

Review Paper

THE THERMODYNAMICAL THEORY OF ELASTO-VISCOPLASTICITY

P. Perzyna

**Institute of Fundamental Technological Research
Polish Academy of Sciences**

Świętokrzyska 21, 00-049 Warsaw, Poland

The main objective of this paper is to survey some recent developments in the constitutive modelling of inelastic polycrystalline solids, which may be used for the description of important problems in modern manufacturing processes, and particularly for mesomechanical issues. This description is needed for the investigation by using the numerical methods how to avoid unexpected plastic strain localization and fracture phenomena in manufacturing technology. Since modern manufacturing processes lead to very complex states of stress and deformation for a solid body under consideration, then in the description we have to take into account the influence of stress triaxiality and plastic spin effects. In this paper emphasis is laid on experimental and physical foundations as well as on mathematical constitutive modelling for the description of localization of plastic deformation and various modes of fracture phenomena in polycrystalline solids. The description of kinematics of finite deformations and the stress tensors is given. The development of a thermo-elasto-viscoplastic model within the thermodynamic framework of the rate-type covariance constitutive structure with finite set of the internal state variables is presented. Particular attention is focused on the determination of the evolution laws for the internal state variables. Fracture criterion based on the evolution of microdamage is formulated. By assuming that the mechanical relaxation time is equal to zero, the thermo-elasto-plastic (rate-independent) response of the damaged material can be accomplished. The thermodynamical theory of elasto-viscoplasticity of polycrystalline solids presented has important features as follows: (i) invariance with respect to diffeomorphism; (ii) finite plastic deformation and plastic spin effects; (iii) plastic non-normality; (iv) softening effects generated by microdamage mechanism; (v) plastic deformation-induced anisotropic effects; (vi) thermomechanical couplings (thermal plastic softening and thermal expansion); (vii) influence of stress triaxiality on the evolution of microdamage; (viii) rate sensitivity; (ix) length scale sensitivity; (x) regularization of the evolution problem; (xi) dissipation and dispersion effects; (xii) synergetic effects generated by cooperative phenomena. All these fundamental features have been carefully discussed. It should be noted that the very important part of constitutive modelling is the identification procedure for the material functions and constants involved in the constitutive equations proposed.

1. PROLOGUE

In this paper emphasis is laid on experimental and physical foundations as well as on mathematical constitutive modelling for the description of polycrystalline solids in modern technological processes.

The understanding of the physical origin and nature of the plastic behaviour of polycrystalline aggregates constitutes one of the major problems in modern materials science.

Modern manufacturing processes generated constitutive modelling of inelastic polycrystalline solids, which may be used for the description of important problems. This description is needed for the investigation by means of numerical methods how to avoid unexpected plastic strain localization and fracture phenomena in manufacturing technology.

Advances in computing as well as measurement instrumentation have recently allowed for the investigation of a wider spectrum of physical phenomena in dynamic failure than those previously possible. With increasing demand for specialized lightweight, high-strength structures, failure of inhomogeneous solids attracts increased attention.

On the other hand, application of metals and polymers at mesoscale (a size scale that ranges from a fraction of micrometer to 100 μm) are recently multiplying rapidly. There is a considerable experimental evidence that plastic flow and particularly fracture phenomena in crystalline solids are inherently size-dependent over mesoscale range. However conventional continuum mechanics models of inelastic deformation processes are size scale-independent. The relatively large numbers of dislocations governing plastic deformation at the micron scale motivate the development of a continuum theory of plasticity incorporating the size-dependence.

The elastic-viscoplastic theory can be developed for this purpose. Based on experimental observations we can suggest that intrinsic microdamage processes very much depend on the strain rate effects. A microdamage process is treated as a sequence of nucleation, growth and coalescence of microcracks. Microdamage kinetics interacts with thermal and load changes to make the failure of a solid a highly rate-temperature- and history-dependent, nonlinear process.

Since modern manufacturing processes lead to very complex states of stress and deformation for a solid body under consideration, then in the description we have to take into account the influence of stress triaxiality and plastic spin effects.

It would be unrealistic to include in the description all the effects observed experimentally. Constitutive modelling is understood as a reasonable choice of effects, which are most important for the explanation of the phenomenon described.

In recent years several models have been proposed to predict the deformation textures, large plastic deformation, strain hardening and strain softening behaviour of polycrystalline solids based on the known behaviour of single crystals. The possibility of making such a prediction rests on the tacit assumption that the main mechanisms of plastic deformation in polycrystalline aggregates are substantially identical with those observed in single crystals.

Recent experimental observations and theoretical investigations have shown that the synergetic effects have great influence on the behaviour of inelastic single crystals. Particularly the adiabatic shear band localization in single crystals is affected very much by cooperative phenomena, cf. PERZYNA [125]. The same conclusion can be drawn for the behaviour of damaged polycrystalline solids and particularly for the fracture phenomena.

Section 2 presents experimental and physical foundations for polycrystalline solids.

First, physical motivations of the new viscoplasticity theory of metallic single crystals have been presented. The discussion of various physical mechanisms of dislocation motion and particularly, the interaction of the thermally activated and phonon damping mechanisms has been given. The relaxation time treated as a microstructural parameter has been introduced. It has been shown that the proposed viscoplastic model accomplishes the description of behaviour of single crystals valid for the entire range of strain rate changes and encompasses the interaction of the thermally activated and phonon damping mechanisms.

Second, experimental justifications for the behaviour of polycrystalline solids are given. Strain rate sensitivity effect is discussed. The relaxation time for the viscoplastic model of polycrystalline solids is investigated. The localized fracture phenomenon of polycrystalline solids is experimentally motivated. The shear band formation and the micro-damage process are discussed. The thermo-mechanical coupling and anisotropy effects are analysed. Experimental observations have suggested that the shear band localization failure in dynamic loading processes is affected by complex cooperative phenomena. The intrinsic microstructure of the shear band region has been investigated and some conclusions important for the constitutive modelling have been drawn.

Section 3 is devoted to the description of kinematics of finite deformations and the stress tensors. The fundamental measures of total deformation are introduced. The decomposition of the strain tensor into the elastic and viscoplastic parts is presented. The rates of the deformation tensor and the stress tensor are defined based on the Lie derivative.

In Sec. 4 the development of a rate-dependent constitutive model within the thermodynamic framework of the rate-type covariance structure with finite set of the internal state variables is presented. This constitutive model is based on the axioms as follows: (i) existence of the free energy function; (ii) invariance with respect to any diffeomorphism (any superposed motion); (iii) assumption of the entropy production inequality; (iv) assumption of the evolution equations for the internal state variables in the particular rate-dependent form.

For our practical purposes it is sufficient to assume that a set of the internal state variables consists of the equivalent viscoplastic deformation and describes the dissipation effects generated by viscoplastic flow phenomena, the volume

fraction porosity which takes account for microdamage effects, and the residual stress tensor (the back stress), which aims at the description of the strain-induced anisotropy (the kinematic hardening effects). Particular attention is focused on the determination of the evolution laws for the internal state variables. The fundamental viscoplastic law for the rate of spatial deformation tensor is assumed to be proportional to the empirical overstress function introduced by the author (cf. PERZYNA [103]). To describe suitably the time and temperature-dependent effects observed experimentally, the kinetics of microdamage and the kinematic hardening law have been modified.

It is noteworthy to stress that viscosity introduces implicitly a length-scale parameter into the dynamical initial-boundary value problem, i.e. $l = \beta c T_m$, where T_m is the relaxation time for mechanical disturbances and is directly related to the viscosity of the material, c denotes the velocity of propagation of the elastic waves in the material, and the proportionality factor β depends on the particular initial-boundary value problem under consideration and may also depend on the microscopic properties of the material.

The relaxation time T_m may be viewed either as a microstructural parameter to be determined from experimental observations or as a mathematical regularization parameter.

Fracture criterion based on the evolution of microdamage is formulated.

By assuming that the mechanical relaxation time is equal to zero, the thermo-elasto-plastic (rate independent) response of the damage material is accomplished, cf. Sec. 5.

An adiabatic inelastic flow process is formulated and investigated in Sec. 6. The conditions for the well-posedness of the Cauchy problem are examined.

The thermodynamical theory of elasto-viscoplasticity of polycrystalline solids presented has important features as follows: (i) invariance with respect to diffeomorphism; (ii) finite plastic deformation and plastic spin effects; (iii) plastic non-normality; (iv) softening effects generated by microdamage mechanism; (v) plastic deformation-induced anisotropic effects; (vi) thermomechanical couplings (thermal plastic softening and thermal expansion); (vii) influence of stress triaxiality on the evolution of microdamage; (viii) rate sensitivity; (ix) length scale sensitivity; (x) regularization of the evolution problem; (xi) dissipation and dispersion effects; (xii) synergetic effects generated by cooperative phenomena. All these fundamental features have been carefully discussed in Sec. 7.

It should be noted that the very important part of the constitutive modelling is the identification procedure for the material functions and constants involved in the constitutive equations proposed. This procedure has to be based on particular experimental observations and it should be developed by using the finite difference or finite element methods.

2. PHYSICAL FOUNDATIONS AND EXPERIMENTAL MOTIVATIONS

2.1. *Physical origin of elastic-viscoplastic response of solids*

The high-rate deformation of face-centered cubic (f.c.c.) metals, such as copper, aluminum, lead and nickel has been recently extensively studied (cf. review paper by FOLLANSBEE [49]). It has been shown that the apparent strain rate sensitivity of f.c.c. metals has two origins: that associated with the finite velocity of dislocations, and that connected with the evolution of the dislocation substructure. The first of these two components – the instantaneous rate sensitivity – is related to the wait – times associated with thermally activated dislocation motion. The second component has more to do with the relative importance of dislocation generation and annihilation at different strain rates, and shall be referred to as the strain-rate history effect.

The rate and temperature dependence of the flow stress of metal crystals can be explained by different physical mechanisms of dislocation motion. The microscopic processes combine in various ways to give several groups of deformation mechanisms, each of which can be limited to the particular range of temperature and strain rate changes.

It will be profitable for further considerations to discuss some of these mechanisms, particularly those which lead to viscoplastic response of the crystal.

Some common thermal obstacles or mechanisms in pure metals are as follows: (i) intersection of forest dislocations; (ii) overcoming Peierls–Nabarro stress; (iii) non-conservative motion of jogs; (iv) cross-slip of screw dislocations; (v) climb of edge dislocations. Forest dislocations, the Peierls–Nabarro stress and jogs represent resistance to the motion of dislocations in the slip plane, while cross-slip and climb represent resistance to the motion out of the slip plane. Schematic representations of the mechanisms in which these obstacles are overcome are given in Fig. 1. In each case, thermal fluctuations assist the applied stress in getting a dislocation segment L past the barrier (cf. CONRAD [17]).

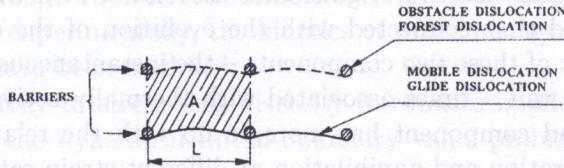
To describe theoretically all the mechanisms we have to introduce three important parameters, namely the density of mobile dislocations α , the density of obstacle dislocations β and the concentration of point defects ζ . Average density of mobile dislocations in deformed metal single crystals is of the order of 10^{15} m^{-2} , average density of obstacle dislocations is 10^{13} m^{-2} , and the average value of the concentration of point defects can be of the order of 10^{15} m^{-3} .

Since plastic flow occurs by the motion of dislocation lines, the rate at which it takes place depends on how fast the dislocations move, how many dislocations are moving in a given volume of material, and how much displacement is carried by each dislocation. The theory of crystal dislocations shows that for the single slip, the inelastic shear strain-rate is as follows

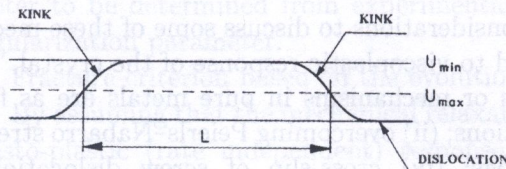
$$(2.1) \quad \dot{\epsilon}^p = \alpha b v,$$

where α is the mean density of mobile dislocations, b is the displacement per dislocation line (the Burgers vector), and v denotes the mean dislocation velocity, cf. ASARO [6,7].

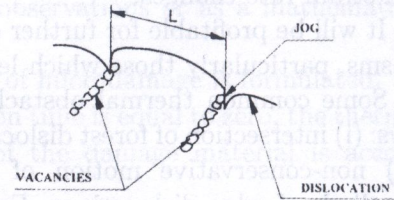
(i) INTERSECTION OF FOREST DISLOCATIONS



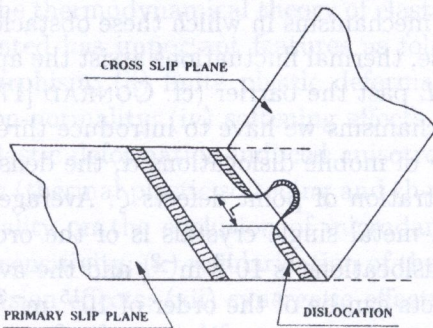
(ii) OVERCOMING PEIERLS-NABARRO STRESS



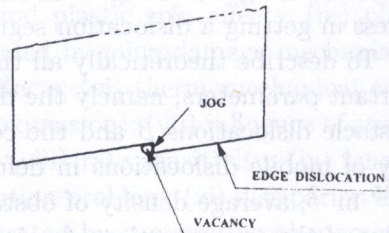
(iii) NON-CONSERVATIVE MOTION OF JOGS



(iv) CROSS-SLIP



(v) CLIMB



- α DENSITY OF MOBILE DISLOCATIONS (10^{10}m^{-2})
- β DENSITY OF OBSTACLE DISLOCATIONS (10^{12}m^{-2})
- ξ CONCENTRATION OF POINT DEFECTS (10^{18}m^{-3})

FIG. 1. Schematic representation of thermal obstacles or mechanisms in pure metals (cf. Conrad [17]).

2.1.1. *Thermally activated mechanism.* It is now generally recognized that the plastic deformation of a crystal is of dynamic nature and has been established as a thermally activated process dependent upon time, temperature and strain rate. The evolution of the activation parameters is a widely used technique for identification of the mechanisms controlling the rate of deformation, and has been applied to b.c.c., f.c.c., h.c.p. metals, intermetallic compounds and ionic and ceramic crystals (cf. the review paper by EVANS and RAWLINGS [48] and books by NABARRO [100], and KOCKS *et al.* [78]).

When a dislocation moves through a crystal lattice, a force is exerted upon it by obstacles present in the lattice. This force can be separated into two components, a long-range force and short-range force.

The stress necessary to overcome the short-range obstacles is temperature-dependent, whereas that needed to surmount fixed long-range obstacles generally depends upon temperature only through the temperature-dependence of the shear modulus. For this reason the obstacles are often referred to as thermal and athermal, respectively. When both types of obstacles are present in a lattice, the applied stress is usually composed of both the thermal and athermal components

$$(2.2) \quad \tau = \tau^\# + \tau_\mu,$$

where $\tau^\#$ is the thermal (or effective) resolved shear stress and τ_μ is the athermal stress, cf. Fig. 2.

THERMALLY ACTIVATED DISLOCATION MECHANISM

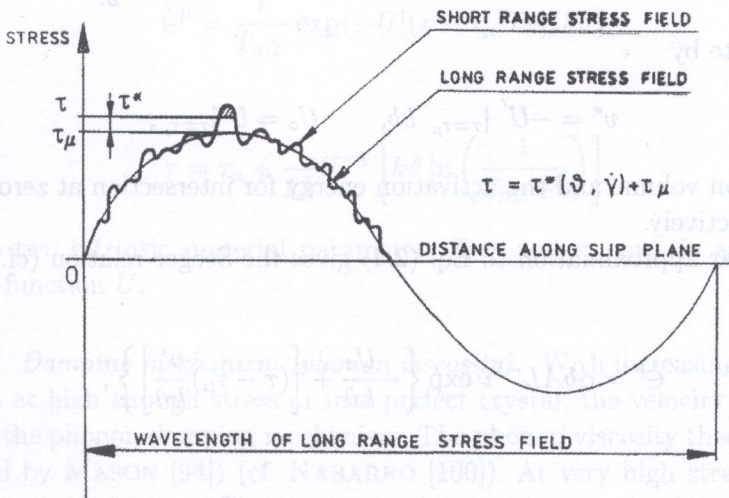


FIG. 2. Thermal and athermal stress field components in a crystal lattice.

Plastic deformation occurs by the movement of a large number of dislocations through an array of obstacles. At any finite temperature, coherent atomic fluctuations can assist the applied stress in moving a dislocation past the obstacles.

The average velocity v of a dislocation that surmounts the obstacles with the assistance of thermal fluctuations is assumed to be an Arrhenius-type relationship

$$(2.3) \quad v = AL^{-1}\nu \exp\left(-\frac{U}{k\vartheta}\right),$$

where ν is the frequency of vibration of the dislocation, AL^{-1} is the distance covered after a successful fluctuation, U is the activation energy (Gibbs free energy), k is the Boltzmann constant and ϑ is the actual absolute temperature.

Equations (2.1) and (2.3) give

$$(2.4) \quad \dot{\epsilon}^p = \alpha b AL^{-1}\nu \exp\left(-\frac{U}{k\vartheta}\right).$$

Let us assume that

$$(2.5) \quad U = U[(\tau - \tau_\mu)Lb],$$

where L is the mean cord distance between the neighboring points at which the dislocation is arrested. Expansion of the function U gives

$$(2.6) \quad U = U|_{\tau=\tau_\mu} + U'|_{\tau=\tau_\mu} (\tau - \tau_\mu)Lb + U''|_{\tau=\tau_\mu} \frac{(\tau - \tau_\mu)^2 L^2 b^2}{2!} + \dots$$

Let us denote by

$$(2.7) \quad v^* = -U'|_{\tau=\tau_\mu} Lb, \quad U_0 = U|_{\tau=\tau_\mu},$$

the activation volume and the activation energy for intersection at zero effective stress, respectively.

The linear approximation to Eq. (2.4) gives the Seeger relation (cf. SEEGER [143, 144])

$$(2.8) \quad \dot{\epsilon}^p = \alpha b AL^{-1}\nu \exp\left\{-\frac{U_0}{k\vartheta} + \left[(\tau - \tau_\mu)\frac{v^*}{k\vartheta}\right]\right\},$$

or

$$(2.9) \quad \tau = \left(\tau_\mu + \frac{U_0}{v^*}\right) + \frac{k\vartheta}{v^*} \ln \frac{\dot{\epsilon}^p}{\alpha b AL^{-1}\nu}.$$

When the activation energy U is a nonlinear function of the effective stress (cf. Eq. (2.5)), the relation (2.4) yields

$$(2.10) \quad \dot{\epsilon}^p = \alpha b A L^{-1} \nu \exp \{ -U [(\tau - \tau_\mu) L b] / k \vartheta \}$$

or

$$(2.11) \quad \tau = \tau_\mu + \frac{1}{L b} U^{-1} [k \vartheta \ln (\alpha b A L^{-1} \nu / \dot{\epsilon}^p)].$$

Let us denote by

$$(2.12) \quad T_{mT} = \frac{1}{\gamma_T} = (\alpha b A L^{-1} \nu)^{-1}, \quad \tau_B = (\tau_\mu + U_o / v^*),$$

the relaxation time for the thermally activated mechanism of dislocation motion (γ_T defines the viscosity coefficient) and the flow stress τ_B , respectively. Then the relations (2.8) and (2.9) take the form

$$(2.13) \quad \dot{\epsilon}^p = \frac{1}{T_{mT}} \exp \left[\frac{v^*}{k \vartheta} (\tau - \tau_B) \right], \quad \tau = \tau_B + (k \vartheta / v^*) \ln (T_{mT} \dot{\epsilon}^p).$$

In this linear theory we have three intrinsic material parameters, namely the relaxation time T_{mT} , the activation volume v^* and the flow stress τ_B .

In the most general case, each of these three parameters may be considered as a function of the three independent variables $\dot{\epsilon}^p$, τ and ϑ .

In the nonlinear theory

$$(2.14) \quad \dot{\epsilon}^p = \frac{1}{T_{mT}} \exp \{ -U [(\tau - \tau_\mu) L b] / k \vartheta \}$$

or

$$(2.15) \quad \tau = \tau_\mu + \frac{1}{L b} U^{-1} \left[k \vartheta \ln \left(\frac{1}{T_{mT} \dot{\epsilon}^p} \right) \right]$$

there are two intrinsic material parameters T_{mT} and τ_μ and, in addition, one response function U .

2.1.2. Damping mechanism (phonon viscosity). With increasing dislocation velocities at high enough stress or in a perfect crystal, the velocity is only governed by the phonon damping mechanism. The phonon viscosity theory has been developed by MASON [94] (cf. NABARRO [100]). At very high strain rates the applied stress is high enough to overcome instantaneously the dislocation barriers without any aid from thermal fluctuations. This is true for the resolved shear

stress $\tau > \tau_B$, where τ_B is attributed to the stress needed to overcome the forest dislocation barriers to the dislocation motion and is called the back stress.

In this region of response, the evolution equation for the inelastic shearing has the form

$$(2.16) \quad \dot{\epsilon}^p = \frac{\alpha b^2 \tau_B}{B} \left[\frac{\tau}{\tau_B} - 1 \right],$$

where B is called the dislocation drag coefficient. If we introduce the notation

$$(2.17) \quad T_{mD} = \frac{B}{\alpha b^2 \tau_B} = \frac{1}{\gamma_D}$$

for the relaxation time of the phonon damping mechanism (γ_D defines the viscosity coefficient for this region), then the evolution equation (2.16) takes the form

$$(2.18) \quad \dot{\epsilon}^p = \frac{1}{T_{mD}} \left(\frac{\tau}{\tau_B} - 1 \right),$$

or

$$(2.19) \quad \tau = \tau_B (1 + T_{mD} \dot{\epsilon}^p).$$

For the phonon damping mechanism we have two intrinsic parameters, namely the relaxation time T_{mD} and the back stress. It is noteworthy that the dislocation drag coefficient B can be interpreted as a generalized damping parameter for phonon viscosity and electron viscosity mechanisms (cf. GORMAN *et al.* [57]) i.e.

$$(2.20) \quad B = B_{pv} + B_{ev}.$$

2.1.3. Interaction of the thermally activated and phonon damping mechanisms. If a dislocation is moving through the rows of barriers, then its velocity can be determined by the expression

$$(2.21) \quad v = AL^{-1}/(t_S + t_B),$$

where AL^{-1} is the average distance of dislocation movement after each thermal activation, t_S is the time a dislocation has spent at the obstacle, and t_B is the time of travelling between the barriers.

The shearing rate in single slip is given by the relationship (cf. KUMAR and KUMBLE [80], TEODOSIU and SIDOROFF [155] and PERZYNA [107, 118])

$$(2.22) \quad \dot{\epsilon}^p = \frac{1}{T_{mT}} \langle \exp \{ U[(\tau - \tau_\mu)Lb]/k\theta \} + BAL^{-1}\nu/(\tau - \tau_B)b \rangle^{-1}$$

where

$$(2.23) \quad \frac{1}{T_{mT}} \frac{b\tau_B}{BAL^{-1}\nu} = \frac{\alpha b^2 \tau_B}{B} = \frac{1}{T_{mD}},$$

and two effective resolved shear stresses

$$(2.24) \quad \tau_T^* = \tau - \tau_\mu \quad \text{and} \quad \tau_D^* = \tau - \tau_B$$

are separately defined for the thermally activated and phonon damping mechanisms, respectively.

If the time t_B taken by the dislocation to travel between the barriers in a viscous phonon medium is negligible when compared with the time t_S spent at the obstacle, then

$$(2.25) \quad v = \frac{AL^{-1}}{t_S}$$

and we can focus our attention on the analysis of the thermally activated process.

When the ratio t_B/t_S increases then the dislocation velocity (2.21) can be approximated by the expression

$$(2.26) \quad v = \frac{AL^{-1}}{t_B}$$

for the phonon damping mechanism.

2.1.4. Viscoplastic model of single crystals. The main idea of the viscoplastic flow mechanism is to accomplish in one model the description of behaviour of single crystals valid for the entire range of strain rate changes. In other words, the main concept is to encompass the interaction of the thermally activated and phonon damping mechanisms.

To achieve this aim, the empirical overstress function Φ has been introduced and the strain rate is postulated in the form as follows (cf. PERZYNA [118]):

$$(2.27) \quad \dot{\epsilon}^p = \frac{1}{T} \left\langle \Phi \left[\frac{\tau}{\tau_Y(\epsilon^p, \vartheta, \beta, \zeta)} - 1 \right] \right\rangle \text{sgn}\tau,$$

where T is the relaxation time, $\langle \cdot \rangle$ denotes the Macauley bracket and τ_Y is the static yield stress function. In this model the static yield stress function depends on the inelastic strain ϵ^p , temperature ϑ , the density of obstacle dislocations β and the concentration of point defects ζ .

It is noteworthy that the empirical overstress function Φ can be determined basing on available experimental results performed under dynamic loading.

To describe the main experimentally observed facts connected with the macroscopic shear band localization of single crystals, namely that the strain-hardening modulus rate h_{crit} at the inception of shear band localization is positive and the direction of the localized shear band is misaligned by some angle δ from the active slip system, we intend to consider the synergetic effects resulting from taking into account spatial covariance effects and thermomechanical couplings (cf. DUSZEK-PERZYNA and PERZYNA [39]).

To take into consideration the evolution of the substructure of crystals we can introduce the density of mobile dislocations $\alpha^{(\nu)}$, the density of obstacle dislocations $\beta^{(\nu)}$ and the concentration of point defects $\zeta^{(\nu)}$ for a particular slip system ν as the internal state variables, cf. PERZYNA [125].

2.2. Strain rate sensitivity

In previous sections fundamental features of finite deformation, rate-dependent plastic flow of crystalline solids were discussed from the microscopic and macroscopic phenomenological points of view. Particular viscoplastic flow model was proposed to predict deformation textures and large strain, temperature and rate-dependent and strain hardening behaviour of polycrystals from the known behaviour of single crystals.

The possibility of making such a prediction rests on the tacit assumption that the mechanisms of plastic deformation in aggregates are substantially identical with those observed in single crystals.

LINDHOLM and YEAKLEY [83] investigated single and polycrystalline specimens of high purity aluminum in compression at strain rates up to 500 s^{-1} using the split Hopkinson pressure bar method. They obtained average stress-strain curves for the six orientations of a single crystal and similar curves for the polycrystalline material. Activation volume as a function of strain can be computed from the data obtained. Results for the single and polycrystalline specimens of high purity aluminum are plotted in Fig. 3. The most interesting feature of these curves is that the activation volume for the polycrystalline material falls within the bounds and near the average of the single crystal data. This implies that the same thermally activated mechanisms control the deformation in single and polycrystals and that the distribution of the activation barriers are essentially the same in both cases. This is in agreement with the previous results obtained by MITRA and DORN [99] for aluminum at low temperature and those of CONRAD [17] for iron and steel, cf. also LINDHOLM [81, 82].

Experimental justifications of the thermally activated and phonon damping mechanisms as well as the discussion of their range rate and temperature changes for particular materials have been given in many papers. Particular importance for our purposes have the results obtained by CAMPBELL and FERGUSON [10]. In their paper an account is given of experiments in which the shear flow stress

of mild steel was measured at temperature from 195 to 713 K and strain rate from 10^{-3} to $4 \cdot 10^4 \text{ s}^{-1}$. The flow stress at lower yield is plotted in Fig. 4 as the shear stress against the logarithm of shear strain rate, for various temperatures used throughout the investigation.

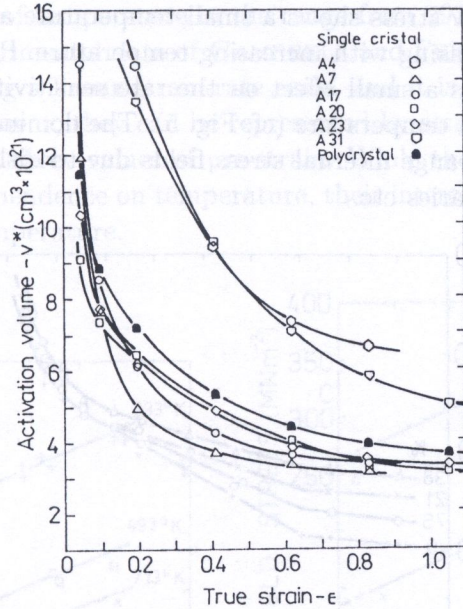


FIG. 3. Activation volume versus true strain for single crystal and polycrystalline aluminium (99.995%). After LINDHOLM and YEAKLEY [83].

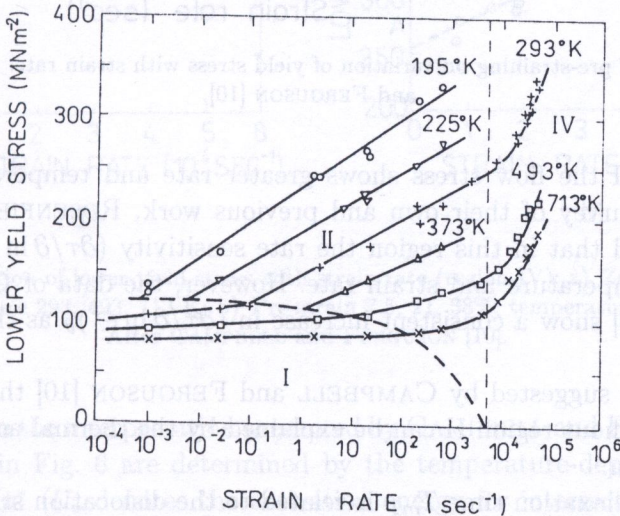


FIG. 4. Variation of lower yield stress with strain rate, at constant temperature. After CAMPBELL and FERGUSON [10].

For the purpose of the discussion which follows, it is convenient to divide the curves into three regions, each corresponding to a certain range of strain rate which is a function of the temperature. Following ROSENFELD and HAHN [138] these will be referred to as region I, II and IV. These regions are indicated in Fig. 4.

In region I the flow stress shows a small temperature and strain rate sensitivity, the latter decreasing with increasing temperature. Prestraining increases the flow stress but has a small effect on the rate sensitivity of the flow stress, $(\partial\tau/\partial \ln \dot{\epsilon}^p)_\vartheta$, at room temperature (cf. Fig. 5). The dominant factor in region I seems to be the long-range internal stress fields due to dislocations, precipitate particles, grain boundaries etc.

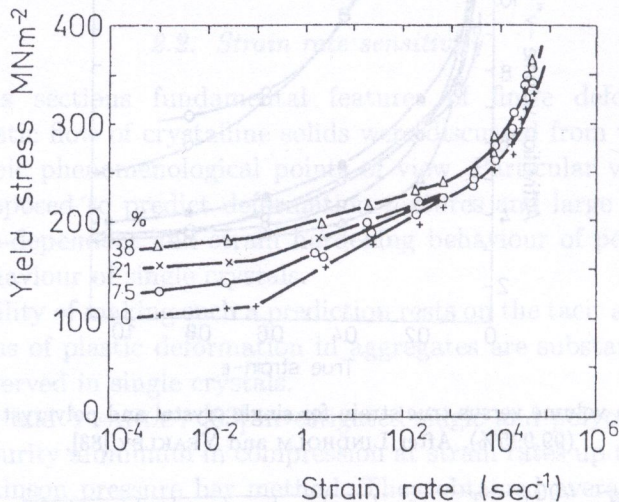


FIG. 5. Effect of pre-straining on variation of yield stress with strain rate. After CAMPBELL and FERGUSON [10].

In region II the flow stress shows greater rate and temperature sensitivities. From a survey of their own and previous work, ROSENFELD and HAHN [138] concluded that in this region the rate sensitivity $(\partial\tau/\partial \ln \dot{\epsilon}^p)_\vartheta$ was independent of temperature and strain rate. However, the data of CAMPBELL and FERGUSON [10] show a consistent increase in $(\partial\tau/\partial \ln \dot{\epsilon}^p)_\vartheta$ as the temperature is reduced.

It has been suggested by CAMPBELL and FERGUSON [10] that the flow behaviour throughout region II can be explained by the thermal activation of dislocation motion.

Since the relaxation time T_{mT} is related to the dislocation structure, it may be governed by the deformation history, rather than a function of the state variables ϵ^p , τ and ϑ .

The experimental data obtained by CAMPBELL and FERGUSON [10] for mild steel in region II are properly interpreted by the linear approximation of the thermally activated theory.

Region IV is characterized by a rapid increase in semi-logarithmic rate sensitivity $(\partial \ln / \partial \ln \dot{\epsilon}^p)_\theta$ with increasing strain rate, this parameter being approximately independent of temperature in the range from 293 to 713 K.

In Fig. 6 the experimental data of CAMPBELL and FERGUSON [10] for region IV are replotted using a linear strain-rate scale, and it is seen that, within the accuracy of measurement, they can be represented by straight lines at all three temperatures and all three values of pre-strain. While the slopes of these lines show only a small dependence on temperature, their intercepts on the stress axis vary greatly with temperature.

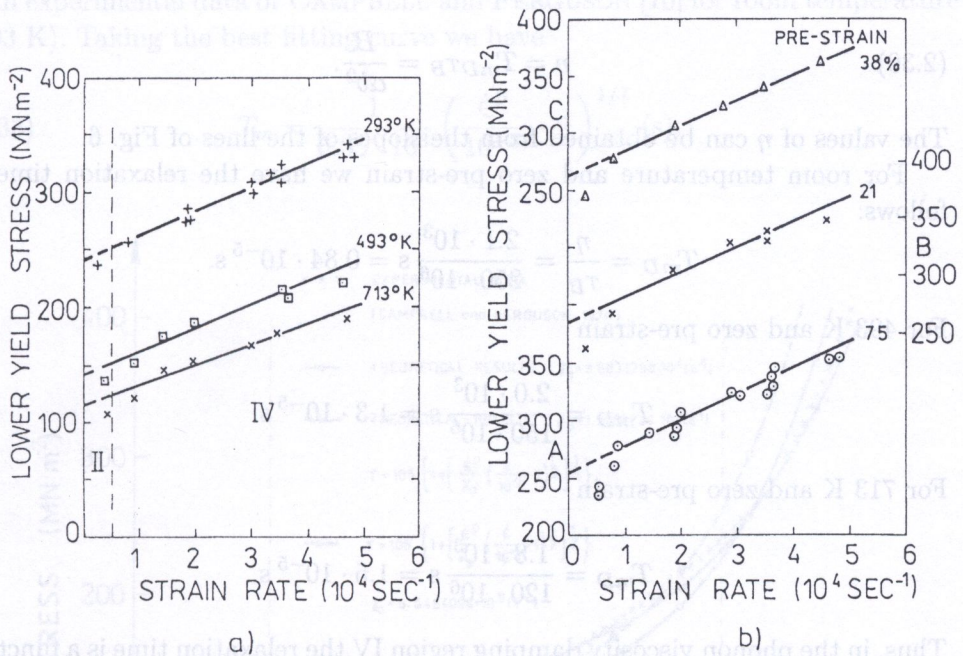


FIG. 6. Variation of lower yield stress with strain rate (region IV); a) Zero pre-strain; temperature 293, 493, 713 K; b) Pre-strain 7.5, 21, 38%; temperature 293 K. After CAMPBELL and FERGUSON [10].

According to the interpretation presented by CAMPBELL and FERGUSON [10], the intercepts in Fig. 6 are determined by the temperature-dependent barrier stress $\tau_\mu + U_o/v^*$ (U_o denotes the activation energy for intersection at zero effective stress and v^* is the activation volume), at which the strain rate reaches $1/T_m T$. When the applied stress exceeds this barrier stress, the time required

to activate a dislocation past the short-range barriers of obstacles is negligible, hence its velocity is controlled by dissipation of energy as it moves through the lattice. Assuming that this dissipation is of a linear viscous nature, the excess stress τ_D will be proportional to the strain rate $\dot{\epsilon}^p$, i.e.

$$(2.28) \quad \tau_D = \eta \dot{\epsilon}^p,$$

where η denotes the macroscopic viscosity. Equating τ_D to the difference between the applied stress and the barrier stress $\tau_B = \tau_\mu + U_o/v^*$, we obtain for region IV

$$(2.29) \quad \tau = \tau_B + \eta \dot{\epsilon}^p.$$

Comparison (2.29) with (2.17) under the condition (2.19) gives

$$(2.30) \quad \eta = T_{mD} \tau_B = \frac{B}{\alpha b^2}.$$

The values of η can be obtained from the slopes of the lines of Fig. 6.

For room temperature and zero pre-strain we have the relaxation time as follows:

$$T_{mD} = \frac{\eta}{\tau_B} = \frac{2.1 \cdot 10^3}{250 \cdot 10^6} \text{ s} = 0.84 \cdot 10^{-5} \text{ s}.$$

For 493 K and zero pre-strain

$$T_{mD} = \frac{2.0 \cdot 10^3}{150 \cdot 10^6} \text{ s} = 1.3 \cdot 10^{-5} \text{ s}.$$

For 713 K and zero pre-strain

$$T_{mD} = \frac{1.8 \cdot 10^3}{120 \cdot 10^6} \text{ s} = 1.5 \cdot 10^{-5} \text{ s}.$$

Thus, in the phonon viscosity damping region IV the relaxation time is a function of temperature and is not sensitive to pre-stressing (for room temperature).

For region II the relaxation time T_{mT} is obtained as a constant value

$$T_{mT} = 2 \cdot 10^{-4} \text{ s},$$

while in region IV the relaxation time T_{mD} is temperature dependent and can change from $T_{mD} = 0.8 \cdot 10^{-5} \text{ s}$ to $T_{mD} = 1.5 \cdot 10^{-5} \text{ s}$.

For the viscoplastic model of polycrystalline solids, the relaxation time T_m governs the viscoplastic flow in the entire range of strain rate changes and can be obtained based on experimental data.

Another possible idea has been presented by PERZYNA [108, 109], namely that

$$(2.31) \quad T_m = \frac{\phi}{\gamma},$$

where ϕ is the control function and γ is the temperature dependent viscosity coefficient. The dimensionless control function ϕ is assumed to depend on the strain rate. Thus we have

$$(2.32) \quad T_m = \frac{1}{\gamma(\dot{\vartheta})} \phi \left(\frac{\dot{\epsilon}^p}{\dot{\epsilon}_s^p} - 1 \right).$$

In Fig. 7 the theoretical results obtained by PERZYNA [108, 109] are compared with experimental data of CAMPBELL and FERGUSON [10] for room temperature (293 K). Taking the best fitting curve we have

$$(2.33) \quad T_m = \frac{1}{6.55 \cdot 10^3} \left(\frac{\dot{\epsilon}^p}{10^{-3}} - 1 \right)^{1/7} \text{ (s)}.$$

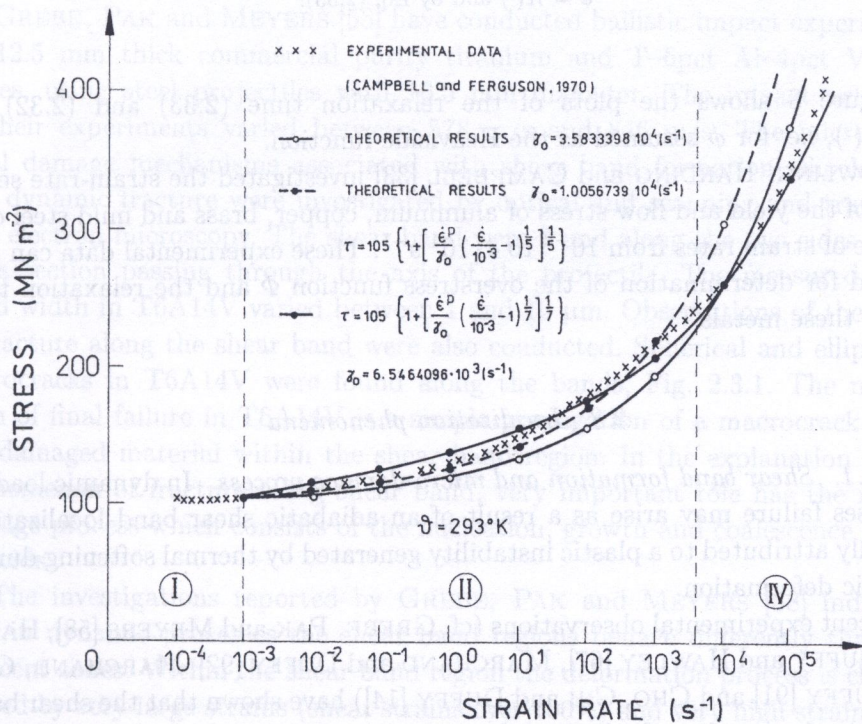


FIG. 7. Comparison of theoretical description with experimental results.

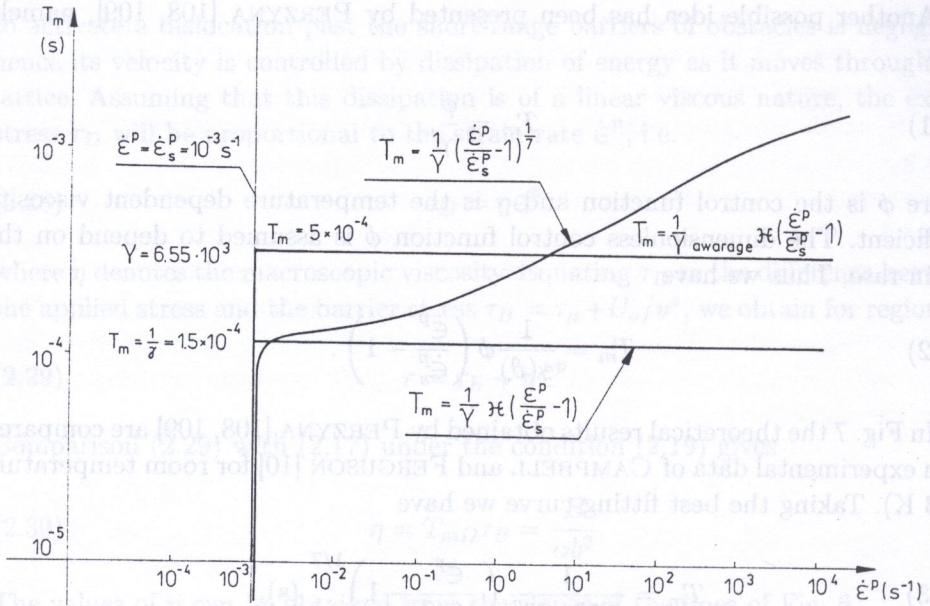


FIG. 8. Variation of the relaxation time with strain rate described by Eq. (2.32) with $\phi = \mathcal{H}(\cdot)$ and by Eq. (2.33).

Figure 8 shows the plots of the relaxation time (2.33) and (2.32) for $\phi \equiv \mathcal{H}(\cdot)$, i.e. for ϕ assumed as the Heaviside function.

DOWLING, HARDING and CAMPBELL [33] investigated the strain-rate sensitivity of the yield and flow stress of aluminum, copper, brass and mild steel over a range of strain rates from 10^{-3} to $4 \cdot 10^4 \text{ s}^{-1}$. These experimental data can also be used for determination of the overstress function Φ and the relaxation time T_m for these metals.

2.3. Localization phenomena

2.3.1. Shear band formation and micro-damage process. In dynamic loading processes failure may arise as a result of an adiabatic shear band localization, generally attributed to a plastic instability generated by thermal softening during dynamic deformation.

Recent experimental observations (cf. GREBE, PAK and MEYERS [58], HARTLEY, DUFFY and HAWLEY [67], MARCHAND and DUFFY [92], MARCHAND, CHO and DUFFY [91] and CHO, CHI and DUFFY [14]) have shown that the shear band procreates in a region of a body deformed where the resistance to plastic deformation is lower and the predisposition for band formation is higher.

Adiabatic shear banding in 4340 steel under pure shear loading in a split Hopkinson torsion bar using a high-speed photography was studied by GIOVANOLA [53]. It was found that shear localization occurs in two sequential stages over width of 60 μm and 20 μm , respectively. Strain rates approaching $1.4 \cdot 10^6 \text{ s}^{-1}$ were measured in the band and temperature elevation was in excess of 1000°C . Fractographic and metallographic observations have shown that the mechanism of shear fracture by microvoid nucleation and growth may, at least in certain situations, provide a plausible explanation for the formation of white-etching bands. General conclusion from experimental observations of GIOVANOLA [53] is that the thermomechanical strain localization and micro-damage mechanisms become main cooperative phenomena responsible for adiabatic shear band localized fracture.

CHAKRABARTI and SPRETNAK [12] investigated the localized fracture mode for tensile steel sheet specimens simulating both plane stress and plane strain processes. The material used in their study was AISI 4340 steel. The principal variable in this flat specimen test was the width-to-thickness ratio. Variation in specimen geometry produces significant changes in the stress state, directions of shear bands and ductility. They found that fracture propagated consistently along the shear band localized region.

GREBE, PAK and MEYERS [58] have conducted ballistic impact experiments on 12.5 mm thick commercial purity titanium and T-6pct Al-4pct V alloy plates, using steel projectiles with 10.5 mm diameter. The impact velocities in their experiments varied between 578 m/s and 846 m/s. The microstructural damage mechanisms associated with shear band formation, shock wave and dynamic fracture were investigated by optical and scanning and transmission electron microscopy. The shear band were found along the two sides of the cross-section passing through the axis of the projectile. The measured shear band width in T6A14V varied between 1 and 10 μm . Observations of the onset of fracture along the shear band were also conducted. Spherical and ellipsoidal microcracks in T6A14V were found along the bands, Fig. 2.3.1. The mechanism of final failure in T6A14V is a simple propagation of a macrocrack along the damaged material within the shear band region. In the explanation of the phenomenon of fracture along shear band, very important role has the micro-damage process which consists of the nucleation, growth and coalescence of microvoids.

The investigations reported by GREBE, PAK and MEYERS [58] indicated that in dynamic processes the shear band regions behave differently than the adjacent zones. Within the shear band region the deformation process is characterized by very large strains (shear strains over 100%) and very high strain rates ($10^3 - 10^5 \text{ s}^{-1}$). The strain rate sensitivity of a material becomes a very important feature of the shear band region and the micro-damage process is intensified.

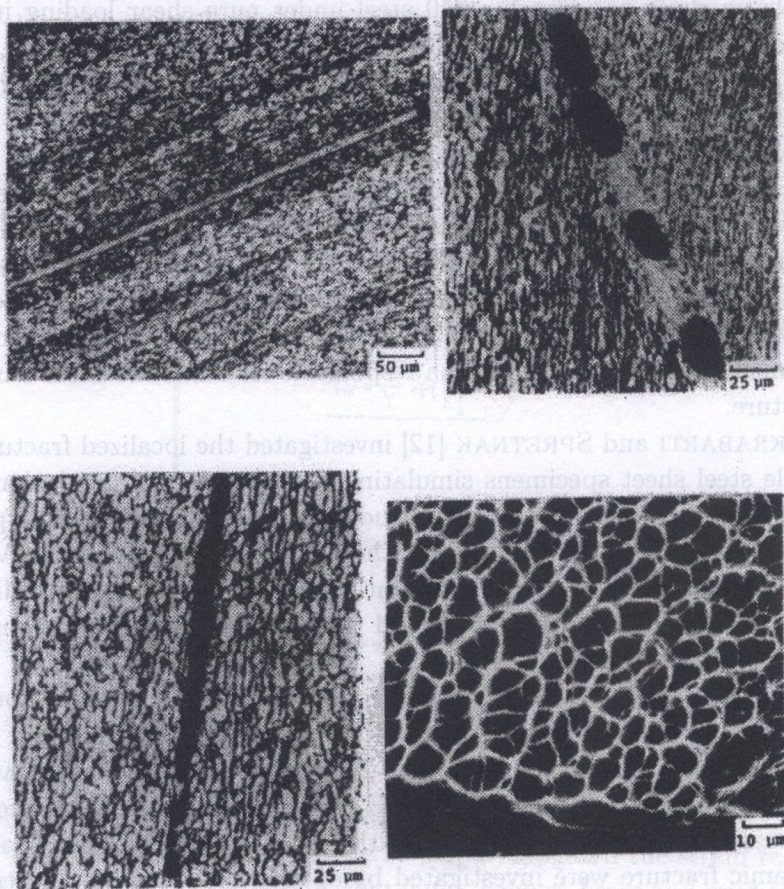


FIG. 9. Shear band in Ti6Al4V target impacted at 846 m/s (After GREBE, PAK and MEYERS [58]). a) Single shear band; b) Microcracks in the shear band region; c) Elongated macrocracks along the shear band; d) Characteristic dimples observed in spall region.

CHO, CHI and DUFFY [14] performed microscopic observations of adiabatic shear bands in three different steels: an AISI cold rolled steel, HY-100 structural steel and AISI 4340 VAR steel subjected to two different heat treatments. Dynamic deformation in shear was imposed to produce shear bands in all the steels tested. It was found that whenever the shear band led to fracture of the specimen, the fracture occurred by a process of void nucleation, growth and coalescence. No cleavage was observed on any fracture surface, included the most brittle of the steel tested. The authors suggested that this is presumably due to softening of the shear band material that results from the local temperature rise occurring during dynamic deformation, Figs. 10 and 11.

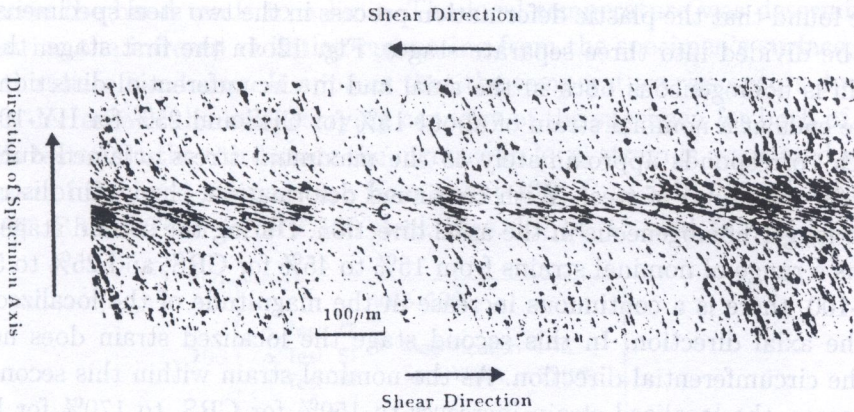


FIG. 10. An optical micrograph of a shear band formed in 1018 CRS. The surface has been polished and etched. An arrested crack is shown within shear band (After CHO, CHI and DUFFY [14]).

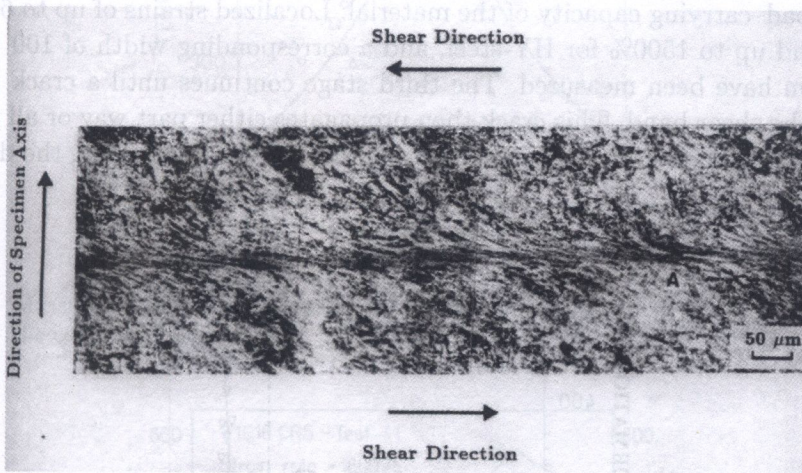


FIG. 11. Optical micrograph of a shear band formed in HY-100 steel, after polishing and etching (After CHO, CHI and DUFFY [14]).

2.3.2. Thermomechanical coupling effects. HARTLEY, DUFFY and HAWLEY [67], MARCHAND and DUFFY [92] and MARCHAND, CHO and DUFFY [91] presented the results of experiments in which the local strain and local temperature were measured during the formation of an adiabatic shear band in an AISI 1018 cold-rolled steel (CRS), and a low alloy structural steel (HY-100). In their experiments a torsional Kolsky bar was used to impose a rapid deformation rate in a short thin-walled tubular specimen. By testing a number of specimens they

have found that the plastic deformation process in the two steel specimens tested can be divided into three separate stages, Fig. 12. In the first stage, the shear strain is homogeneous both in the axial and in circumferential directions. This stage ends at a nominal strain of about 15% for CRS and 25% for HY-100 steel, which corresponds approximately to the maximum stress attained during the test for each kind of steel. With continued deformation, the strain distribution is no longer homogeneous in the axial direction. During the second stage, which spans a range of nominal strains from 15% to 45% for CRS, and 25% to 50% for HY-100, there is a continuous increase in the magnitude of the localized strain in the axial direction. In this second stage the localized strain does not vary in the circumferential direction. As the nominal strain within this second stage increases, the localized strain increases to 150% for CRS, to 170% for HY-100 steel and the width of the band decreases from about 1100 μm to 350 μm for CRS, and 600 μm to 150 μm for HY-100 steel. In this stage of deformation, the flow stress level does not vary greatly. The third stage in the deformation process in each of two steel kinds tested involves a sharp drop in stress, i.e. a loss in the load-carrying capacity of the material. Localized strains of up to 600% for CRS, and up to 1500% for HY-steel, and a corresponding width of 100 μm and of 20 μm have been measured. The third stage continues until a crack appears within the shear band. This crack then propagates either part way or all the way around the specimen. It has been observed that, in the third stage, the deforma-

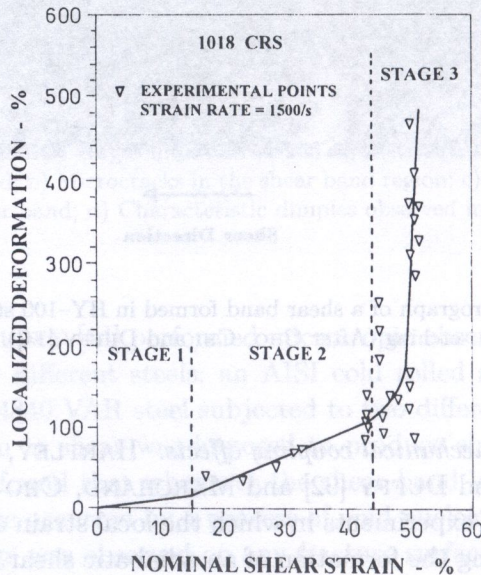


FIG. 12. The maximum localized strain as a function of the nominal shear strain (After MARCHAND, CHO and DUFFY [91]).

tion outside the band tends to a limit. The local temperature was determined by measuring the infrared radiation emanating from the specimen's surface, including the shear band area. It appears that the temperature rise occurs during the sharp decrease in the load-carrying capacity of the specimen for both of the two steels tested. In the third stage the increase in local strain is associated with an increase of the local temperature from about 235° C to 575° C for CRS and about 460° C to 900° C for HY-100 steel, Figs. 13, 14, 15, and 16.

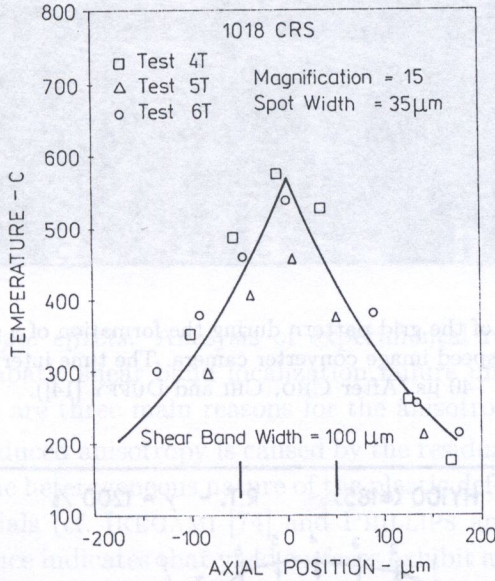


FIG. 13. Measured values of the temperature as a function of axial position with respect to the centre of the shear band (After MARCHAND, CHO and DUFFY [91]).

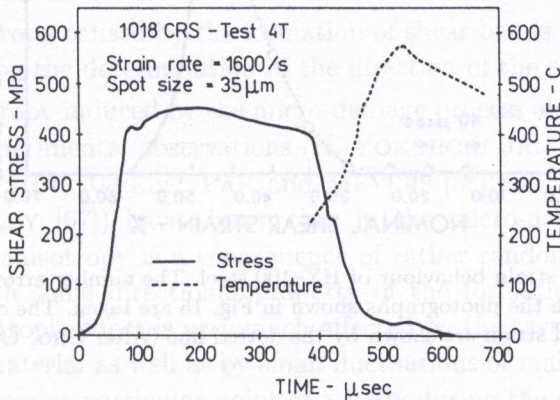


FIG. 14. Shear band temperature and stress as a function of time in 1018 CRS (After HARTKEY, DUFFY and HAWLEY [67]).

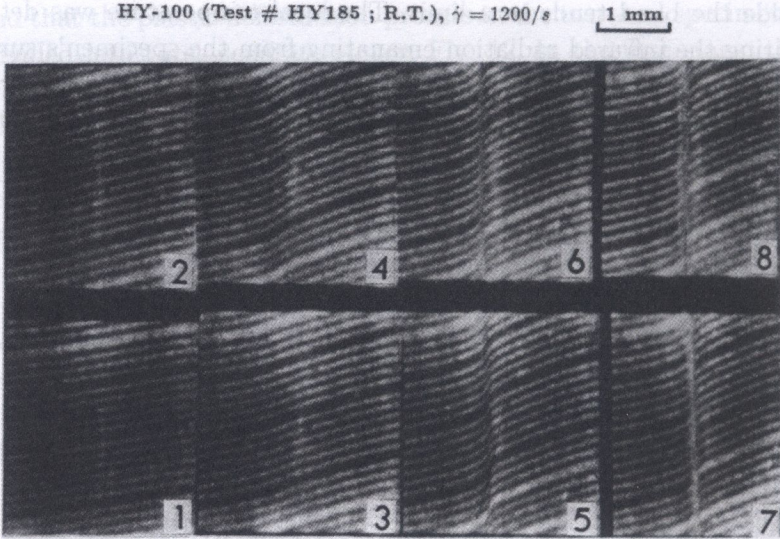


FIG. 15. Photographs of the grid pattern during the formation of a shear band in HY-100 steel taken by a high speed image converter camera. The time interval between frames is 40 μs (After CHO, CHI and DUFFY [14]).

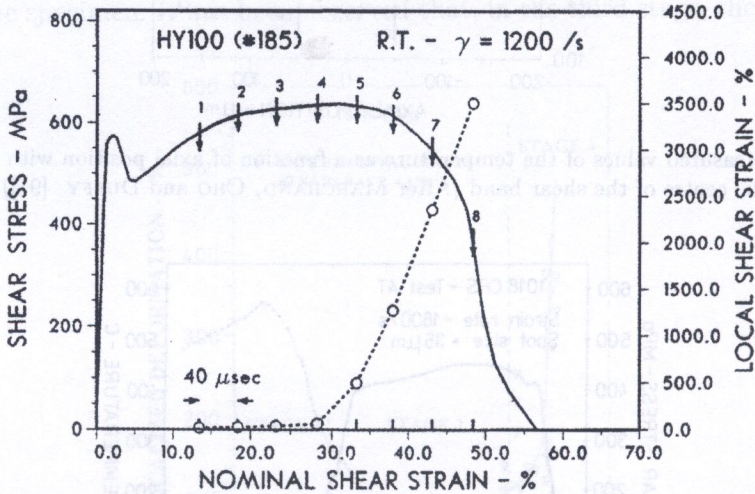


FIG. 16. The stress-strain behaviour of HY-100 steel. The number arrows indicate nominal strain values at which the photographs shown in Fig. 15 are taken. The corresponding values of the maximum local strain are shown by the dotted line (After CHO, CHI and DUFFY [14]).

It is generally accepted that shear bands nucleate in the presence of a local inhomogeneity or defects, causing enhanced local deformation and heating. Once

nonuniform flow procreates, the deformation becomes increasingly unstable as the dynamic process goes on if the heat that is produced during deformation is given insufficient time to be conducted away.

Experimental results have shown that localization occurs more readily in materials with a low strain hardening rate, a low strain rate sensitivity, a low thermal conductivity and a high thermal softening rate. Shear bands also form readily in high strength materials where the heat generated by plastic deformation is greater for a given plastic strain increment (cf. HARTLEY, DUFFY and HAWLEY [67]).

Along the shear band, the deformation process is characterized by very intense strain and very large strain rates (cf. GREBE, PAK and MEYERS [58] and HARTLEY, DUFFY and HAWLEY [67]). Strain rate sensitivity of a material becomes a very important feature of the shear band region. It causes an increase in the flow stress with a corresponding decrease in ductility.

2.3.3. Anisotropic effects. Analysis of experimental results concerning investigations of adiabatic shear band localization failure under dynamic loading suggests that there are three main reasons for the anisotropic effects:

1. The strain-induced anisotropy is caused by the residual type stresses which result from the heterogeneous nature of the plastic deformation in polycrystalline materials (cf. IKEGAMI [74] and PHILLIPS and LU [132]). Experimental evidence indicates that yield surfaces exhibit anisotropic hardening. Subsequent yield surfaces are both translated and deformed in the stress space. In phenomenological description this kind of anisotropy is modelled by the shift of the yield surface in the stress space. This shift of the yield surface might be described by the residual stress tensor α .
2. The anisotropy caused by the formation of shear bands. This effect can be described by the determination of the direction of the shear band formed.
3. The anisotropy induced by the micro-damage process along the shear band region. Experimental observations (cf. YOKOBORI JR., YOKOBORI, SATO and SYOJI [167], GREBE, PAK and MEYERS [58] and HARTLEY, DUFFY and HAWLEY [67]) have shown that in the micro-damage process, the generated anisotropy is a consequence of rather random phenomena connected with some directional property of the formation of microcracks. This anisotropic effect is very much affected by the crystallographic structure of a material as well as by small fluctuations of main directions of the applied stress at particular point of a body during the dynamic process.

To describe this kind of anisotropy one has to introduce an additional set of the internal state variables, cf. PERZYNA [119].

2.3.4. Analysis of cooperative phenomena. An analysis of experimental results has clearly shown that the shear band localization failure in dynamic loading processes is affected by complex cooperative phenomena. From this analysis it is also evident that such cooperative phenomena as the thermomechanical flow process, the instability of the flow process along localized adiabatic shear bands, the micro-damage process which consists of the nucleation, growth and coalescence of microcracks and the final mechanism of failure are the most important for proper description of the fracture phenomenon under dynamic loading.

All these cooperative phenomena might be influenced by different additional effects such as the strain rate sensitivity, the induced anisotropy, the thermomechanical couplings and others.

2.3.5. Self-organization and physical interpretation of instability hierarchies. We are interested in the fracture phenomenon which is preceded by shear band localization. In this case the instability of the plastic flow process plays a fundamental role as a precursor of fracture.

Let us consider a thermodynamic plastic flow process of a system. Synergetics suggests that a system is self-organized if it acquires a spatial, temporal or functional structure without specific interference from the outside, cf. HAKEN [62, 63, 64]. As a result of instability of plastic flow process we observe the macroscopic shear band pattern. A system has been self-organized in a new system – the shear band pattern system. The situation is very similar to that considered for single crystals, cf. PERZYNA [123, 125].

The instability phenomenon of plastic flow process can be considered at different levels. At the mesoscopic level we consider single crystals and their deformation. We describe the crystal lattice, consider movement of dislocations through the rows of barriers and take into account interactions of dislocations. At the macroscopic level, by consideration of polycrystalline solids we are interested in description of the instability phenomenon of plastic flow processes. In particular we study the localization of plastic deformation along shear bands. So, we can expect the evolving macroscopic shear band pattern.

It seems that the study of instability hierarchies plays a very important role in the explanation of the interrelation between macroscopic deformation modes and dislocation structures evolved in single crystals.

2.3.6. Intrinsic microstructure of the shear band region. Adiabatic shear band is a term used to describe the localization of plastic flow that occurs in many metals when they are deformed at high strain rates to large plastic deformations. It usually manifests itself as zones of intense shear deformation

and microstructural modification of the original material up to hundreds of micrometres wide, located between regions of relatively homogeneous deformation, cf. TIMOTHY [157] and MEYERS [97].

It can be proposed that shear bands in different metals could be broadly classified as either "transformed" or "deformed" on the basis of their appearance in metallographic section. A permanent change in structure is associated with the former, whereas the latter are manifested merely as zones of intense shear deformation of the original microstructure. The relative temperature rise within developing "transformed" shear zones is therefore assumed to be larger by definition.

As it has been suggested by TIMOTHY [157], shear bands in steels can be classified specifically on this basis, since the distinctive structure of "transformed" shear bands has been shown to be generally martensitic in nature, and they follow on from "deformed" shear bands when the adiabatic shear deformation becomes sufficiently localized.

Basing on experimental investigations performed for steels, ROGERS and SHASTRY [137] have pointed out that under some conditions during dynamic processes, a deformed shear band of some form first develops, followed by the formation of a short transformed band. Figure 17 shows a typical transformed shear band preceded by a precursor deformed band in AISI 1040 steel, generated by the impact process.

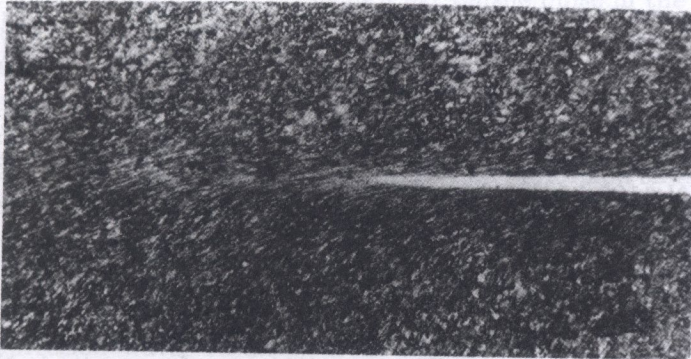


FIG. 17. Transformed shear band preceded by a deformed band in AISI 1040 steel (After ROGERS and SHASTRY [137]).

Examination of the microstructure has given evidence of a transverse structural gradient within the white-etching band. This is shown for a comparable band in AISI 4340 steel in Fig. 18. Although the band is still white over the entire transformed zone, the central zone is essentially featureless while the two outer regions appear granular in nature and have lower hardness.

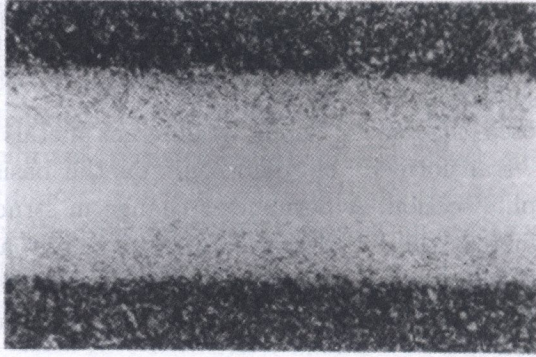


FIG. 18. Transformed shear band in AISI 4340 steel, quenched and tempered at 400°C
(After ROGERS and SHASTRY [137]).

Very recently WITTMAN, MEYERS and PAK [165] have taken experimental investigations to identify the microstructure of a white-etching shear band in a hollow AISI 4340 steel cylinder subjected to dynamic expansion by using high-voltage transmission electron microscopy. They have determined the microstructure of an adiabatic shear band formed at a minimum strain rate of $0.8 \times 10^6 \text{ s}^{-1}$ and with an accumulated shear strain of 3.92.

It has been found that the microstructure inside the shear band is martensitic and contains carbides which exist only after a significant amount of tempering. This structure is similar to that of the surrounding matrix and has been highly deformed. There was no evidence that the material had transformed to austenite at any time during the deformation process.

Microhardness traverses were made perpendicular to the length and along the length of the band, cf. ROGERS and SHASTRY [137]. The average hardness value of KHN 1195 in the shear band is similar to that expected in quenched AISI 4340 microstructure.

The sample was also tested after being immersed in liquid nitrogen for 1 hour. This would transform any possible austenite to martensite. The hardness measurement of the band remained unchanged, as did the observed microstructure in the optical microscope. Thus, no evidence of austenite in the band was produced by this test.

To aid in the explanation of the microstructure of shear band observed, WITTMAN, MEYERS and PAK [165] have modelled the thermal history of the band region by using the finite difference method.

On the basis of the thermal history analysis and the TEM observations, WITTMAN, MEYERS and PAK [165] have concluded that the observed white etching of the band region is an artifact of the etching. The white etching is not a particular indication of a phase transformation.

WITTMAN, MEYERS and PAK [165] have also observed that the band often contained voids of smaller microcracks. These spherical voids are thought to have been produced from tensile stresses acting within the band. The band, being at very high temperature and therefore ductile, deforms readily in tension by void nucleation and growth. Material within the band has, by virtue of the higher temperature, a lower flow stress than the matrix. It has been pointed out that near the tip of the shear bands, these voids and microcracks were less prominent.

The reason that the results obtained by WITTMAN, MEYERS and PAK [165] have a great importance for the constitutive modelling of the shear band region is twofold.

1. It has been clearly shown that the response of the material within the shear band region is different from that in the surrounding zones.
2. It has been proved that the phase transformation in AISI 4340 steel does not accompany the adiabatic shear band formation.

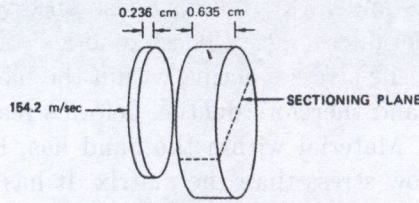
2.4. Ductile fracture

2.4.1. Experimental results and physical foundations. The most popular dynamical experiment¹⁾ in the investigation of the fracture phenomenon in metals is a plate-impact configuration system. This experimental system consists of two plates, a projectile plane plate impacts against a target plane. This is a good example of a dynamic deformation process. If the impact velocity is sufficiently high, the propagation of a plastic wave through the target is generated. The reflection and interaction of waves result in a net tensile pulse in the target plate. If this stress pulse has sufficient amplitude and sufficient time duration, it will cause separation of the material and the spalling process.

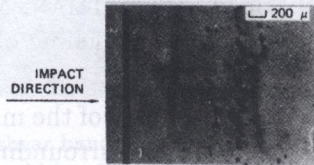
The reason for choosing this particular kind of dynamical experiment is that postshot photomicrographic observations of the residual porosity are available, and the stress amplitude and pulse duration can be performed sufficiently great to produce substantial porosity and the spall of the target plate.

The experimental data presented by SEAMAN, CURRAN and SHOCKEY [141] illustrate damage phenomena and provide a common basis for considering the damage criteria. They have used a plate-impact configuration system. Following the compression waves resulting from the impact, rarefaction waves have intersected near the middle of the target plate to cause damage in the form of nearly spherical voids. The heaviest damage is localized in a narrow zone, which is called the spall plane. Both the number and the size of voids decrease with distance from this zone. This type of damage is termed ductile fracture because of high ductility (ability to flow) required of the plate material, Fig. 19.

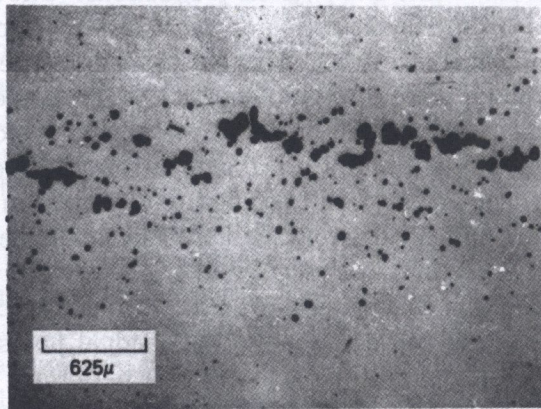
¹⁾For a thorough discussion of the experimental and theoretical works in the field of dynamic fracture and spalling of metals please consult the review papers by MEYERS and AIMONE [98] and CURRAN, SEAMAN and SHOCKEY [18], cf. also MEYERS [97].



(a)



(b)



(c)

FIG. 19. A cross section of an aluminum target plate that has undergone a planar impact by another aluminum plate (After SEAMAN, CURRAN and SHOCKEY [141]).

The final damage of the target plate (aluminium 1145) for a constant shot geometry but for different impact velocities has been performed by BARBEE, SEAMAN, CREWDSON and CURRAN [9]. The results suggest dependence of the spalling process on the pulse amplitude, Fig. 20. On the other hand an example of brittle fracture in armco iron (cf. SEAMAN, CURRAN and SHOCKEY [141]) shows dependence of damage on the tensile pulse duration. In this experimental performance an Armco iron target was impacted by a flyer plate, which was

tapered on the back to provide a varying tensile wave duration across the plate. The damage, which appears as randomly oriented microcracks, varies in proportion to the tensile wave duration. A sample of full separation is shown in Fig. 21, an aluminium target impacted by a plate has been damaged to the extent that full separation occurred near the center of the target, cf. SEAMAN, CURRAN and SHOCKEY [141]. The authors suggested that this full separation appears as a macrocrack propagating through a heavily damaged material. The macrocrack occurs as a result of coalescence of microvoids which is also visible in Fig. 21.

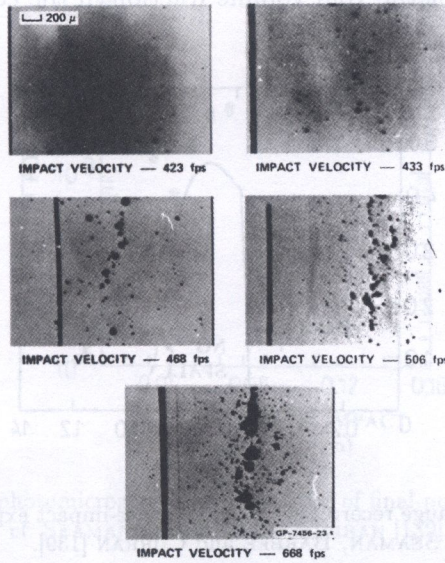


FIG. 20. The final damage of the aluminum 1145 target plate for a constant shot geometry but for different impact velocities (After BARBEE, SEAMAN, CREWDSON and CURRAN [9]).

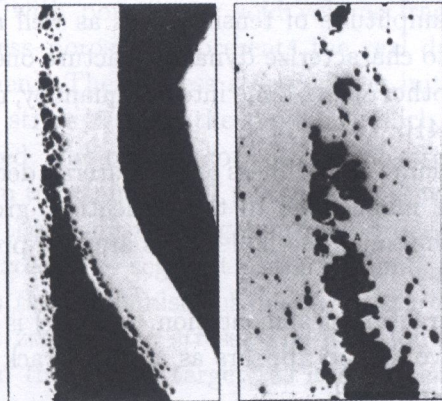


FIG. 21. A sample of full separation of an aluminum target. Impact test performed by SEAMAN, CURRAN and SHOCKEY [141].

Similar experimental test data have been obtained for copper by SEAMAN, BARBEE and CURRAN [139]²⁾. This is also a plate-impact experiment in which a 0.6 mm thick copper plate strikes a 1.6 mm copper target backed by a relatively thick plate of PMMA (polymethylmethacrylate) in which a manganin pressure gauge is embedded. The impact velocity of 0.016 cm/ μ s implies a 29-kbar peak tensile stress in the copper target, and pulse duration about 0.3 μ s which are sufficient to produce porosity up to 32% at the spall plane. The manganin pressure gauge record are shown in Fig. 22. The postshot photomicrographic observations of final porosity or the void volume fraction in the copper target is shown in Fig. 23.

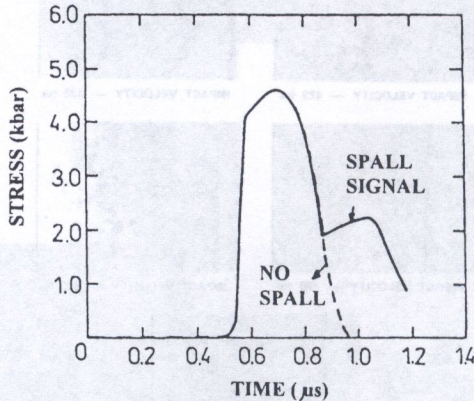


FIG. 22. The pressure gauge record for copper. A plate-impact experiment performed by SEAMAN, BARBEE and CURRAN [139].

From the experimental investigation we have the following conclusions:

1. Damage (spalling) in ductile metals (aluminium, copper, mild steel, etc.) depends on the amplitude of tensile stress as well as on the duration of stress pulse. So, to characterize dynamic fracture one has to use the stress impulse or some other stress-time integral quantity, cf. SEAMAN, CURRAN and SHOCKEY [141].
2. As the damage occurs, the stiffness of the material decreases. This softening of the material is mainly due to the nucleation, growth and coalescence of microvoids (sometimes thermal effects are also pronounced), cf. WRAY [166].
3. Full separation (fracture, fragmentation, spalling) is the result of the coalescence of microvoids and appears as a macrocrack propagating through heavily damaged material.

²⁾The experimental results of this unpublished report can be found in the paper by JOHNSON [77].

4. The propagation of the shock plastic wave induced by the impact process produces significant structural changes and affect the mechanical properties. In general, one observes an increase in the flow stress with a corresponding decrease of ductility.

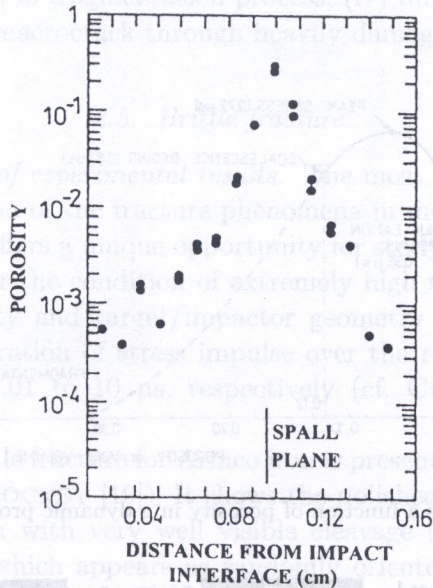


FIG. 23. The postshot photomicrographic observations of final porosity in a copper target, cf. SEAMAN, BARBEE and CURRAN [139].

2.4.2. Physical mechanisms of ductile dynamic fracture. To understand better the physical mechanism of ductile dynamic fracture let us consider the variation of tensile stress with porosity or void volume fraction, cf. Fig. 24. The trajectory "tensile stress-porosity" represents the real dynamic process in the copper target (specimen). The process starts at the initial porosity ξ_0 and in about $0.55 \mu\text{s}$ tensile stress reaches the point at which the nucleation of microvoids can be detected. The process goes on, tensile stress peaks up at $0.72 \mu\text{s}$ and slowly breaks down to attain in $0.87 \mu\text{s}$ the point at which the coalescence of microvoids begins. At this point the fragmentation processes by the coalescence of microcracks has started. The segment of the dynamic process marked by the dashed line represents the mechanism of ductile fracture (spalling or fragmentation) which ends at zero tensile stress. The duration of the entire dynamic deformation process in the copper target (as it has been suggested by experimental observations) is approximately $1.25 \mu\text{s}$.

Very recent experimental investigation of dynamic fracture in metals at high strain rate performed by CHENGWEI *et al.* [13] and GILATH [52] have confirmed

previous results. CHENGWEI *et al.* [13] used an electric-gun-driven plate impact (EGDPI) assembly and laser-driven shock wave (LDSW) assembly to investigate the spall strength of various metals, cf. Figs. 25 and 26. Gilath investigated the spall behaviour and dynamic fracture of various metals and composite materials.

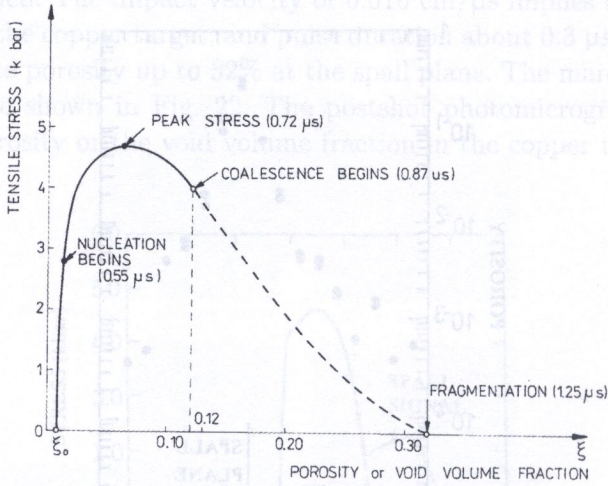


FIG. 24. Tensile stress as a function of porosity in a dynamic process for copper specimen.

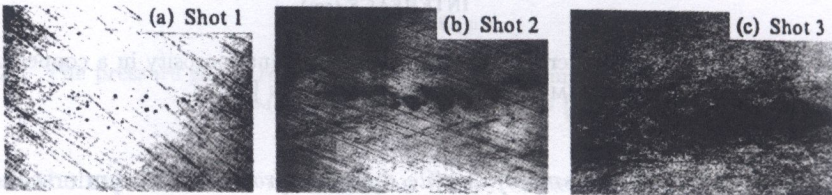


FIG. 25. Microvoids in aluminum specimens loaded by EGDPI (After CHENGWEI, SHIMING, YANPING and CANGLI [13]).

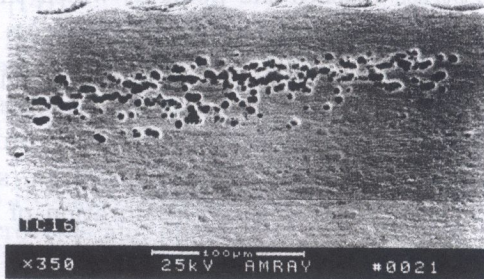


FIG. 26. Microvoids in Ti-6Al-4V specimens loaded by LDSW at $3.5 \times 10^{12} \text{ W/cm}^2$ (After CHENGWEI, SHIMING, YANPING and CANGLI [13]).

From this analysis of the dynamic deformation process one can see that the main cooperative phenomena which are most important for proper description of dynamic fracture (spalling) are as follows: (i) the plastic deformation wave phenomena; (ii) the nucleation and growth of microvoids; (iii) the coalescence of microvoids which leads to fragmentation process; (iv) full separation as a result of the propagation of macrocrack through heavily damaged material.

2.5. Brittle fracture

2.5.1. Discussion of experimental results. The most popular dynamical experimental investigation of the fracture phenomena in metals as a plate-impact configuration system offers a unique opportunity for studying microvoid and microcrack kinetics under the condition of extremely high tensile stress. By varying the impact velocity and target/impactor geometry it provides to change the amplitude and duration of stress impulse over the range of approximately 0.1 to 10 GPa and 0.01 to 10 μ s, respectively (cf. CURRAN, SEAMAN and SHOCKEY [19]).

An example of brittle fracture for Armco iron is presented in Fig. 27 (cf. CURRAN, SEAMAN and SHOCKEY [19]). It shows the polished cross-section through plate impact specimen with very well visible cleavage (penny-shaped) microcracks. The damage, which appears as randomly oriented planar microcracks, depends on the impact velocity as well as on the duration of the tensile wave. The second property is directly observed from the results presented in Fig. 28, (cf. CURRAN, SEAMAN and SHOCKEY [18]). Use of a tapered flyer results in longer tensile impulses at the thicker end. As it is shown in Fig. 28, these longer pulses lead to greater damage in the Armco iron target (the inset gives to approximate durations of the tensile pulses).



FIG. 27. Internal cleavage (penny shape) microcracks caused by shock loading in the polished cross section of an Armco iron specimen (After CURRAN, SEAMAN and SHOCKEY [19]).

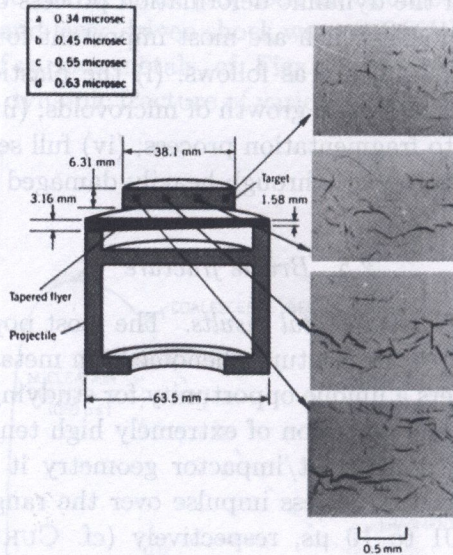


FIG. 28. Tapered flyer impact experimental results for the Armco iron target (After CURRAN, SEAMAN and SHOCKEY [18]).

The damage observed in this experiment is termed brittle, although the microcrack growth is much slower than the elastic crack velocities, indicating considerable plastic flow at micro-crack tips.

2.5.2. Physical mechanism of brittle dynamic fracture. When subjected to high rate loads from impact, Armco iron undergoes relatively brittle failure from nucleation, growth and coalescence of planar microcracks.

To understand better the physical mechanism of brittle dynamic fracture let us consider the variation of tensile stress with specific volume (or porosity), Fig. 29 (cf. CURRAN, SEAMAN and SHOCKEY [18]). The trajectory "tensile stress-specific volume" represents the real dynamic process in the Armco iron target (specimen) subjected to a constant strain rate of $1.3 \times 10^5 \text{ s}^{-1}$. From this trajectory we can follow the events in the order in which things naturally happen during the dynamic process. The process starts at the initial specific volume of about 0.1272 and when the tensile stress reaches the threshold value for nucleation, the nucleation, process begins. The process goes on, the tensile stress peaks up the value of specific volume 0.1310 and dramatically breaks down to attain at 0.1323 the point at which the coalescence of microcracks begins.

If no stress relaxation were allowed, the tensile stress-specific volume trajectory would follow that determined by the constitutive laws of the elastic-plastic

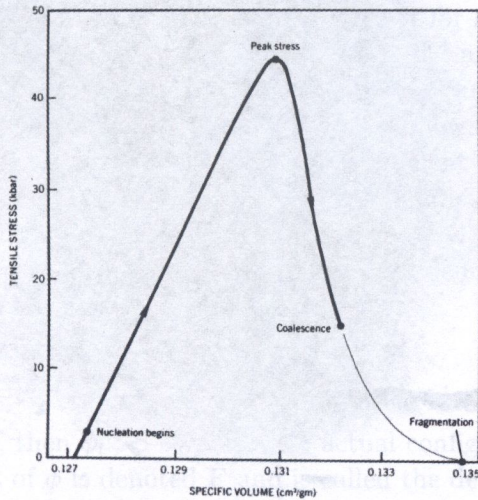


FIG. 29. Stress-specific volume trajectory of Armco iron loaded to fragmentation at constant strain rate (After CURRAN, SEAMAN, SHOCKEY [18]).

flow theory, and the stress would increase indefinitely. However, the microcrack nucleation and growth processes cause the stress to peak up and decay.

The segment of the dynamic process marked by the gray line represents the mechanism of brittle fracture (or fragmentation process) by microcrack coalescence which ends at zero tensile stress, at that point volume reaches the value 0.135. As it has been suggested by SEAMAN, CURRAN and MURRI [142], the physical process of coalescence occurs when the planar microcracks become so large that they begin to intersect other microcracks. They may intersect in the same plane, thus forming larger microcracks, and they may intersect at right angles, forming corners of fragments. Also, microcracks of the same orientation, but on different planes, may coalesce by developing crack extensions out of the plane to join the nearby microcracks. Thus a family of microcracks of one orientation can coalesce and form a rough, multifaceted spall plane.

SHOCKEY, SEAMAN and CURRAN [147] have recently investigated the coalescence process for the XAR30 armor steel under plate impact loading conditions. Their experimental results are presented in Fig. 30, which shows two parallel but nonplanar macrofractures in the process of coalescing. A profusion of tiny microfractures has formed in a path linking the tips of macrocracks, suggesting that coalescence is a nucleation and growth process on a smaller scale.

From this analysis of the dynamic deformation process in the Armco iron target and from the analysis of the previously discussed experimental results, one can see that the main cooperative phenomena which are most important for proper description of brittle dynamic fracture are as follows:



FIG. 30. Stress-specific volume trajectory of Armco iron loaded to fragmentation at constant strain rate (After CURRAN, SEAMAN, SHOCKEY [18]).

1. The inelastic deformation wave phenomena. The propagation of the shock inelastic wave induced by the impact process produces significant structural changes and affects the mechanical properties. In general, one observes an increase in the flow stress with a corresponding decrease of ductility.
2. The nucleation and growth processes of microcracks. Damage in brittle metals as Armco iron depends on the amplitude of tensile stress as well as on the duration of stress impulse. As the damage occurs, the stiffness of the material decreases. This softening of the material is mainly due to nucleation and growth of microcracks. The nucleation and growth processes may be accompanied by thermal effects.
3. The coalescence of microcracks which leads to fragmentation process. As the number and sizes of microcracks increase, fragments form until the entire material disintegrates into fragments.
4. Full separation as a result of the propagation of a macrocrack through heavily damaged material.

3. KINEMATICS OF FINITE DEFORMATION AND FUNDAMENTAL DEFINITIONS

3.1. Fundamental measures of total deformation

Our notation throughout is as follows: \mathcal{B} and \mathcal{S} are manifolds, points in \mathcal{B} are denoted by \mathbf{X} and those in \mathcal{S} by \mathbf{x} . The tangent spaces are written $T_{\mathbf{X}}\mathcal{B}$ and

$T_{\mathbf{x}}\mathcal{S}$. Coordinate systems are denoted $\{X^A\}$ and $\{x^a\}$ for \mathcal{B} and \mathcal{S} , respectively, with corresponding bases \mathbf{E}_A and \mathbf{e}_a and dual bases \mathbf{E}^A and \mathbf{e}^a .

Let us take the Riemannian spaces on manifolds \mathcal{B} and \mathcal{S} , i.e. $\{\mathcal{B}, \mathbf{G}\}$ and $\{\mathcal{S}, \mathbf{g}\}$, the metric tensors \mathbf{G} and \mathbf{g} are defined as follows $\mathbf{G} : T\mathcal{B} \rightarrow T^*\mathcal{B}$ and $\mathbf{g} : T\mathcal{S} \rightarrow T^*\mathcal{S}$, where $T\mathcal{B}$ and $T\mathcal{S}$ denote the tangent bundles of \mathcal{B} and \mathcal{S} , respectively, and $T^*\mathcal{B}$ and $T^*\mathcal{S}$ their dual tangent bundles.

Let the metric tensor G_{AB} be defined by $G_{AB}(\mathbf{X}) = (\mathbf{E}_A, \mathbf{E}_B)_{\mathbf{X}}$, and similarly define g_{ab} by $g_{ab}(\mathbf{x}) = (\mathbf{e}_a, \mathbf{e}_b)_{\mathbf{x}}$, where $(,)_{\mathbf{X}}$ and $(,)_{\mathbf{x}}$ denote the standard inner products in \mathcal{B} and \mathcal{S} , respectively.

Let

$$(3.1) \quad \mathbf{x} = \phi(\mathbf{X}, t)$$

be a regular motion, then $\phi_t : \mathcal{B} \rightarrow \mathcal{S}$ is a C^1 actual configuration (at time t) of \mathcal{B} in \mathcal{S} . The tangent of ϕ is denoted \mathbf{F} and is called the deformation gradient of ϕ ; thus $\mathbf{F} = T\phi$. For $\mathbf{X} \in \mathcal{B}$, we let $\mathbf{F}(\mathbf{X})$ denote the restriction of \mathbf{F} to $T_{\mathbf{X}}\mathcal{B}$.

Thus

$$(3.2) \quad \mathbf{F}(\mathbf{X}, t) : T_{\mathbf{X}}\mathcal{B} \rightarrow T_{\mathbf{x}=\phi(\mathbf{X}, t)}\mathcal{S}$$

is a linear transformation for each $\mathbf{X} \in \mathcal{B}$ and $t \in I \subset \mathbb{R}$. For each $\mathbf{X} \in \mathcal{B}$ there exists an orthogonal transformation $\mathbf{R}(\mathbf{X}) : T_{\mathbf{X}}\mathcal{B} \rightarrow T_{\mathbf{x}}\mathcal{S}$ such that $\mathbf{F} = \mathbf{R} \cdot \mathbf{U} = \mathbf{V} \cdot \mathbf{R}$. Notice that \mathbf{U} and \mathbf{V} operate within each fixed tangent space. We call \mathbf{U} and \mathbf{V} the right and left stretch tensor, respectively. For each $\mathbf{X} \in \mathcal{B}$, $\mathbf{U}(\mathbf{X}) : T_{\mathbf{X}}\mathcal{B} \rightarrow T_{\mathbf{X}}\mathcal{B}$ and for each $\mathbf{x} \in \mathcal{S}$, $\mathbf{V}(\mathbf{x}) : T_{\mathbf{x}}\mathcal{S} \rightarrow T_{\mathbf{x}}\mathcal{S}$.

The material (or Lagrangian) strain tensor $\mathbf{E} : T_{\mathbf{X}}\mathcal{B} \rightarrow T_{\mathbf{X}}\mathcal{B}$ is defined by

$$(3.3) \quad 2\mathbf{E} = \mathbf{C} - \mathbf{I}, \quad (\mathbf{I} \text{ denotes the identity on } T_{\mathbf{X}}\mathcal{B}),$$

where

$$(3.4) \quad \mathbf{C} = \mathbf{F}^T \cdot \mathbf{F} = \mathbf{U}^2 = \mathbf{B}^{-1}.$$

The spatial (or Eulerian) strain tensor $\mathbf{e} : T_{\mathbf{x}}\mathcal{S} \rightarrow T_{\mathbf{x}}\mathcal{S}$ is defined by

$$(3.5) \quad 2\mathbf{e} = \mathbf{i} - \mathbf{c}, \quad (\mathbf{i} \text{ denotes the identity on } T_{\mathbf{x}}\mathcal{S}),$$

where

$$(3.6) \quad \mathbf{c} = \mathbf{b}^{-1} \quad \text{and} \quad \mathbf{b} = \mathbf{F} \cdot \mathbf{F}^T = \mathbf{V}^2.$$

The various strain tensors can be redefined in terms of pull-back and push-forward operations. For the material strain tensor \mathbf{E} and the spatial strain tensor \mathbf{e} we have

$$(3.7) \quad \mathbf{E}^b = \phi^*(\mathbf{e}^b), \quad E_{AB}(\mathbf{X}) = e_{ab}(\mathbf{x})F_A^a(\mathbf{X})F_B^b(\mathbf{X}),$$

$$\mathbf{e}^b = \phi_*(\mathbf{E}^b), \quad e_{ab}(\mathbf{x}) = E_{AB}(\mathbf{X})(\mathbf{F}(\mathbf{X})^{-1})_a^A(\mathbf{F}(\mathbf{X})^{-1})_b^B,$$

where the symbol b denotes the index lowering operator.

3.2. Finite elasto-viscoplastic deformation

Motivated by the micromechanics of single crystal plasticity we postulate a local multiplicative decomposition of the form

$$(3.8) \quad \mathbf{F}(\mathbf{X}, t) = \mathbf{F}^e(\mathbf{X}, t) \cdot \mathbf{F}^p(\mathbf{X}, t),$$

where \mathbf{F}^{e-1} is interpreted as the local deformation that releases the stresses from each neighborhood $\mathcal{N}(\mathbf{x}) \subset \phi(B)$ in the current configuration of the body, cf. Fig. 31.

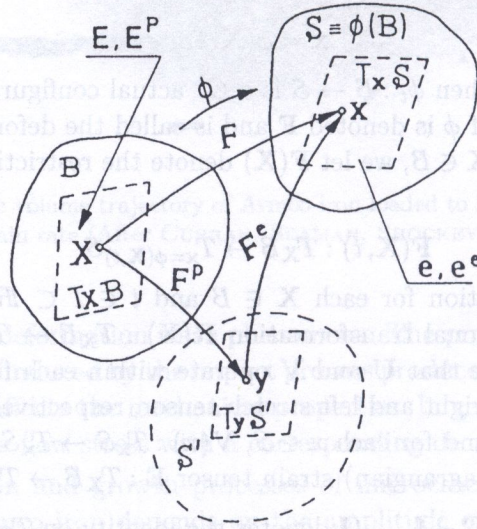


FIG. 31. Schematic representation of the multiplicative decomposition of the deformation gradient.

Let us consider a particle X , which at time $t = 0$ occupied the place \mathbf{X} in the reference (material) configuration \mathcal{B} , its current place at time t in the actual (spatial) configuration \mathcal{S} is $\mathbf{x} = \phi(\mathbf{X}, t)$ and its position in the unloaded actual configuration \mathcal{S}' is denoted by \mathbf{y} . Thus we have

$$(3.9) \quad \mathbf{F}^e : T_{\mathbf{y}}\mathcal{S}' \rightarrow T_{\mathbf{x}}\mathcal{S}, \quad \mathbf{F}^p : T_{\mathbf{X}}\mathcal{B} \rightarrow T_{\mathbf{y}}\mathcal{S}',$$

where $T_{\mathbf{y}}\mathcal{S}'$ denotes the tangent space in the unloaded actual configuration \mathcal{S}' . It is noteworthy that \mathbf{F}^e and \mathbf{F}^p defined by (3.9) are linear transformations.

We shall treat the tangent space $T_{\mathbf{y}}\mathcal{S}'$ as an auxiliary tool which helps to define the plastic strain tensors³⁾.

³⁾For precise definition of the finite elasto-plastic deformation see PERZYNA [122] and DUSZEK-PERZYNA and PERZYNA [43]. Different approach to define the finite elasto-plastic deformation has been presented by NEMAT-NASSER [101].

The plastic strain tensor $\mathbf{E}^p : T_{\mathbf{X}}\mathcal{B} \rightarrow T_{\mathbf{X}}\mathcal{B}$ is defined by

$$(3.10) \quad \mathbf{E}^p = \frac{1}{2}(\mathbf{C}^p - \mathbf{I}),$$

where

$$(3.11) \quad \mathbf{C}^p = \mathbf{F}^{pT} \cdot \mathbf{F}^p = \mathbf{U}^{p2} = \mathbf{B}^{p-1} \quad \text{and} \quad \mathbf{E}^e \stackrel{\text{def}}{=} \mathbf{E} - \mathbf{E}^p.$$

Similarly the elastic strain tensor $\mathbf{e}^e : T_x\mathcal{S} \rightarrow T_x\mathcal{S}$ is defined by

$$(3.12) \quad \mathbf{e}^e = \frac{1}{2}(\mathbf{i} - \mathbf{c}^e),$$

where

$$(3.13) \quad \mathbf{c}^e = \mathbf{b}^{e-1}, \quad \mathbf{b}^e = \mathbf{F}^e \cdot \mathbf{F}^{eT} = \mathbf{V}^{e2} \quad \text{and} \quad \mathbf{e}^p \stackrel{\text{def}}{=} \mathbf{e} - \mathbf{e}^e.$$

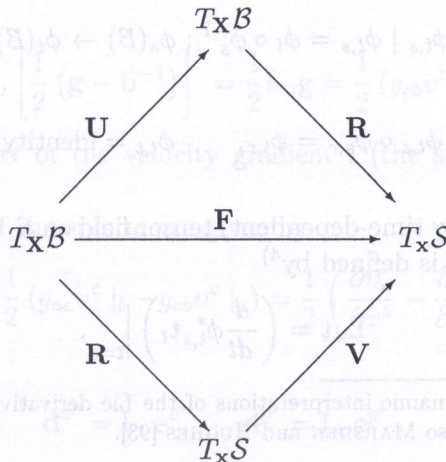
It is noteworthy to compare the relation

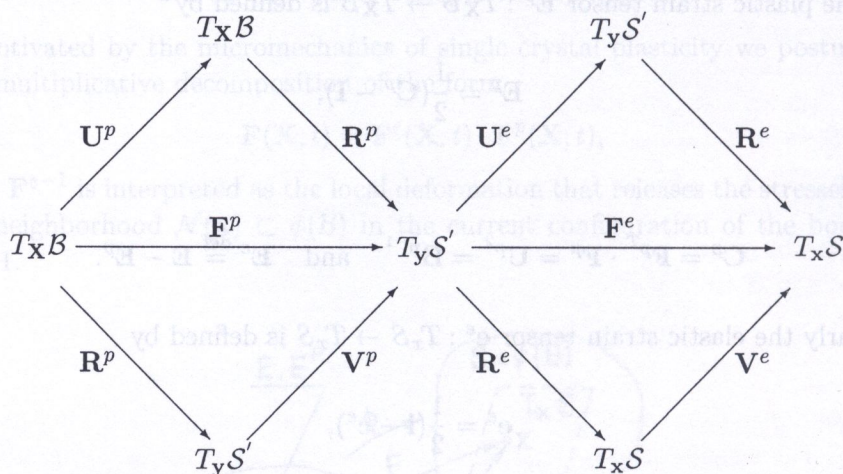
$$(3.14) \quad \mathbf{F} = \mathbf{R} \cdot \mathbf{U} = \mathbf{V} \cdot \mathbf{R}$$

with

$$(3.15) \quad \mathbf{F} = \mathbf{F}^e \cdot \mathbf{F}^p = \mathbf{R}^e \cdot \mathbf{U}^e \cdot \mathbf{R}^p \cdot \mathbf{U}^p = \mathbf{V}^e \cdot \mathbf{R}^e \cdot \mathbf{V}^p \cdot \mathbf{R}^p.$$

The following commutative diagrams summarize the situation.





From the second diagram it is clear that the tangent space T_yS' is playing an auxiliary role indeed.

The plastic tensors \mathbf{E}^p and \mathbf{e}^p operate within each fixed tangent space; that is $\mathbf{E}^p : T_{\mathbf{X}}\mathcal{B} \rightarrow T_{\mathbf{X}}\mathcal{B}$ and $\mathbf{e}^p : T_{\mathbf{x}}\mathcal{S} \rightarrow T_{\mathbf{x}}\mathcal{S}$.

We can show that the following relations are valid:

$$(3.16) \quad \phi_*(\mathbf{E}^{p^b}) = \mathbf{e}^{p^b}, \quad \phi^*(\mathbf{e}^{e^b}) = \mathbf{E}^{e^b}.$$

3.3. Rates of the deformation tensor

Let $\phi(\mathbf{X}, t)$ be a C^2 motion of \mathcal{B} . Then the spatial velocity is $\mathbf{v}_t = \mathbf{V}_t \circ \phi_t^{-1}$, where $\mathbf{V}_t = \frac{\partial \phi}{\partial t}$ is the material velocity, i.e. $\mathbf{v} : S \times I \rightarrow T\mathcal{S}$, $I \subset \mathbb{R}$.

The collection of maps $\phi_{t,s}$ such that for each s and \mathbf{x} , $t \rightarrow \phi_{t,s}(\mathbf{x})$ is an integral curve of \mathbf{v} , and $\phi_{s,s}(\mathbf{x}) = \mathbf{x}$, is called the flow or evolution operator of \mathbf{v} , i.e.

$$(3.17) \quad \{\phi_{t,s} \mid \phi_{t,s} = \phi_t \circ \phi_s^{-1} : \phi_s(\mathcal{B}) \rightarrow \phi_t(\mathcal{B})\}$$

and

$$(3.18) \quad \phi_{t,s} \circ \phi_{s,r} = \phi_{t,r}, \quad \phi_{t,t} = \text{identity}$$

for all $r, s, t \in I \subset \mathbb{R}$.

If \mathbf{t} is a C^1 (possibly time-dependent) tensor field on \mathcal{S} , then the Lie derivative of \mathbf{t} with respect to \mathbf{v} is defined by⁴⁾

$$(3.19) \quad L_{\mathbf{v}}\mathbf{t} = \left(\frac{d}{dt} \phi_{t,s}^* \mathbf{t}_t \right) \Big|_{t=s}.$$

⁴⁾The algebraic and dynamic interpretations of the Lie derivative have been presented by ABRAHAM *et al.* [2], cf. also MARSDEN and HUGHES [93].

If we hold t fixed in \mathbf{t}_t , we obtain the autonomous Lie derivative

$$(3.20) \quad \mathcal{L}_{\mathbf{v}}\mathbf{t} = \left(\frac{d}{dt} \phi_{t,s}^* \mathbf{t}_s \right) \Big|_{t=s}.$$

Thus

$$(3.21) \quad \mathbf{L}_{\mathbf{v}}\mathbf{t} = \frac{\partial \mathbf{t}}{\partial t} + \mathcal{L}_{\mathbf{v}}\mathbf{t}.$$

If $\mathbf{t} \in \mathbf{T}^r_s(\mathcal{S})$ (elements of $\mathbf{T}^r_s(\mathcal{S})$ are called tensors on \mathcal{S} , contravariant of order r and covariant of order s) then $\mathbf{L}_{\mathbf{v}}\mathbf{t} \in \mathbf{T}^r_s(\mathcal{S})$.

The spatial velocity gradient \mathbf{l} is defined by

$$(3.22) \quad \mathbf{l} = D\mathbf{v} : T_x\mathcal{S} \rightarrow T_x\mathcal{S}, \quad \text{i.e.} \quad l_b^a = v^a |_{|b} = \frac{\partial v^a}{\partial x^b} + \gamma_{bc}^a v^c,$$

where γ_{bc}^a denotes the Christoffel symbol for \mathbf{g} .

The spatial velocity gradient \mathbf{l} can be expressed as follows

$$(3.23) \quad \mathbf{l} = D\mathbf{v} = \dot{\mathbf{F}} \cdot \mathbf{F}^{-1} = \dot{\mathbf{F}}^e \cdot \mathbf{F}^{e^{-1}} + \mathbf{F}^e \cdot (\dot{\mathbf{F}}^p \cdot \mathbf{F}^{p^{-1}}) \cdot \mathbf{F}^{e^{-1}} \\ = \mathbf{l}^e + \mathbf{l}^p = \mathbf{d} + \boldsymbol{\omega} = \mathbf{d}^e + \boldsymbol{\omega}^e + \mathbf{d}^p + \boldsymbol{\omega}^p,$$

where \mathbf{d} denotes the spatial rate of deformation tensor and $\boldsymbol{\omega}$ is called the spin.

Let us define the material (or Lagrangian) rate of deformation tensor \mathbf{D} as follows

$$(3.24) \quad \mathbf{D}(\mathbf{X}, t) = \frac{\partial}{\partial t} \mathbf{E}(\mathbf{X}, t).$$

We have a very important relation

$$(3.25) \quad \mathbf{d}^b = \mathbf{L}_{\mathbf{v}}\mathbf{e}^b = \phi_* \frac{\partial}{\partial t} (\phi^* \mathbf{e}^b) = \phi_* \left(\frac{\partial}{\partial t} \mathbf{E}^b \right) = \phi_* (\mathbf{D}^b).$$

On the other hand,

$$(3.26) \quad \mathbf{d}^b = \mathbf{L}_{\mathbf{v}}\mathbf{e}^b = \mathbf{L}_{\mathbf{v}} \left[\frac{1}{2} (\mathbf{g} - \mathbf{b}^{-1}) \right]^b = \frac{1}{2} \mathbf{L}_{\mathbf{v}}\mathbf{g} = \frac{1}{2} (g_{cb} v^c |_{|a} + g_{ac} v^c |_{|b}) \mathbf{e}^a \otimes \mathbf{e}^b,$$

i.e. the symmetric part of the velocity gradient \mathbf{l} (the symbol \otimes denotes the tensor product).

The components of the spin $\boldsymbol{\omega}$ are given by

$$(3.27) \quad \omega_{ab} = \frac{1}{2} (g_{ac} v^c |_{|b} - g_{cb} v^c |_{|a}) = \frac{1}{2} \left(\frac{\partial v_a}{\partial x^b} - \frac{\partial v_b}{\partial x^a} \right),$$

and

$$(3.28) \quad \mathbf{d}^{e^b} = \mathbf{L}_{\mathbf{v}}\mathbf{e}^{e^b}, \quad \mathbf{d}^{p^b} = \mathbf{L}_{\mathbf{v}}\mathbf{e}^{p^b}.$$

3.4. Rates of the stress tensors

The first Piola–Kirchhoff stress tensor P^{aA} is the two–point tensor obtained by performing a Piola transformation on the second index of the Cauchy stress tensor σ , i.e.

$$(3.29) \quad P^{aA} = J(\mathbf{F}^{-1})^A_b \sigma^{ab},$$

where J denotes the Jacobian of the deformation.

The second Piola–Kirchhoff stress tensor \mathbf{S} is defined as follows

$$(3.30) \quad S^{AB} = (\mathbf{F}^{-1})^A_a P^{aB} = J(\mathbf{F}^{-1})^A_a (\mathbf{F}^{-1})^B_b \sigma^{ab} = (\mathbf{F}^{-1})^A_a (\mathbf{F}^{-1})^B_b \tau^{ab},$$

i.e.

$$(3.31) \quad \mathbf{S} = \phi^*(\boldsymbol{\tau}),$$

where $\boldsymbol{\tau} = J\boldsymbol{\sigma}$ is called the Kirchhoff stress tensor.

The rate of the Kirchhoff stress tensor $\boldsymbol{\tau}$ is given by

$$(3.32) \quad L_{\mathbf{v}}\boldsymbol{\tau} = \phi_* \frac{\partial}{\partial t} (\phi^* \boldsymbol{\tau}) = \phi_* \left(\frac{\partial}{\partial t} \mathbf{S} \right) = \mathbf{F} \cdot \left(\frac{\partial}{\partial t} \mathbf{S} \right) \cdot \mathbf{F}^T \circ \phi_t^{-1}.$$

Let us define

$$(3.33) \quad \begin{aligned} \boldsymbol{\tau}_1 &= \tau^{ab} \mathbf{e}_a \otimes \mathbf{e}_b \in \mathbf{T}^2_0(\mathcal{S}), \\ \boldsymbol{\tau}_2 &= \tau_a^b \mathbf{e}^a \otimes \mathbf{e}_b \in \mathbf{T}^1_1(\mathcal{S}), \\ \boldsymbol{\tau}_3 &= \tau^a_b \mathbf{e}_a \otimes \mathbf{e}^b \in \mathbf{T}^1_1(\mathcal{S}). \end{aligned}$$

Then

$$(3.34) \quad (L_{\mathbf{v}}\boldsymbol{\tau}_1)^{ab} = \frac{\partial \tau^{ab}}{\partial t} + \frac{\partial \tau^{ab}}{\partial x^c} v^c - \tau^{cb} \frac{\partial v^a}{\partial x^c} - \tau^{ac} \frac{\partial v^b}{\partial x^c}$$

is the rate associated with the name Oldroyd (cf. OLDROYD [102]). The Zaremba–Jaumann rate (cf. ZAREMBA [168, 169] and JAUMANN [76]) is defined as follows

$$(3.35) \quad \frac{1}{2} \left[(L_{\mathbf{v}}\boldsymbol{\tau}_3)^a_c g^{cb} + g^{ac} (L_{\mathbf{v}}\boldsymbol{\tau}_2)_c^b \right] = \frac{\partial \tau^{ab}}{\partial t} + \frac{\partial \tau^{ab}}{\partial x^c} v^c + \tau^{ad} \omega_d^b - \tau^{db} \omega_d^a.$$

3.5. Fundamental properties of the Lie derivatives

Let us take again $\mathbf{t} \in \mathbf{T}^r_s(\mathcal{S})$ a given time-dependent spatial tensor field on \mathcal{S} and let $\boldsymbol{\xi}$ be a diffeomorphism of \mathcal{S} to another manifold $\boldsymbol{\xi}(\phi(\mathcal{B}))$, cf. Fig. 32.

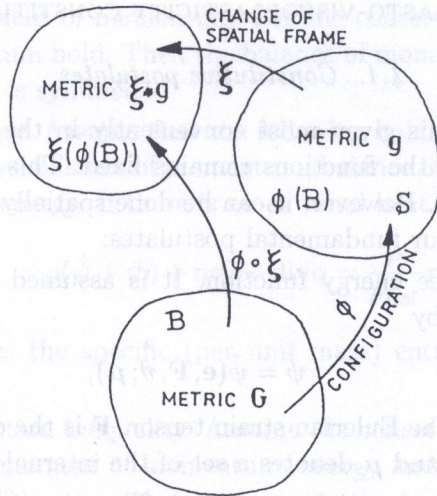


FIG. 32. Schematic representation of the change of spatial frame generated by superposed spatial diffeomorphism.

Any spatial tensor field $\mathbf{t} \in \mathbf{T}'_s(\mathcal{S})$ is said to transform objectively under the superposed diffeomorphism ξ if it transforms according to the rule

$$(3.36) \quad \mathbf{t}' = \xi_* \mathbf{t},$$

where ξ_* is the push-forward operation.

Let \mathbf{v}' be the velocity field of $\xi_t \circ \phi_t$. Then we have (cf. MARS DEN and HUGHES, [93])

$$(3.37) \quad L_{\mathbf{v}'} \mathbf{t}' = \xi_* (L_{\mathbf{v}} \mathbf{t}).$$

This means that objective tensors have objective Lie derivatives. It is noteworthy to recall here that the rates which are objective with respect to diffeomorphisms are called covariant.

The Oldroyd rate of the Kirchhoff stress tensor (3.34) is objective with respect to diffeomorphisms while the Zaremba–Jaumann rate (3.35) is objective with respect to isometries. The reason of it is caused by the fact that the operations of raising and lowering indices do not commute with Lie differentiation. This corollary has very important consequences for the formulation of the objective constitutive structures.

4. THERMO-ELASTO-VISCOPLASTICITY CONSTITUTIVE MODEL

4.1. Constitutive postulates

Constitutive theory is given most conveniently in the material picture because the domain \mathcal{B} of the functions remains fixed. This helps to develop the identification procedure. However, it can be done spatially as well.

We introduce the four fundamental postulates:

- (i) Existence of the free energy function. It is assumed that the free energy function is given by

$$(4.1) \quad \psi = \hat{\psi}(\mathbf{e}, \mathbf{F}, \vartheta; \boldsymbol{\mu}),$$

where \mathbf{e} denotes the Eulerian strain tensor, \mathbf{F} is the deformation gradient, ϑ is temperature and $\boldsymbol{\mu}$ denotes a set of the internal state variables.

- (ii) Axiom of objectivity (spatial covariance). The constitutive structure should be invariant with respect to any diffeomorphism $\boldsymbol{\xi} : \mathcal{S} \rightarrow \mathcal{S}$ (MARSDEN and HUGHES, [93]). Assuming that $\boldsymbol{\xi} : \mathcal{S} \rightarrow \mathcal{S}$ is a regular, orientation preserving map transforming \mathbf{x} into \mathbf{x}' and $T\boldsymbol{\xi}$ is an isometry from $T_{\mathbf{x}}\mathcal{S}$, to $T_{\mathbf{x}'}\mathcal{S}$, we obtain the axiom of material frame indifference, cf. Fig. 32.

Before the formulation of the third axiom let us discuss thermodynamic restrictions. Consider the balance principles as follows:

1. Conservation of mass. Let assume that $\phi(\mathbf{X}, t)$ is a C^1 regular motion. A mass density function $\rho(\mathbf{x}, t)$ is said to obey the law of conservation of mass if

$$(4.2) \quad \dot{\rho} + \rho \operatorname{div} \mathbf{v} = 0 \quad \text{or} \quad \rho(\mathbf{x}, t) J(\mathbf{X}, t) = \rho_{\text{Ref}}(\mathbf{X}).$$

For a damaged solid body the mass density $\rho(\mathbf{x}, t)$ is given by

$$(4.3) \quad \rho = \rho_M(1 - \xi) + \rho_V \xi,$$

where ρ_M is the mass density of the matrix material and ρ_V the mass density of voids. Assuming $\rho_V \ll \rho_M$ we have

$$(4.4) \quad \rho = \rho_M(1 - \xi).$$

Thus a function $\rho(\mathbf{x}, t)$ is said to obey the conservation of mass if

$$(4.5) \quad \rho_M(1 - \xi) J(\mathbf{X}, t) = \rho_M^0(\mathbf{X}) (1 - \xi_0) = \rho_{\text{Ref}}.$$

2. Balance of momentum. Assume that conservation of mass and balance of momentum hold. If there is no external body force field, then

$$(4.6) \quad \rho \dot{\mathbf{v}} = \operatorname{div} \left(\frac{1}{J} \boldsymbol{\tau} \right).$$

- 3. Balance of moment of momentum. Let the conservation of mass and balance of momentum hold. Then the balance of moment of momentum holds if and only if τ is symmetric.
- 4. Balance of energy. Assume that the following balance principles hold: conservation of mass, balance of momentum, balance of moment of momentum and balance of energy. If there is no external heat supply then

$$(4.7) \quad \rho(\dot{\psi} + \vartheta\dot{\eta} + \eta\dot{\vartheta}) + \text{div}\mathbf{q} = \frac{\rho}{\rho_{\text{Ref}}}\boldsymbol{\tau} : \mathbf{d},$$

where η denotes the specific (per unit mass) entropy and \mathbf{q} is the heat vector field.

- 5. Entropy production inequality. Assume the conservation of mass, balance of momentum, moment of momentum, energy and entropy production inequality hold. Then the reduced dissipation inequality is satisfied:

$$(4.8) \quad \frac{1}{\rho_{\text{Ref}}}\boldsymbol{\tau} : \mathbf{d} - (\eta\dot{\vartheta} + \dot{\psi}) - \frac{1}{\rho\vartheta}\mathbf{q} \cdot \text{grad}\vartheta \geq 0.$$

- (iii) The axiom of entropy production. For any regular process $\phi_t, \vartheta_t, \boldsymbol{\mu}_t$ of a body \mathcal{B} the constitutive functions are assumed to satisfy the reduced dissipation inequality (4.8). MARS DEN and HUGHES [93] proved that the reduced dissipation inequality (4.8) is equivalent to the entropy production inequality first introduced by COLEMAN and NOLL [16] in the form of the Clausius–Duhem inequality. In fact the Clausius–Duhem inequality gives a statement of the second law of thermodynamics within the framework of mechanics of continuous media.
- (iv) The evolution equation for the internal state variable vector $\boldsymbol{\mu}$ is assumed in the form as follows

$$(4.9) \quad L_{\nu}\boldsymbol{\mu} = \hat{\mathbf{m}}(\mathbf{e}, \mathbf{F}, \vartheta, \boldsymbol{\mu}),$$

where the evolution function $\hat{\mathbf{m}}$ has to be determined based on careful physical interpretation of a set of the internal state variables and analysis of the available experimental observations.

The determination of the evolution function $\hat{\mathbf{m}}$ (in practice a finite set of the evolution functions) appears to be the main problem of the modern constitutive modelling.

4.2. Fundamental assumptions

The main objective is to develop the rate-type constitutive structure for an elastic-viscoplastic material in which the effects of the plastic non-normality,

plastic spin, plastic strain-induced anisotropy (kinematic hardening), microdamaged mechanism and thermomechanical coupling are taken into consideration. To do this it is sufficient to assume a finite set of the internal state variables. Let us postulate

$$(4.10) \quad \boldsymbol{\mu} = (\boldsymbol{\zeta}, \xi, \boldsymbol{\alpha}),$$

where $\boldsymbol{\zeta}$ denotes the new internal state vector which describes the dissipation effects generated by viscoplastic flow phenomena, ξ is volume fraction porosity and takes account for microdamaged effects and $\boldsymbol{\alpha}$ denotes the residual stress (the back stress) and aims at the description of the kinematic hardening effects.

Let us introduce the plastic potential function $f = f(\tilde{J}_1, \tilde{J}_2, \vartheta, \boldsymbol{\mu})$, where \tilde{J}_1, \tilde{J}_2 denote the first two invariants of the stress tensor $\tilde{\boldsymbol{\tau}} = \boldsymbol{\tau} - \boldsymbol{\alpha}$.

Let us postulate the evolution equations as follows:

$$(4.11) \quad \mathbf{d}^p = \Lambda \mathbf{P}, \quad \boldsymbol{\omega}^p = \Lambda \boldsymbol{\Omega}, \quad L_v \boldsymbol{\zeta} = \Lambda \mathbf{Z}, \quad \dot{\xi} = \Xi, \quad L_v \boldsymbol{\alpha} = \mathbf{A},$$

where for elasto-viscoplastic model of a material we assume (cf. PERZYNA [103, 104, 105, 122, 123])

$$(4.12) \quad \Lambda = \frac{1}{T_m} \left\langle \Phi \left(\frac{f}{\kappa} - 1 \right) \right\rangle,$$

T_m denotes the relaxation time for mechanical disturbances, the isotropic work-hardening-softening function κ is

$$(4.13) \quad \kappa = \hat{\kappa}(\epsilon^p, \vartheta, \xi), \quad \epsilon^p = \int_0^t \left(\frac{2}{3} \mathbf{d}^p : \mathbf{d}^p \right)^{1/2} dt,$$

Φ is the empirical overstress function, the bracket $\langle \cdot \rangle$ defines the ramp function,

$$(4.14) \quad \mathbf{P} = \frac{\partial f}{\partial \boldsymbol{\tau}} \Big|_{\xi = \text{const}} \left(\left\| \frac{\partial f}{\partial \boldsymbol{\tau}} \right\| \right)^{-1},$$

$\boldsymbol{\Omega}, \mathbf{Z}, \Xi$ and \mathbf{A} denote the evolution functions which have to be determined.

It is noteworthy that the material function \mathbf{Z} is intrinsically determined by the constitutive assumptions postulated. To show this it is sufficient to perform a Legendre transformation what has been presented by DUSZEK and PERZYNA [37].

For our practical purposes it is sufficient to assume that the internal state vector $\boldsymbol{\zeta}$ is equal to the equivalent plastic deformation ϵ^p , i.e.

$$(4.15) \quad \boldsymbol{\mu} = (\epsilon^p, \xi, \boldsymbol{\alpha}).$$

Then the material function Z is directly determined from

$$(4.16) \quad \dot{\epsilon}^p = \Lambda Z = \left(\frac{2}{3} \mathbf{d}^p : \mathbf{d}^p \right)^{1/2} = \sqrt{\frac{2}{3}} \Lambda,$$

i.e.

$$(4.17) \quad Z = \sqrt{\frac{2}{3}}.$$

4.3. Constitutive assumption for the plastic spin

The constitutive laws for the plastic spin⁵⁾ based on the application of the tensor function formulation have been proposed by MANDEL [88, 89], KRATOCHVIL [79], DAFALIAS [21, 23, 24, 25] and LORET [84]. Different proposition by using generalized normality condition has been introduced by HALPHEN [66], MANDEL [90], DAFALIAS [22] and VAN DER GIESSEN [161, 162].

Let us postulate that Ω has the form (cf. DAFALIAS [21] and LORET [84])

$$(4.18) \quad \Omega = \eta^*(\alpha \cdot \mathbf{P} - \mathbf{P} \cdot \alpha),$$

where η^* denotes the scalar-valued function of the invariants of the tensors α and \mathbf{P} , and may depend on temperature ϑ and porosity ξ .

4.4. Intrinsic microdamage process

An analysis of the experimental observations for cycle fatigue damage mechanisms at high temperature of metals performed by SIDEY and COFFIN [149] suggests that the intrinsic microdamage process does very much depend on the strain rate effects as well as on the wave shape effects, cf. Sec. 2.

To take into consideration these observed time-dependent effects it is advantageous to use the proposition of the description of the intrinsic microdamage process presented by PERZYNA [116, 117] and DUSZEK-PERZYNA and PERZYNA [40].

Let us assume that the intrinsic microdamage process consists of the nucleation and growth mechanisms⁶⁾.

⁵⁾For the thorough discussion of the concept of the plastic spin and its constitutive description in phenomenological theories for macroscopic large plastic deformations please consult the critical review paper by VAN DER GIESSEN [163].

⁶⁾Recent experimental observation results (cf. SHOCKEY *et al.* [147]) have shown that coalescence mechanism can be treated as nucleation and growth process on a smaller scale. This conjecture simplifies very much the description of the intrinsic microdamage process by taking account only of the nucleation and growth mechanisms.

Physical considerations (cf. CURRAN *et al.* [20] and PERZYNA [116, 117]) have shown that the nucleation of microvoids in dynamic loading processes which are characterized by very short time duration is governed by the thermally-activated mechanism. Based on this heuristic suggestion and taking into account the influence of the stress triaxiality on the nucleation mechanism, we postulate for rate-dependent plastic flow

$$(4.19) \quad (\dot{\xi})_{\text{nucl}} = \frac{1}{T_m} h^*(\xi, \vartheta) \left[\exp \frac{m^*(\vartheta) | \tilde{I}_n - \tau_n(\xi, \vartheta, \epsilon^p) |}{k\vartheta} - 1 \right],$$

where k denotes the Boltzmann constant, $h^*(\xi, \vartheta)$ represents a void nucleation material function which is introduced to take account of the effect of microvoid interaction effect, $m^*(\vartheta)$ is a temperature-dependent coefficient, $\tau_n(\xi, \vartheta, \epsilon^p)$ is the porosity, temperature and equivalent plastic strain-dependent threshold stress for microvoid nucleation,

$$(4.20) \quad \tilde{I}_n = a_1 \tilde{J}_1 + a_2 \sqrt{\tilde{J}_2} + a_3 (\tilde{J}_3)^{1/3}$$

defines the stress intensity invariant for nucleation, a_i ($i = 1, 2, 3$) are the material constants, \tilde{J}_1 denotes the first invariant of the stress tensor $\tilde{\tau} = \tau - \alpha$, \tilde{J}_2 and \tilde{J}_3 are the second and third invariants of the stress deviator $\tilde{\tau}' = (\tau - \alpha)'$.

For the growth mechanism we postulate (cf. CARROLL and HOLT [11]), JOHNSON [77], PERZYNA [116, 117, 119], PERZYNA and DRABIK [127, 128])

$$(4.21) \quad (\dot{\xi})_{\text{grow}} = \frac{1}{T_m} \frac{g^*(\xi, \vartheta)}{\sqrt{\kappa_0}} \left[\tilde{I}_g - \tau_{\text{eq}}(\xi, \vartheta, \epsilon^p) \right],$$

where $T_m \sqrt{\kappa_0}$ denotes the dynamic viscosity of a material, $g^*(\xi, \vartheta)$ represents a void growth material function and takes account of void interaction, $\tau_{\text{eq}}(\xi, \vartheta, \epsilon^p)$ is the porosity, temperature and equivalent plastic strain-dependent void growth threshold stress,

$$(4.22) \quad \tilde{I}_g = b_1 \tilde{J}_1 + b_2 \sqrt{\tilde{J}_2} + b_3 (\tilde{J}_3)^{1/3},$$

defines the stress intensity invariant for growth and b_i ($i = 1, 2, 3$) are the material constants.

Finally the evolution equation for the porosity ξ has the form

$$(4.23) \quad \dot{\xi} = \frac{h^*(\xi, \vartheta)}{T_m} \left[\exp \frac{m^*(\vartheta) | \tilde{I}_n - \tau_n(\xi, \vartheta, \epsilon^p) |}{k\vartheta} - 1 \right] + \frac{g^*(\xi, \vartheta)}{T_m \sqrt{\kappa_0}} \left[\tilde{I}_g - \tau_{\text{eq}}(\xi, \vartheta, \epsilon^p) \right].$$

To have a consistent theory of elasto-viscoplasticity we can replace the exponential function in the nucleation term and the linear function in the growth term by the empirical overstress function Φ , then the evolution equation for the porosity ξ takes the form as follows:

$$(4.24) \quad \dot{\xi} = \frac{1}{T_m} h^*(\xi, \vartheta) \left\langle \Phi \left[\frac{\tilde{I}_n}{\tau_n(\xi, \vartheta, \epsilon^p)} - 1 \right] \right\rangle + \frac{1}{T_m} g^*(\xi, \vartheta) \left\langle \Phi \left[\frac{\tilde{I}_g}{\tau_{eq}(\xi, \vartheta, \epsilon^p)} - 1 \right] \right\rangle.$$

This determines the evolution function Ξ .

4.5. Kinematic hardening

For a constitutive model describing the behaviour of a material under cyclic loading processes, the crucial role plays the evolution equation for the back stress α , which is responsible for the description of the induced plastic strain anisotropy effects.

We shall follow some fundamental results obtained by DUSZEK and PERZYNA [36] (cf. also DUSZEK and PERZYNA [34, 35]). Let us postulate

$$(4.25) \quad L_v \alpha = A(\mathbf{d}^p, \tilde{\tau}, \vartheta, \xi).$$

Making use of the tensorial representation of the function A and taking into account that there is no change of α when $\tilde{\tau} = 0$ and $\mathbf{d}^p = 0$ the evolution law (4.25) can be written in the form (cf. TRUESDELL and NOLL [159])

$$(4.26) \quad L_v \alpha = \eta_1 \mathbf{d}^p + \eta_2 \tilde{\tau} + \eta_3 \mathbf{d}^{p^2} + \eta_4 \tilde{\tau}^2 + \eta_5 (\mathbf{d}^p \cdot \tilde{\tau} + \tilde{\tau} \cdot \mathbf{d}^p) + \eta_6 (\mathbf{d}^{p^2} \cdot \tilde{\tau} + \tilde{\tau} \cdot \mathbf{d}^{p^2}) + \eta_7 (\mathbf{d}^p \cdot \tilde{\tau}^2 + \tilde{\tau}^2 \cdot \mathbf{d}^p) + \eta_8 (\mathbf{d}^{p^2} \cdot \tilde{\tau}^2 + \tilde{\tau}^2 \cdot \mathbf{d}^{p^2}),$$

where η_1, \dots, η_8 are functions of the basic invariant of \mathbf{d}^p and $\tilde{\tau}$, the porosity parameter ξ and temperature ϑ .

A linear approximation of the general evolution law (4.26) leads to the result

$$(4.27) \quad L_v \alpha = \eta_1 \mathbf{d}^p + \eta_2 \tilde{\tau}.$$

This kinetic law represents the linear combination of the Prager and Ziegler kinematic hardening rules.

To determine the connection between the material functions η_1 and η_2 we take advantage of the geometrical relation (cf. DUSZEK and PERZYNA [36, 37])

$$(4.28) \quad (L_v \alpha - r \mathbf{d}^p) : \mathbf{Q} = 0,$$

where

$$(4.29) \quad \mathbf{Q} = \left[\frac{\partial f}{\partial \tau} + \left(\frac{\partial f}{\partial \xi} - \frac{\partial \kappa}{\partial \xi} \right) \frac{\partial \xi}{\partial \tau} \right] \left\| \frac{\partial f}{\partial \tau} + \left(\frac{\partial f}{\partial \xi} - \frac{\partial \kappa}{\partial \xi} \right) \frac{\partial \xi}{\partial \tau} \right\|^{-1},$$

and r denotes the new material function.

The relation (4.28) leads to the result

$$(4.30) \quad \eta_2 = \frac{1}{T_m} \left\langle \Phi \left(\frac{f}{\kappa} - 1 \right) \right\rangle [r(\xi, \vartheta) - \eta_1] \frac{\mathbf{P} : \mathbf{Q}}{\tilde{\tau} : \mathbf{Q}}.$$

Finally the kinematic hardening evolution law takes the form

$$(4.31) \quad L_v \alpha = \frac{1}{T_m} \left\langle \Phi \left(\frac{f}{\kappa} - 1 \right) \right\rangle \left[r_1(\xi, \vartheta) \mathbf{P} + r_2(\xi, \vartheta) \frac{\mathbf{P} : \mathbf{Q}}{\tilde{\tau} : \mathbf{Q}} \tilde{\tau} \right],$$

where

$$(4.32) \quad r_1(\xi, \vartheta) = \eta_1, \quad r_2(\xi, \vartheta) = r - \eta_1.$$

It is noteworthy to add that the developed procedure can be used as a general approach for obtaining various particular kinematic hardening laws. As an example let us assume that the evolution function A in (4.25) instead of \mathbf{d}^p and $\tilde{\tau}$ depends on \mathbf{d}^p and α only (cf. AGAH-TEHRANI *et al.* [3, 4]). Then instead of (4.31) we obtain

$$(4.33) \quad L_v \alpha = \frac{1}{T_m} \left\langle \Phi \left(\frac{f}{\kappa} - 1 \right) \right\rangle [\zeta_1(\xi, \vartheta) \mathbf{P} - \zeta_2(\xi, \vartheta) \alpha],$$

where

$$(4.34) \quad \zeta_1 = r_1, \quad \zeta_2 = -r_2(\xi, \vartheta) \frac{\mathbf{P} : \mathbf{Q}}{\alpha : \mathbf{Q}}.$$

When the infinitesimal deformations and rate-independent response of a material are assumed and the intrinsic microdamage effects are neglected, then the kinematic hardening law (4.33) reduces to that proposed by ARMSTRONG and FREDERICK [5].

The kinematic hardening law (4.33) leads to the nonlinear stress-strain relation with the characteristic saturation effect. The material function $\zeta_1(\xi, \vartheta)$ for $\xi = \xi_0$ and $\vartheta = \vartheta_0$ can be interpreted as an initial value of the kinematic hardening modulus and the material function $\zeta_2(\xi, \vartheta)$ determines the character of the nonlinearity of kinematic hardening. The particular forms of the functions ζ_1 and ζ_2 have to take into account the degradation nature of the influence of the intrinsic microdamage process on the evolution of anisotropic hardening.

4.6. Thermodynamic restrictions and rate type constitutive relations

Suppose the axiom of the entropy production holds. Then the constitutive assumption (4.1) and the evolution equations (4.11) lead to the results as follows:

$$(4.35) \quad \boldsymbol{\tau} = \rho_{\text{Ref}} \frac{\partial \hat{\psi}}{\partial \mathbf{e}}, \quad \eta = -\frac{\partial \hat{\psi}}{\partial \vartheta}, \quad -\frac{\partial \hat{\psi}}{\partial \boldsymbol{\mu}} \cdot \mathbf{L}_v \boldsymbol{\mu} - \frac{1}{\rho \vartheta} \mathbf{q} \cdot \text{grad} \vartheta \geq 0.$$

The rate of internal dissipation is determined by

$$(4.36) \quad \vartheta \dot{\eta} = -\frac{\partial \hat{\psi}}{\partial \boldsymbol{\mu}} \cdot \mathbf{L}_v \boldsymbol{\mu} = -\left[\frac{\partial \hat{\psi}}{\partial \epsilon^p} \sqrt{\frac{2}{3}} + \frac{\partial \hat{\psi}}{\partial \boldsymbol{\alpha}} : \left(r_1 \mathbf{P} + r_2 \frac{\mathbf{P} : \mathbf{Q}}{\bar{\boldsymbol{\tau}} : \mathbf{Q}} \bar{\boldsymbol{\tau}} \right) \right] \Lambda - \frac{\partial \hat{\psi}}{\partial \xi} \Xi.$$

Operating on the stress relation (4.35)₁ with the Lie derivative and keeping the internal state vector constant, we obtain (cf. DUSZEK-PERZYNA and PERZYNA [40])

$$(4.37) \quad \mathbf{L}_v \boldsymbol{\tau} = \mathcal{L}^e : \mathbf{d} - \mathcal{L}^{\text{th}} \dot{\vartheta} - [(\mathcal{L}^e + \mathbf{g} \boldsymbol{\tau} + \boldsymbol{\tau} \mathbf{g} + \mathcal{W}) : \mathbf{P}] \frac{1}{T_m} \left\langle \Phi \left(\frac{f}{\kappa} - 1 \right) \right\rangle,$$

where

$$(4.38) \quad \begin{aligned} \mathcal{L}^e &= \rho_{\text{Ref}} \frac{\partial^2 \hat{\psi}}{\partial \mathbf{e}^2}, \\ \mathcal{L}^{\text{th}} &= -\rho_{\text{Ref}} \frac{\partial^2 \hat{\psi}}{\partial \mathbf{e} \partial \vartheta}, \\ \mathcal{W} &= \eta^* [(\mathbf{g} \boldsymbol{\tau} - \boldsymbol{\tau} \mathbf{g}) : (\boldsymbol{\alpha} \mathbf{g} - \mathbf{g} \boldsymbol{\alpha})]. \end{aligned}$$

Substituting $\dot{\psi}$ into the energy balance equation and taking into account the results (4.35)₃ and (4.36) we obtain

$$(4.39) \quad \rho \vartheta \dot{\eta} = -\text{div} \mathbf{q} + \rho \vartheta \dot{\eta}.$$

Operating on the entropy relation (4.35)₂ with the Lie derivative and substituting the result into (4.39) we obtain

$$(4.40) \quad \rho c_p \dot{\vartheta} = -\text{div} \mathbf{q} + \vartheta \frac{\rho}{\rho_{\text{Ref}}} \frac{\partial \boldsymbol{\tau}}{\partial \vartheta} : \mathbf{d} + \rho \chi^* \boldsymbol{\tau} : \mathbf{d}^p + \rho \chi^{**} \dot{\xi},$$

where the specific heat

$$(4.41) \quad c_p = -\vartheta \frac{\partial^2 \hat{\psi}}{\partial \vartheta^2}$$

and the irreversibility coefficients χ^* and χ^{**} are determined by

$$(4.42) \quad \chi^* = - \left[\left(\frac{\partial \hat{\psi}}{\partial \epsilon^p} - \vartheta \frac{\partial^2 \hat{\psi}}{\partial \vartheta \partial \epsilon^p} \right) \sqrt{\frac{2}{3}} + \left(\frac{\partial \hat{\psi}}{\partial \alpha} - \vartheta \frac{\partial^2 \hat{\psi}}{\partial \vartheta \partial \alpha} \right) : \left(r_1 \mathbf{P} + r_2 \frac{\mathbf{P} : \mathbf{Q}}{\tilde{\tau} : \mathbf{Q}} \tilde{\tau} \right) \right] \frac{1}{\tau : \mathbf{P}},$$

$$\chi^{**} = - \left(\frac{\partial \hat{\psi}}{\partial \xi} - \vartheta \frac{\partial^2 \hat{\psi}}{\partial \vartheta \partial \xi} \right).$$

4.7. Fracture criterion based on the evolution of microdamage

We base the fracture criterion on the evolution of the porosity internal state variable ξ . The volume fraction porosity ξ takes account of microdamage effects.

Let us assume that for $\xi = \xi^F$ a catastrophe takes place (cf. PERZYNA [113, 114]), that is

$$(4.43) \quad \kappa = \hat{\kappa}(\epsilon^p, \vartheta, \xi)|_{\xi=\xi^F} = 0.$$

It means that for $\xi = \xi^F$ the material loses its carrying capacity. The condition (4.43) describes the main feature observed experimentally that the load tends to zero at the fracture point.

It is noteworthy that the isotropic hardening-softening material function $\hat{\kappa}$ proposed in Eq. (4.13)₁ should satisfy the fracture criterion (4.43).

5. RATE-INDEPENDENT PLASTIC RESPONSE

5.1. Rate-independent plastic response as a limit case

Let us assume that the relaxation time $T_m = 0$, then from (4.11)₁ and (4.12) we have the yield criterion

$$(5.1) \quad f - \kappa = 0.$$

The coefficient Λ can now be determined from the consistency condition

$$(5.2) \quad \dot{f} - \dot{\kappa} = 0,$$

which yields

$$(5.3) \quad \Lambda = \left\langle \frac{1}{H} \{ \mathbf{Q} : [\dot{\tau} - (\mathbf{d} \cdot \alpha + \alpha \cdot \mathbf{d})] + \pi \dot{\vartheta} \} \right\rangle,$$

where

$$\begin{aligned}
 H &= H^* + H^{**}, \\
 H^* &= \sqrt{\frac{2}{3}} \left[\frac{\partial \hat{\kappa}}{\partial \epsilon^p} - \left(\frac{\partial f}{\partial \xi} - \frac{\partial \hat{\kappa}}{\partial \xi} \right) \frac{\partial \xi}{\partial \epsilon^p} \right] \left\| \frac{\partial f}{\partial \tau} + \left(\frac{\partial f}{\partial \xi} - \frac{\partial \hat{\kappa}}{\partial \xi} \right) \frac{\partial \xi}{\partial \tau} \right\|^{-1}, \\
 H^{**} &= \tau \mathbf{P} : \mathbf{Q}, \\
 \pi &= \left[\left(\frac{\partial f}{\partial \xi} - \frac{\partial \hat{\kappa}}{\partial \xi} \right) \frac{\partial \xi}{\partial \vartheta} + \frac{\partial f}{\partial \vartheta} - \frac{\partial \hat{\kappa}}{\partial \vartheta} \right] \left\| \frac{\partial f}{\partial \tau} + \left(\frac{\partial f}{\partial \xi} - \frac{\partial \hat{\kappa}}{\partial \xi} \right) \frac{\partial \xi}{\partial \tau} \right\|^{-1}.
 \end{aligned}
 \tag{5.4}$$

The relations (5.3) and (5.4) suggest the interpretation of H^* and H^{**} as the isotropic and anisotropic hardening modulus rates, respectively.

Finally, we have for rate-independent plastic response

$$\mathbf{d}^p = \left\langle \frac{1}{H} \{ \mathbf{Q} : [\dot{\boldsymbol{\tau}} - (\mathbf{d} \cdot \boldsymbol{\alpha} + \boldsymbol{\alpha} \cdot \mathbf{d})] + \pi \dot{\vartheta} \} \right\rangle \mathbf{P}.
 \tag{5.5}$$

5.2. Rate-independent intrinsic micro-damage process

For rate-independent response when $T_m = 0$ the evolution equation for porosity (4.24) yields

$$\dot{\tilde{I}}_n = \dot{\tilde{I}}_g = \tau_n(\xi, \vartheta, \epsilon^p) = \tau_{eq}(\xi, \vartheta, \epsilon^p) = \kappa.
 \tag{5.6}$$

To obtain the evolution equation for porosity parameter ξ we shall follow the procedure developed by DUSZEK-PERZYNA and PERZYNA [121]. The result (5.6) leads to the evolution equation as follows

$$\dot{\xi} = A_1 \dot{\tilde{J}}_1 + A_2 \dot{\tilde{J}}_2 + A_3 \dot{\tilde{J}}_3 + B \dot{\epsilon}^p + C \dot{\vartheta},
 \tag{5.7}$$

where A_1, A_2, A_3, B and C are determined material functions. The evolution equation (5.7) can be directly related to the Gurson proposition modified by Tvergaard (cf. GURSON [59], MEAR and HUTCHINSON [96], TVERGAARD [160], DUSZEK and PERZYNA [34]) by the assumptions

$$\begin{aligned}
 A_1 \dot{\tilde{J}}_1 &= k_1 \dot{\tilde{J}}_1, & A_2 &= A_3 = 0, \\
 B \dot{\epsilon}^p &= k_2 \tilde{\boldsymbol{\tau}} : \mathbf{d}^p + k_3 \mathbf{g} : \mathbf{d}^p.
 \end{aligned}
 \tag{5.8}$$

Introducing the assumptions (5.8) into (5.7) we obtain

$$\dot{\xi} = k_1 \dot{\tilde{J}}_1 + k_2 \tilde{\boldsymbol{\tau}} : \mathbf{d}^p + k_3 \mathbf{g} : \mathbf{d}^p + C \dot{\vartheta}.
 \tag{5.9}$$

The first two terms in (5.9) are responsible for the description of the nucleation, the first due to the cracking of the second-phase particles and the second is generated by debonding of the second-phase particles from the matrix material as the plastic work progressively increases. The third term describes the growth process and is assumed to be controlled only by the plastic flow phenomena. The last term can be interpreted as the description of the nucleation induced by the transient change of temperature. For processes in which temperature change is smooth and small, this term can be neglected (i.e. we can assume $C = 0$).

5.3. Fundamental rate-type constitutive equations

The rate equation (4.37) can also be written in the form as follows:

$$(5.10) \quad L_v \tau = \mathcal{L}^e : \mathbf{d} - (\mathcal{L}^e : \mathbf{P} + \mathbf{b})\Lambda - \mathcal{L}^{th} \dot{\vartheta},$$

where

$$(5.11) \quad \mathbf{b} = (\mathbf{P} + \mathbf{\Omega}) \cdot \tau + \tau \cdot (\mathbf{P} - \mathbf{\Omega})$$

(cf. here the results for single crystals presented by HILL and RICE [69] and DUSZEK-PERZYNA and PERZYNA [39]).

Substituting in (5.10) Λ and $\mathbf{\Omega}$ from Eqs. (5.3) and (4.18) we finally obtain the rate-type constitutive equation for the Kirchhoff stress tensor τ in the form

$$(5.12) \quad L_v \tau = \mathcal{L} : \mathbf{d} - \mathcal{M} \dot{\vartheta},$$

where the fundamental elasto-plastic matrix \mathcal{L} and the thermal tensor \mathcal{M} are defined as follows:

$$(5.13) \quad \mathcal{L} = \mathcal{L}^e - \frac{(\mathcal{L}^e + \mathbf{g}\tau + \tau\mathbf{g} + \mathcal{W}) : \mathbf{P}\mathbf{Q} : (\mathcal{L}^e + \tilde{\tau}\mathbf{g} + \mathbf{g}\tilde{\tau})}{H + \mathbf{P} : (\mathcal{L}^e + \mathbf{g}\tau + \tau\mathbf{g}) : \mathbf{Q} + \mathbf{P} : \mathcal{W} : \mathbf{Q}},$$

$$\mathcal{M} = \mathcal{L}^{th} - \frac{(\mathcal{L}^e + \mathbf{g}\tau + \tau\mathbf{g} + \mathcal{W}) : \mathbf{P}(\mathbf{Q} : \mathcal{L}^{th} - \pi)}{H + \mathbf{P} : (\mathcal{L}^e + \mathbf{g}\tau + \tau\mathbf{g}) : \mathbf{Q} + \mathbf{P} : \mathcal{W} : \mathbf{Q}}.$$

It is noteworthy to point out here that the fundamental elasto-plastic matrix \mathcal{L} determined by (5.13)₁ is nonsymmetric. There are three reasons for the nonsymmetry of the fundamental elasto-plastic matrix \mathcal{L} , namely the kinematic hardening effects (i.e. the stress tensor $\tilde{\tau} = \tau - \alpha$ arises in the second bracket in the numerator of the second term instead of τ), the plastic non-normality (i.e. $\mathbf{P} \neq \mathbf{Q}$) and the plastic spin (this effect is represented by the additional term \mathcal{W}). For the particular case when these three effects are neglected we have a very important result, namely the fundamental elasto-plastic matrix \mathcal{L} becomes symmetric.

The rate equation (4.40) for rate-independent response takes the form

$$(5.14) \quad \rho c_p \dot{\vartheta} = -\text{div} \mathbf{q} + \vartheta \frac{\rho}{\rho_{\text{Ref}}} \frac{\partial \boldsymbol{\tau}}{\partial \vartheta} : \mathbf{d} + \rho \chi_1 \Lambda + \rho \chi_2 [\mathbf{L}_v \boldsymbol{\tau} : \mathbf{g} + (\mathbf{g} \cdot \tilde{\boldsymbol{\tau}} + \tilde{\boldsymbol{\tau}} \cdot \mathbf{g}) : \mathbf{d}],$$

where the irreversibility coefficients χ_1 and χ_2 are defined as follows

$$(5.15) \quad \chi_1 = - \left[\left(\frac{\partial \hat{\psi}}{\partial \boldsymbol{\zeta}} - \vartheta \frac{\partial^2 \hat{\psi}}{\partial \vartheta \partial \boldsymbol{\zeta}} \right) \sqrt{\frac{2}{3}} + \left(\frac{\partial \hat{\psi}}{\partial \boldsymbol{\alpha}} - \vartheta \frac{\partial^2 \hat{\psi}}{\partial \vartheta \partial \boldsymbol{\alpha}} \right) : \left(r_1 \mathbf{P} + r_2 \frac{\mathbf{P} : \mathbf{Q}}{\tilde{\boldsymbol{\tau}} : \mathbf{Q}} \tilde{\boldsymbol{\tau}} \right) + \left(\frac{\partial \hat{\psi}}{\partial \boldsymbol{\xi}} - \vartheta \frac{\partial^2 \hat{\psi}}{\partial \vartheta \partial \boldsymbol{\xi}} \right) (k_2 \tilde{\boldsymbol{\tau}} : \mathbf{P} + k_3 \mathbf{g} : \mathbf{P}) \right],$$

$$\chi_2 = - \left(\frac{\partial \hat{\psi}}{\partial \boldsymbol{\xi}} - \vartheta \frac{\partial^2 \hat{\psi}}{\partial \vartheta \partial \boldsymbol{\xi}} \right) k_1.$$

It is noteworthy that the rate-type equations (5.12) and (5.14) take into account such effects as the plastic spin, plastic non-normality, plastic strain-induced anisotropy (kinematic hardening, i.e. nonsymmetry of the fundamental matrix \mathcal{L}), covariant terms, micro-damage process (i.e. softening generated by microcrack nucleation and growth mechanisms), thermomechanical couplings (i.e. thermal plastic softening and thermal expansion) and of course, due to cooperative phenomena the synergetic effects.

6. ADIABATIC INELASTIC FLOW PROCESS

6.1. Formulation of an adiabatic inelastic flow process

Let us define an adiabatic inelastic flow process as follows (cf. PERZYNA [121, 122] and ŁODYGOWSKI and PERZYNA [85, 86]). Find ϕ , \mathbf{v} , ρ , $\boldsymbol{\tau}$, $\boldsymbol{\alpha}$, $\boldsymbol{\xi}$ and ϑ as function of t and \mathbf{x} such that

(i) the field equations

$$(6.1) \quad \begin{aligned} \dot{\phi} &= \mathbf{v}, \\ \dot{\mathbf{v}} &= \frac{1}{\rho_{\text{Ref}}} \left(\frac{\boldsymbol{\tau}}{\rho} \text{grad} \rho + \text{div} \boldsymbol{\tau} \right), \\ \dot{\rho} &= -\rho \text{div} \mathbf{v}, \\ \dot{\boldsymbol{\tau}} &= \left(\mathcal{L}^e - \frac{\vartheta}{c_p \rho_{\text{Ref}}} \mathcal{L}^{\text{th}} \frac{\partial \boldsymbol{\tau}}{\partial \vartheta} \right) : \text{sym} \frac{\partial \mathbf{v}}{\partial \mathbf{x}} + 2 \text{sym} \left\langle \boldsymbol{\tau} : \frac{\partial \mathbf{v}}{\partial \mathbf{x}} \right\rangle \\ &\quad - \frac{1}{T_m} \left\langle \Phi \left(\frac{f}{\kappa} - 1 \right) \right\rangle \left[\left(\mathcal{L}^e + \frac{\chi^*}{\rho c_p} \mathcal{L}^{\text{th}} \boldsymbol{\tau} + \mathbf{g} \boldsymbol{\tau} + \boldsymbol{\tau} \mathbf{g} + \mathcal{W} \right) : \mathbf{P} \right] - \frac{\chi^{**} \Xi}{\rho c_p} \mathcal{L}^{\text{th}}, \end{aligned}$$

$$\dot{\alpha} = 2\text{sym} \left(\alpha : \frac{\partial \mathbf{v}}{\partial \mathbf{x}} \right) + \frac{1}{T_m} \left\langle \Phi \left(\frac{f}{\kappa} - 1 \right) \right\rangle \left[r_1(\xi, \vartheta) \mathbf{P} + r_2(\xi, \vartheta) \frac{\mathbf{P} : \mathbf{Q}}{\tilde{\tau} : \mathbf{Q}} \tilde{\tau} \right],$$

(6.1)
[cont.] $\dot{\xi} = \Xi,$

$$\dot{\vartheta} = \frac{\vartheta}{c_p \rho_{\text{Ref}}} \frac{\partial \tau}{\partial \vartheta} : \text{sym} \frac{\partial \mathbf{v}}{\partial \mathbf{x}} + \frac{1}{T_m} \left\langle \Phi \left(\frac{f}{\kappa} - 1 \right) \right\rangle \frac{\chi^*}{c_p} \tau : \mathbf{P} + \frac{\chi^{**}}{c_p} \Xi;$$

(ii) the boundary conditions

- (a) displacement ϕ is prescribed on a part ∂_ϕ of $\partial\phi(\mathcal{B})$ and tractions $(\tau \cdot \mathbf{n})^a$ are prescribed on part ∂_τ of $\partial\phi(\mathcal{B})$, where $\partial_\phi \cap \partial_\tau = 0$ and $\overline{\partial_\phi \cup \partial_\tau} = \partial\phi(\mathcal{B})$;
- (b) heat flux $\mathbf{q} \cdot \mathbf{n} = 0$ is prescribed on $\partial\phi(\mathcal{B})$;
- (iii) the initial conditions $\phi, \mathbf{v}, \rho, \tau, \alpha, \xi$ and ϑ are given at each particle $X \in \mathcal{B}$ at $t = 0$;

are satisfied.

6.2. Formulation of the evolution problem

Find φ as function of t and \mathbf{x} satisfying⁷⁾

$$(6.2) \quad \begin{cases} \text{(i)} & \dot{\varphi} = \mathcal{A}(t, \varphi)\varphi + \mathbf{f}(t, \varphi); \\ \text{(ii)} & \varphi(0) = \varphi^0(\mathbf{x}); \\ \text{(iii)} & \text{The boundary conditions} \\ & \text{(e.g. as have been postulated in Sec. 6.1),} \end{cases}$$

where the unknown φ takes values in a Banach space, $\mathcal{A}(t, \varphi)$ is a spatial linear differential operator (in general unbounded) depending on t and φ , and \mathbf{f} is a nonlinear function.

The evolution problem (6.2) describes an adiabatic inelastic flow process formulated in Section 6.1 provided

$$\varphi = \begin{bmatrix} \mathbf{v} \\ \rho \\ \tau \\ \alpha \\ \xi \\ \vartheta \end{bmatrix},$$

⁷⁾We shall follow here some fundamental results which have been discussed in RICHTMYER and MORTON [136], STRANG and FIX [152], HUGHES, KATO and MARSDEN [72], RICHTMYER [135], DAUTRAY and LIONS [26], GUSTAFSSON, KREISS and OLIGER [61] and ŁODYGOWSKI and PERZYNA [85, 86].

$$\mathbf{f} = \begin{bmatrix} 0 \\ 0 \\ -\frac{1}{T_m} \left\langle \Phi \left(\frac{f}{\kappa} - 1 \right) \right\rangle \left[\left(\mathcal{L}^e + \frac{\chi^*}{\rho c_p} \mathcal{L}^{th} \boldsymbol{\tau} + \mathbf{g} \boldsymbol{\tau} + \boldsymbol{\tau} \mathbf{g} + \mathcal{W} \right) : \mathbf{P} \right] \\ - \frac{\chi^{**} \Xi}{\rho c_p} \mathcal{L}^{th} \\ \frac{1}{T_m} \left\langle \Phi \left(\frac{f}{\kappa} - 1 \right) \right\rangle \left[r_1(\xi, \vartheta) \mathbf{P} + r_2(\xi, \vartheta) \frac{\mathbf{P} : \mathbf{Q}}{\tilde{\boldsymbol{\tau}} : \mathbf{Q}} \tilde{\boldsymbol{\tau}} \right] \\ \Xi \\ \frac{1}{T_m} \left\langle \Phi \left(\frac{f}{\kappa} - 1 \right) \right\rangle \frac{\chi^*}{\rho c_p} \boldsymbol{\tau} : \mathbf{P} + \frac{\chi^{**}}{\rho c_p} \Xi \end{bmatrix}, \tag{6.3}$$

$$\mathcal{A} = \begin{bmatrix} 0 & \frac{\boldsymbol{\tau}}{\rho_{Ref} \rho} \text{grad} & \frac{1}{\rho_{Ref}} \text{div} & 0 & 0 & 0 \\ -\rho \text{div} & 0 & 0 & 0 & 0 & 0 \\ \mathbb{E} : \text{sym} \frac{\partial}{\partial \mathbf{x}} + 2 \text{sym} \left(\boldsymbol{\tau} : \frac{\partial}{\partial \mathbf{x}} \right) & 0 & 0 & 0 & 0 & 0 \\ 2 \text{sym} \left(\boldsymbol{\alpha} : \frac{\partial}{\partial \mathbf{x}} \right) & 0 & 0 & 0 & 0 & 0 \\ 0 & 0 & 0 & 0 & 0 & 0 \\ \frac{\vartheta}{c_p \rho_{Ref}} \frac{\partial \boldsymbol{\tau}}{\partial \vartheta} : \text{sym} \frac{\partial}{\partial \mathbf{x}} & 0 & 0 & 0 & 0 & 0 \end{bmatrix},$$

where

$$\mathbb{E} = \mathcal{L}^e - \frac{\vartheta}{c_p \rho_{Ref}} \mathcal{L}^{th} \frac{\partial \boldsymbol{\tau}}{\partial \vartheta}. \tag{6.4}$$

It is noteworthy that the spatial operator \mathcal{A} has the same form as in thermo-elastodynamics while all dissipative effects generated by viscoplastic flow phenomena influence the process through the nonlinear function \mathbf{f} .

6.3. Strict solution of the evolution problem

A strict solution of (6.2) with $\mathbf{f}(t, \varphi) \equiv 0$ (i.e. the homogeneous evolution problem) is defined as a function $\varphi(t) \in E$ (a Banach space) such that

$$\varphi(t) \in \mathcal{D}(\mathcal{A}), \quad \text{for all } t \in [0, t_f], \tag{6.5}$$

$$\lim_{\Delta t \rightarrow 0} \left\| \frac{\varphi(t + \Delta t) - \varphi(t)}{\Delta t} - \mathcal{A} \varphi(t) \right\|_E = 0 \quad \text{for all } t \in [0, t_f].$$

The boundary conditions are taken care of by restricting the domain $\mathcal{D}(\mathcal{A})$ to elements of E that satisfy those conditions; they are assumed to be linear and homogeneous, so that the set S of all φ that satisfy them is a linear manifold; $\mathcal{D}(\mathcal{A})$ is assumed to be contained in S .

The choice of the Banach space E , as well as the domain of \mathcal{A} , is an essential part of the formulation of the evolution problem.

6.4. Well-posedness of the evolution problem

The homogeneous evolution problem (i.e. for $\mathbf{f} \equiv 0$) is called well posed (in the sense of Hadamard) if it has the following properties (cf. RICHTMYER [135] and HUGHES *et al.* [72]):

- (i) The strict solutions are uniquely determined by their initial elements;
- (ii) The set Y of all initial elements of strict solutions is dense in the Banach space E ;
- (iii) For any finite interval $[0, t_0]$, $t_0 \in [0, t_f]$ there is a constant $K = K(t_0)$ such that every strict solution satisfies the inequality

$$(6.6) \quad \|\varphi(t)\| \leq K \|\varphi^0\|, \quad \text{for } 0 \leq t \leq t_0.$$

The inhomogeneous evolution problem (6.2) will be called well posed if it has a unique solution for all reasonable choices of φ^0 and $\mathbf{f}(t, \varphi)$ and if the solution depends continuously, in some sense, on those choices.

It is evident that any solution is unique, because of the uniqueness of the solutions of the homogeneous evolution problem. Namely, the difference of two solutions, for given φ^0 and given $\mathbf{f}(\cdot)$, is a solution of the homogeneous problem with zero as an initial element, hence must be zero for all t .

It is possible to show (cf. RICHTMYER [135]) that strict solutions exist for sets of φ^0 and $\mathbf{f}(\cdot)$ that are dense in E and E_1 (a new Banach space), respectively.

Of course it is easier to do this for the initial value problem (the Cauchy problem) than for the initial-boundary value problem (the evolution problem).

Let us consider the initial value problem (6.2)(i),(ii), i.e.

$$(6.7) \quad \dot{\varphi} = \mathcal{A}(t, \mathbf{x}, \varphi)\varphi + \mathbf{f}(t, \mathbf{x}, \varphi), \quad t \in [0, t_f], \quad \varphi(0, \mathbf{x}) = \varphi^0(\mathbf{x}).$$

In order to examine the existence, uniqueness and well-posedness of the initial value problem (6.7) let us assume that the spatial differential operator \mathcal{A} has domain $\mathcal{D}(\mathcal{A})$ and range $\mathcal{R}(\mathcal{A})$, both contained in a real Banach space E and the nonlinear function $\mathbf{f} : E \rightarrow E$. To investigate the existence as well as stability of solutions to (6.7) it is necessary to characterize their properties without actually constructing the solutions. This can be done by considering the properties of a nonlinear semi-group.

Let $\{F_t^*; t \geq 0\}$ be a semi-group generated by the operator $\mathcal{A} + \mathbf{f}(\cdot)$ and $\{F_t; t \geq 0\}$ be a semi-group generated by the operator \mathcal{A} .

Then we can write the generalized solution of the nonhomogenous initial-value problem (6.7) in alternative forms

$$(6.8) \quad \begin{aligned} \varphi(t, \mathbf{x}) &= F_t^*(t)\varphi^0(\mathbf{x}) \\ &= F(t)\varphi^0(\mathbf{x}) + \int_0^t F(t-s)\mathbf{f}(s, \varphi(s))ds. \end{aligned}$$

We say that the problem (6.7) is well posed if F_t^* is continuous (in the topology on $\mathcal{D}(\mathcal{A})$ and $\mathcal{R}(\mathcal{A})$ assumed) for each $t \in [0, t_f]$.

Let us postulate as follows:

(i) the strong ellipticity conditions in the form:

$$(6.9) \quad E = \mathcal{L}^e - \frac{1}{c_p \rho_{Ref}} \vartheta \mathcal{L}^{th} \frac{\partial \tau}{\partial \vartheta}$$

is strongly elliptic (at a particular deformation ϕ) if there is an $\varepsilon > 0$ such that

$$(6.10) \quad E^{abcd} \zeta_a \zeta_c \xi_b \xi_d \geq \varepsilon \|\zeta\|^2 \|\xi\|^2$$

for all vectors ζ and $\xi \in \mathbb{R}^3$;

(ii) for positive numbers λ_f^1 and λ_f^2 and for $T_m > 0$

$$(6.11) \quad \begin{aligned} \mathbf{f}(t, \varphi) \in E, \quad \|\mathbf{f}(t, \varphi)\|_E &\leq \lambda_f^1, \\ \|\mathbf{f}(t, \varphi') - \mathbf{f}(t, \varphi)\|_E &\leq \lambda_f^2 \|\varphi' - \varphi\|_E, \end{aligned}$$

and

$$(6.12) \quad t \rightarrow \mathbf{f}(t, \varphi) \in E \text{ is continuous.}$$

Using the results presented by HUGHES *et al.* [72] and MARDEN and HUGHES [93] it is possible to show (cf. PERZYNA [121, 122]) that the conditions (i) and (ii) guarantee the existence of (locally defined) evolution operators $F_t^* : E \rightarrow E$ that are continuous in all variables. In other words, the solution of the Cauchy problem (6.7) in the form (6.8)₁ exists, is unique and well-posed.

The generalized solution of the nonhomogeneous initial-value problem (6.7) in the form (6.8)₂ is the integral equation.

The successive approximations for (6.8)₂ are defined to be the functions $\varphi_0, \varphi_1, \dots$, given by the formulas

$$(6.13) \quad \begin{aligned} \varphi_0(t) &= \varphi^0, \\ \varphi_{k+1}(t) &= F(t)\varphi^0 + \int_0^t F(t-s)\mathbf{f}(s, \varphi_k(s))ds, \\ k &= 0, 1, 2, \dots; \quad t \in [0, t_f]. \end{aligned}$$

It is possible to show that these functions actually exist on $t \in [0, t_f]$ if the continuous function \mathbf{f} is Lipschitz-continuous with respect to the second argument uniformly with respect to $t \in [0, t_f]$. Then (6.8)₂ has a unique solution (cf. IONESCU and SOFONEA [75]).

To prove the well-posedness of the initial-value problem (6.7) we can also use recent results obtained for the symmetrizable hyperbolic systems (cf. TAYLOR [154]).

Let us write the system of equations (6.7) in the form

$$(6.14) \quad \frac{\partial \varphi}{\partial t} = \sum_{j=1}^3 B_j(t, \mathbf{x}, \varphi) \partial_j \varphi + \mathbf{f}(t, \mathbf{x}, \varphi).$$

The system (6.14) due to the condition (6.10) is strictly hyperbolic, however is not symmetric⁸).

We shall use the following

PROPOSITION 1. (cf. TAYLOR [154]). Whenever the system (6.14) is strictly hyperbolic, it is symmetrizable.

So, there exist $A_0(t, \mathbf{x}, \varphi)$ positive definite, such that

$$(6.15) \quad A_0(t, \mathbf{x}, \varphi) B_j(t, \mathbf{x}, \varphi) = A_j(t, \mathbf{x}, \varphi)$$

are all symmetric, i.e.

$$(6.16) \quad A_j = A_j^* \quad \text{and} \quad A_0 \geq cI > 0.$$

The initial-value problem (6.7) can be written in the form

$$(6.17) \quad A_0(t, \mathbf{x}, \varphi) \frac{\partial \varphi}{\partial t} = \sum_{j=1}^3 A_j(t, \mathbf{x}, \varphi) \partial_j \varphi + \mathbf{g}(t, \mathbf{x}, \varphi),$$

$$\varphi(0, \mathbf{x}) = \varphi^0(\mathbf{x}),$$

with the domain $\mathcal{D} \subset E$. We shall use the following

THEOREM 1: (cf. TAYLOR [154]). If the system (6.14) is symmetrizable, in particular if it is strictly hyperbolic, the initial value problem (6.7), with $\varphi(0, \mathbf{x}) = \varphi^0(0, \mathbf{x}) \in H^k(\mathcal{D})$, has a unique local solution $\varphi \in C(I, H^k(\mathcal{D}))$ whenever $k > \frac{n}{2} + 1$; $n = 3$ and $I = [0, t_f]$.

We can also use here the results of FRIEDRICHS [50, 51] for the symmetric hyperbolic systems (cf. MARSDEN and HUGHES [93]).

⁸For all examples considered for an elastic-viscoplastic model of the material, the system (6.14) will be strictly hyperbolic.

7. ANALYSIS OF THE FUNDAMENTAL FEATURES OF THE MODEL

7.1. *Invariance with respect to diffeomorphism*

Our description of the thermo-elasto-viscoplastic constitutive structure is invariant with respect to any diffeomorphism, cf. Fig. 32. It means that the constitutive structure is invariant to any superposed motion. Such constitutive structure is called covariant, cf. MARS DEN and HUGHES [93].

As it has been already mentioned in Sec. 4.1 (see Postulate (ii)) when $\xi : \mathcal{S} \rightarrow \mathcal{S}$ is a regular, orientation preserving map transforming \mathbf{x} into \mathbf{x}' and $T\xi$ is an isometry from $T_{\mathbf{x}}\mathcal{S}$ to $T_{\mathbf{x}'}\mathcal{S}$, we obtain the invariance with respect to any rigid motion, i.e. the axiom of material frame indifference, cf. TRUESDELL and NOLL [159].

The covariance property of the constitutive structure has been achieved due to the assumption that the rates of the deformation tensors and the stress tensors (as well as all vectors and tensors) are defined based on the Lie derivative. Of course, the covariance description has very important consequence for proper mathematical investigations of some phenomena which will be discussed in the solution of the evolution problems. It will be also crucial for proper description of mesomechanical problems and particularly in their numerical solutions.

7.2. *Finite plastic deformation; plastic spin effects*

The kinematics of finite elasto-viscoplastic deformation is based on notions of the Riemann space on manifolds and tangent spaces, cf. MARS DEN and HUGHES [93]. A multiplicative decomposition of the deformation gradient into elastic and viscoplastic parts is assumed, and Lie derivative is used to define all objective rates for vectors and tensors.

The viscoplastic spin has been also taken into account in the constitutive structure.

Due to these assumptions we obtain the consistent description of finite elasto-viscoplastic deformations.

The main effect generated by the viscoplastic spin can be observed from the rate-type constitutive relation for the Kirchhoff stress tensor $\boldsymbol{\tau}$ (cf. Eq. (4.37)). In this equation the additional term $\frac{1}{T_m} \left\langle \Phi \left(\frac{f}{\kappa} - 1 \right) \right\rangle \mathcal{W} : \mathbf{P}$ describes the influence of the viscoplastic spin. For thermo-elasto-plastic (rate independent) constitutive structure we observe a similar influence of the plastic spin on the fundamental rate constitutive equation for the Kirchhoff stress tensor $\boldsymbol{\tau}$ (cf. Eq. (5.13)). Namely, both matrices \mathcal{L} and \mathcal{M} are affected by the additional term \mathcal{W} . In this case it caused the asymmetry of the fundamental elasto-plastic matrix \mathcal{L} . This property, of course, has a very important influence on the description of localization phenomena.

7.3. Plastic non-normality

Plastic non-normality (i.e. $\mathbf{P} \neq \mathbf{Q}$) is generated by the influence of microdamage mechanisms. This effect is clear from the comparison of \mathbf{P} (cf. Eq. (4.14)) and \mathbf{Q} (cf. Eq. (4.29)). It has very important influence on the description of localization and localized fracture phenomena.

7.4. Softening effects generated by microdamage mechanisms

By introducing the internal state variable ξ , i.e. volume fraction porosity in the constitutive structure (cf. Sec. 4), the description of the intrinsic microdamage process has been achieved. From the available experimental observations we learn that there are three main mechanisms responsible for the evolution of microdamage, namely nucleation, growth and coalescence of microcracks. Taking advantage of the conjecture that the coalescence mechanism can be treated as nucleation and growth process on a smaller scale, we simplified the description of the intrinsic microdamage by making allowance only for the nucleation and growth mechanisms.

From the fundamental rate equation for temperature ϑ (cf. Eq. (4.40)) we observe that the microdamage mechanism generates dissipation effects. On the other hand, from the form of the isotropic work-hardening-softening function κ (cf. Eq. (4.13)) we see the direct description of softening effects caused by the intrinsic microdamage process.

It is noteworthy to add that the fundamental fracture criterion (cf. Eq. (4.43)) is also based on the evolution of microdamage. The evolution equation for the porosity internal state variable ξ is assumed in the form (4.24) which takes into consideration the influence of the stress triaxiality on the nucleation and growth mechanisms. This assumption has crucial importance for the description of fatigue fracture phenomena.

7.5. Plastic deformation-induced anisotropic effects

Experimental observations of plastic flow processes have shown that finite plastic deformations induced the effect of anisotropy of a material. To describe this effect, the residual stress (the back stress) α has been introduced to the constitutive structure as the internal state variable. The aim of this is to take into account the kinematic hardening phenomenon, which can be treated as the first approximation of the description of plastic deformation-induced anisotropy.

The evolution equation postulated for the back stress α represents the linear combination of the Prager and Ziegler kinematic hardening rules. As a result of this description of plastic deformation-induced elasto-plastic matrix \mathcal{L} (cf. Eq. (5.13)), i.e. the stress tensor $\tilde{\tau} = \tau - \alpha$ arises in the second bracket in the numerator of the second term instead of τ .

This kind of anisotropy generated by the kinematic hardening law will have very important influence on the localized fracture phenomena in thermo-viscoplastic flow processes under cyclic dynamic loadings.

7.6. *Thermomechanical couplings (thermal plastic softening and thermal expansion)*

An analysis of thermomechanical coupling effects can be based on the investigation of the evolution problem formulated for a thermo-elasto-viscoplastic model (cf. Eqs. (6.2) and (6.3)). Thermal expansion effect influences the fundamental matrix \mathbb{E} (cf. Eq. (6.4)) for an adiabatic process, so it can have very important influence on the propagation and interaction of the deformation waves.

On the other hand, the thermal plastic softening as a typical dissipative effect influences an adiabatic process through the nonlinear function \mathbf{f} (cf. Eq. (6.3)). Of course, it will have a lot of influence on the localization phenomena as well as on the fracture phenomena⁹⁾.

7.7. *Influence of stress triaxiality on the evolution of microdamage*

The introduced modification of the kinetics of microdamage presented in Sec. 4.4 leads to the description of the influence of stress triaxiality. This has been done by assumption that the stress intensity invariants for nucleation and growth depend on three invariants of the stress tensor, cf. Eqs. (4.20) and (4.22).

It has been shown by Dornowski and Perzyna [27, 28, 29, 30, 31, 32] that this modification helps to describe the accumulation of damage during the dynamic loading process.

7.8. *Rate sensitivity*

To analyse the influence of the strain rate effect let us write the evolution constitutive equation (4.11)₁ in the form as follows:

$$(7.1) \quad \|\mathbf{d}^P\| = \frac{1}{T_m} \left\langle \Phi \left(\frac{f}{\kappa} - 1 \right) \right\rangle \|\mathbf{P}\|,$$

where $\|\cdot\|$ denotes the norm of the vectors in the 6-dimensional space.

The equation (7.1) yields the following dynamical yield criterion

$$(7.2) \quad f = \hat{\kappa}(\epsilon^P, \vartheta, \xi) \left[1 + \Phi^{-1} \left(T_m \frac{\|\mathbf{d}^P\|}{\|\mathbf{P}\|} \right) \right].$$

⁹⁾For a thorough analytical discussion of the thermal plastic softening and thermal expansion effects on the localization of plastic deformation please consult the papers by DUSZEK-PERZYNA and PERZYNA [40, 43].

This relation may be interpreted as a description of actual change of the yield surface during the thermodynamical process, cf. Fig. 33. This change is caused by isotropic and anisotropic work-hardening-softening effects, by dependence on temperature and by the influence of the strain rate effects. It is noteworthy to add that the relation (7.2) constitutes a basis for experimental investigations which seek to examine the theoretical assumptions.

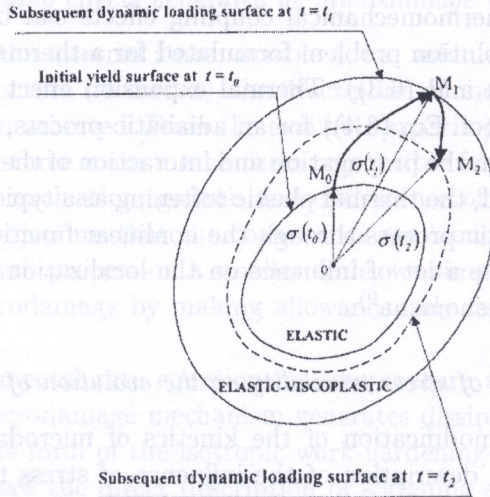


FIG. 33. Dynamic loading surface for the elasto-viscoplastic response.

To show this possibility deeper let us take assumptions concerning the plastic potential function f and the isotropic work-hardening-softening function κ as have been postulated in DORNOWSKI and PERZYNA [29], cf. also EFTIS [44] and EFTIS and NEMES [45, 46, 47]. Then we have a particular form of the dynamical yield criterion

$$\begin{aligned}
 (7.3) \quad & \left\{ \tilde{J}_2 + [n_1(\vartheta) + n_2(\vartheta)\xi] \tilde{J}_1^2 \right\}^{1/2} \\
 & = \left\{ \kappa_s(\vartheta) - [\kappa_s(\vartheta) - \kappa_0(\vartheta)] \exp[-\delta(\vartheta) \epsilon^P] \right\} \\
 & \quad \left[1 - \left(\frac{\xi}{\xi_F} \right)^{\beta(\vartheta)} \right] \left[1 + \Phi^{-1} \left(T_m \frac{\|d^P\|}{\|P\|} \right) \right].
 \end{aligned}$$

7.9. Length-scale sensitivity of the constitutive model

The constitutive equations for a thermo-elastic-viscoplastic model introduce implicitly a length-scale parameter into the dynamic initial-boundary value problem, i.e.

$$(7.4) \quad l = \beta c T_m,$$

where T_m is the relaxation time for mechanical disturbances and is directly related to the viscosity of the material, c denotes the velocity of the propagation of the elastic waves in the problem under consideration, and the proportionality factor β depends on the particular initial-boundary value problem and may also be conditioned on the microscopic properties of the material.

The relaxation time T_m can be viewed either as a microstructural parameter to be determined from experimental observations or as a mathematical regularization parameter.

To go deeply into length-scale sensitivity of the constitutive model let us consider one-dimensional longitudinal wave propagation for an elastic-viscoplastic material. The constitutive equations are assumed in the form as follows

$$(7.5) \quad \dot{\epsilon}^P = \dot{\epsilon} - \frac{\dot{\sigma}}{E}, \quad \dot{\sigma} = h\dot{\epsilon}^P + \frac{\sigma_0}{\gamma} \frac{\partial \dot{\epsilon}^P}{\partial t},$$

where γ denotes the viscosity parameter, σ_0 the yield stress and h the hardening-softening parameter.

The wave equation takes the form

$$(7.6) \quad \zeta \left(\frac{1}{c^2} \frac{\partial^2 v}{\partial t^2} - \frac{\partial^3 v}{\partial x^2 \partial t} \right) + \frac{E+h}{c^2} \frac{\partial^2 v}{\partial t^2} - h \frac{\partial^2 v}{\partial x^2} = 0,$$

where

$$(7.7) \quad \zeta = \frac{\sigma_0}{\gamma} = \sigma_0 T_m$$

denotes the macroscopic viscosity (or dynamic viscosity) and $c = (E/\rho)^{1/2}$.

For $\gamma \rightarrow \infty \Rightarrow \zeta \rightarrow 0$ (7.6) reduces to the wave equation for an elastic-plastic rate-independent material. To investigate the dispersive nature of wave propagation in an elastic-viscoplastic medium, a general solution for a single linear harmonic wave with angular frequency ω and wave number k is assumed

$$(7.8) \quad v = A e^{i(kx - \omega t)}, \quad k = \frac{2\pi}{\lambda},$$

and A denotes the amplitude.

To satisfy the equation (7.6), constants k and ω have to be related by the dispersion relation

$$(7.9) \quad \zeta \left(\frac{1}{c^2} \omega^3 - k^2 \omega \right) i - \frac{E+h}{c^2} \omega^2 + h k^2 = 0.$$

By sophisticated analysis of the dispersion relation (7.9) we can obtain the result for the internal length-scale parameter (cf. SLUYS [151])

$$(7.10) \quad l = \frac{2\sigma_0}{E} cT_m.$$

Comparison (7.10) with (7.4) gives

$$(7.11) \quad \beta = \frac{2\sigma_0}{E}$$

for a one-dimensional longitudinal wave propagation problem.

It is noteworthy to stress that the length-scale sensitivity of the constitutive structure is of great importance for proper description of mesomechanical problems.

7.10. Regularization of the evolution problem

The analysis of shear band development in nonhomogeneously deforming solids requires a full initial-boundary value problem solution. Such a solution can be obtained only by means of numerical methods. In recent years the initial-boundary value problems with the development of shear bands have been solved by using numerical methods. All solutions obtained for a rate-independent plastic flow model with the development of shear bands have some shortcomings: (i) They are mesh-dependent. In other words, the pathological mesh size effects influence the results obtained. (ii) They are obtained by superposing some artificial inhomogeneities. Without some mechanism to make the deformation nonhomogeneous, the solid body considered will undergo unlimited homogeneous deformation and no shear band localization will occur. Very recently, it has been widely recognized to consider an elastic-viscoplastic model of a material as a regularization method for solving mesh-dependent problems of plasticity. In these regularized initial-boundary value problems, wave propagation phenomena play a fundamental role. Since an elastic-viscoplastic model introduces dissipative as well as dispersive nature for the propagated waves, the analysis of dispersive, dissipative waves and particularly their interactions and reflections have to be considered as the most important problem, cf. GLEMA, ŁODYGOWSKI and PERZYNA [54, 55, 56]. The dispersion property implies that in the elastic-viscoplastic medium any initial disturbance can break up into a system of groups of oscillations or wavelets. On the other hand, the dissipation property causes the amplitude of a harmonic wavetrain to decay with time. In the evolution problem considered in such a dissipative and dispersive medium, the stress deformation due to wave reflections and interactions are not uniformly distributed, and this kind of heterogeneity can lead to strain localization in the absence of geometrical or material imperfections.

It may happen that for some constitutive models the nonhomogeneous evolution problem (6.2) is not well posed (e.g. for a rate-independent plastic model).

Then we can find a parameter $\delta \in [0, \delta^*]$ (δ^* is given) such that the new evolution problem

$$(7.12) \quad \begin{cases} \dot{\varphi} = \mathcal{A}_\delta(t, \varphi)\varphi + \mathbf{f}_\delta(t, \varphi); \\ \varphi(0) = \varphi^0, \quad t \in [0, t_f]; \\ \text{The boundary conditions;} \end{cases}$$

has the generalized solution

$$(7.13) \quad \varphi(t, \mathbf{x}) = \mathbb{F}_\delta(t)\varphi^0(\mathbf{x}) + \int_0^t \mathbb{F}_\delta(t-s)\mathbf{f}_\delta(s)ds$$

which satisfies the assertions as follows:

(i) The evolution operator $\mathbb{F}_\delta(t)$ is continuous in the topology on $\mathcal{D}(\mathcal{A}_\delta) \subset E$ assumed for each $t \in [0, t_f]$;

(ii) The function $\mathbf{f}_\delta(t)$ satisfies the conditions

$$(7.14) \quad \begin{aligned} \mathbf{f}_\delta(t, \varphi) \in E, \quad \|\mathbf{f}_\delta(t, \varphi)\|_E &\leq \lambda_f^1, \\ \|\mathbf{f}_\delta(t, \varphi') - \mathbf{f}_\delta(t, \varphi)\|_E &\leq \lambda_f^2 \|\varphi' - \varphi\|_E \end{aligned}$$

and $t \rightarrow \mathbf{f}_\delta(t, \varphi) \in E$ is continuous;

(iii)

$$(7.15) \quad \begin{aligned} \mathbb{F}_\delta(t) |_{\delta=0} &= \mathbb{F}(t), \\ \mathbf{f}_\delta(t, \varphi(t)) |_{\delta=0} &= \mathbf{f}(t, \varphi(t)). \end{aligned}$$

It means that the regularized evolution problem (7.12) is well-posed. Then the parameter δ is called **the regularization parameter**.

For the regularized evolution problem formulated by means of an elastic-viscoplastic constitutive model (6.2), (6.3), (6.4), that is for an adiabatic inelastic flow process, the regularization parameter $\delta = T_m$. Thus, the relaxation time T_m (or viscosity) can be viewed either as a mathematical regularization parameter or as a microstructural parameter to be determined from experimental observations.

It is possible to prove that the regularization evolution problem (6.2), (6.3), (6.4) is well-posed, cf. Sec. 6.4.

Let us postulate as follows:

1. The strong ellipticity condition in the form: the adiabatic-elastodynamic matrix \mathbb{E} defined by (6.4) is strongly elliptic (at a particular deformation ϕ) if there is an $\varepsilon > 0$ such that

$$(7.16) \quad \mathbb{E}^{abcd} \zeta_a \zeta_c \eta_b \eta_d \geq \varepsilon \|\zeta\|^2 \|\eta\|^2$$

2. The condition (ii) (cf. Eq. (7.14)) is satisfied for the function \mathbf{f}_δ .

For an elasto-viscoplastic model the strong ellipticity condition is satisfied provided it is assumed that the elastic properties of the material are reasonable. The condition (ii) for the function \mathbf{f}_δ is also satisfied if and only if we postulate: The material functions $f = f(J_1, J_2, \xi, \vartheta)$, $\kappa = \hat{\kappa}(\in^P, \xi, \vartheta)$, $g^* = g^*(\xi, \vartheta)$ and $\tau_{eq} = \tau_{eq}(\in^P, \xi, \vartheta)$ are continuous functions in all variables and the overstress viscoplastic function $\Phi = \Phi\left(\frac{f}{\kappa} - 1\right)$ is an absolutely continuous function, cf. PERZYNA [121].

Then the rate dependence (viscosity) allows the spatial differential operator in the governing equation to retain its ellipticity and the regularized evolution problem is well-posed. Viscosity introduces implicitly a length-scale parameter into the dynamical initial-boundary value problem.

Since the rate-independent plastic response can be obtained as the limit case when the regularization parameter (the relaxation time) $\delta = T_m$ is equal to zero, hence the theory of elasto-viscoplasticity offers regularization procedure for the solution of the initial-boundary value problems under dynamic loadings.

7.11. Dissipation and dispersion effects

Internal dissipation for the thermo-elasto-viscoplastic model is as follows (cf. Eq. (4.36)):

$$(7.17) \quad \vartheta \dot{i} = - \left[\frac{\partial \hat{\psi}}{\partial \in^P} \sqrt{\frac{2}{3}} + \frac{\partial \hat{\psi}}{\partial \alpha} : \left(r_1 \mathbf{P} + r_2 \frac{\mathbf{P} : \mathbf{Q}}{\bar{\tau} : \mathbf{Q}} \bar{\tau} \right) \right] \frac{1}{T_m} \left\langle \Phi \left(\frac{f}{\kappa} - 1 \right) \right\rangle \\ - \frac{\partial \hat{\psi}}{\partial \xi} \left\{ \frac{1}{T_m} h^* \left\langle \Phi \left[\frac{\tilde{I}_n}{\tau_n(\xi, \vartheta, \in^P)} - 1 \right] \right\rangle + \frac{1}{T_m} g^* \left\langle \Phi \left[\frac{\tilde{I}_g}{\tau_{eq}(\xi, \vartheta, \in^P)} - 1 \right] \right\rangle \right\}.$$

From this equation we observe that for an adiabatic process, the dissipation effects are generated by the following phenomena: (i) viscoplastic flow; (ii) viscoplastic deformation-induced anisotropy; and (iii) microdamage mechanisms.

For an adiabatic process ($\mathbf{q} = 0$) Eq. (4.40) takes the form

$$(7.18) \quad c_p \dot{\vartheta} = \vartheta \frac{1}{\rho_{Ref}} \frac{\partial \tau}{\partial \vartheta} : \mathbf{d} + \chi * \tau : \mathbf{d}^P + \chi^{**} \xi.$$

The first term on the right-hand side of Eq. (7.18) has not a dissipative nature and is of the second order when compared with the internal dissipation terms.

The second term on the right-hand side of Eq. (7.18) represents the rate of internal dissipation due to plastic flow process while the last term gives the

contribution to the rate of internal dissipation generated by the intrinsic microdamage mechanism.

When the nondissipative term is neglected, then Eq. (7.18) takes the form

$$(7.19) \quad c_p \dot{\vartheta} = \chi^* \boldsymbol{\tau} : \mathbf{d}^p + \chi^{**} \dot{\xi}.$$

From Eq. (7.19) we can compute the irreversibility coefficient χ^* . It gives

$$(7.20) \quad \chi^* = \frac{c_p \dot{\vartheta} - \chi^{**} \dot{\xi}}{\boldsymbol{\tau} : \mathbf{d}^p}.$$

For $\chi^{**} = 0$, i.e. when the influence of the intrinsic microdamage mechanism is not taken into consideration, Eq. (7.20) takes the form

$$(7.21) \quad \chi^* = \frac{c_p \dot{\vartheta}}{\boldsymbol{\tau} : \mathbf{d}^p}.$$

For this particular case the irreversibility coefficient χ^* has a simple interpretation as the heat rate conversion to plastic work rate fraction. However, Eq. (7.20) shows that the remaining work rate is attributed to the energy rate lost for microdamage effects.

When modelling the thermomechanical behaviour of materials, χ^* is usually assumed to be a constant in the range 0.85 – 0.95 (a practice that dates back to the work of TAYLOR and QUINNEY [153]).

Recent experimental investigations performed by MASON *et al.* [95] by using a Kolsky (split Hopkinson) pressure bar and a high-speed infrared detector array have clearly shown that this assumption may not be correct for all metals, cf. Fig. 34.

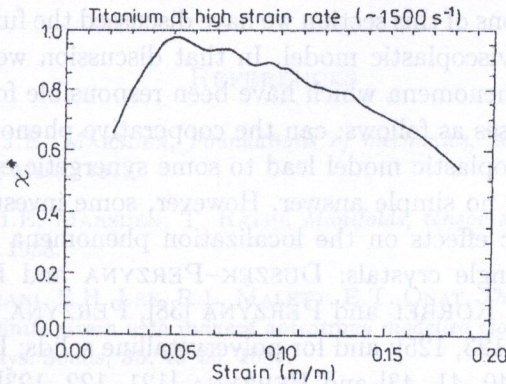


FIG. 34. The irreversibility coefficient χ^* versus strain calculated for Ti-6Al-4V titanium using the average of the temperature of the two detectors (after MASON *et al.* [95].)

The reason for this considerable discrepancy is clearly visible from Eq. (7.20). The rate of the stored energy implied by the evolution of microdamage is responsible for the decreasing of χ^* (e.g. as it has been observed for Ti-6Al-4V deformed at high strain rates χ^* decreases from 0.975 to 0.5, cf. Fig. 34).

MASON *et al.* [95] observed that the irreversibility coefficient χ^* depends on strain and strain rate in a range of metals. Their experimental observations have significant implications in the study of the conditions preceding and governing adiabatic shear band formation and shear band growth as well as on the establishment of a criterion governing dynamic fracture mode selection in rate-sensitive materials.

It is a very well known fact that the stress wave propagation in an elasto-viscoplastic medium has a dispersive nature. We can observe a dispersive character of waves in a very simple example considered in Sec. 7.8, namely one-dimensional longitudinal wave propagation in an elastic-viscoplastic model of a material. From this consideration it can be seen that the dispersion relation (7.9) suggests the dispersive nature of elasto-viscoplastic waves, while the elastic-plastic (rate independent) waves (i.e. when $\zeta = 0$) are non-dispersive, because for $\zeta = 0$ the dispersion relation (7.9) gives the linear dependence between the angular frequency ω and the wave number k .

The dispersion effect is very crucial for the development of regularization procedure for the rate independent plastic flow evolution problems, cf. Sec 7.10.

Of course, the dispersion effects will also influence very much the initiation and development of the localization phenomena. A thorough analysis of these consequences has been presented in GLEMA, ŁODYGOWSKI and PERZYNA [54].

7.12. Synergetic effects generated by cooperative phenomena

In previous sections of this section we have discussed the fundamental features of a thermo-elastic-viscoplastic model. In that discussion we have investigated many cooperative phenomena which have been responsible for these features.

The question arises as follows: can the cooperative phenomena described by a thermo-elasto-viscoplastic model lead to some synergetic effects? This fundamental question has no simple answer. However, some investigations of the influence of synergetic effects on the localization phenomena have been already presented, cf. for single crystals: DUSZEK-PERZYNA and PERZYNA [39, 42], DUSZEK-PERZYNA, KORBEL and PERZYNA [38], PERZYNA and KORBEL [130, 131] and PERZYNA [123, 125]; and for polycrystalline solids: DUSZEK-PERZYNA and PERZYNA [39, 40, 41, 43] and PERZYNA [121, 122, 123]. Numerical investigation of synergetic effects for localization and fracture phenomena has been given in DUSZEK-PERZYNA and PERZYNA [40, 43].

8. EPILOGUE

It is noteworthy that the thermodynamical theory of elasto-viscoplasticity of polycrystalline solids presented in this paper has been inspired by the experimental observations and physical concepts discussed in Sec. 2. The mentioned experimental works have brought deep understanding of the intrinsic microdamage mechanism during dynamic loading processes and have clearly shown that fracture mechanism of metals does very much depend on the strain rate and wave shape effects.

The crucial idea in this theory is the very efficient interpretation of a finite set of the internal state variables as the equivalent plastic deformation, volume fraction porosity and the residual stress (the back stress). To describe suitably the time and temperature-dependent effects observed experimentally and the accumulation of the plastic deformation and damage during dynamic loading processes, the thermomechanical coupling has been taken into account and the kinetics of microdamage and kinematic hardening law have been modified and generalized.

Since the rate-independent plastic response is obtained as the limit case when the relaxation time is equal to zero, hence the theory of elasto-viscoplasticity offers a regularization procedure for the solution of the dynamical initial-boundary value problems. The existence of a solution to the initial-boundary value problem is examined and its stability property is investigated based on the application of nonlinear semi-group methods and on the analysis of continuity of evolution operators.

The viscoplastic regularization procedure assures a stable integration algorithm by using the finite difference and finite element methods.

All fundamental features of the thermo-elasto-viscoplastic model have been deeply examined and discussed.

REFERENCES

1. R. ABRAHAM, J.E. MARSDEN, *Foundations of mechanics*, Second Edition, Addison-Wesley, Reading Mass., 1978.
2. R. ABRAHAM, J.E. MARSDEN, T. RATIU, *Manifolds, tensor analysis and applications*, Springer, Berlin 1988.
3. A. AGAH-TEHRANI, E.H. LEE, R.L. MALETT, E.T. ONAT, *The theory of elastic-plastic deformation at finite strain with induced anisotropy modelled isotropic-kinematic hardening*, J. Mech. Phys. Solids, **35**, 43-60, 1987.
4. A. AGAH-TEHRANI, E.H. LEE, R.L. MALETT, E.H. ONAT, *The theory of elastic-plastic deformation at finite strain with induced anisotropy modelled as combined isotropic-kinematic hardening*, J. Mech. Phys. Solids, **35**, 519-539, 1987.

5. P.J. ARMSTRONG, C.O. FREDERICK, *A mathematical representation of the multiaxial Baushinger effect*, CEGB Report RD/B/N731, Central Electricity Generating Board, 1966.
6. R.J. ASARO, *Crystal plasticity*, J. Appl. Mech., **50**, 921-934, 1983.
7. R.J. ASARO, *Micromechanics of crystals and polycrystals*, Adv. Appl. Mech., **23**, 1-115, 1983.
8. R.J. ASARO, A. NEEDLEMAN, *Texture development and strain hardening in rate dependent polycrystals*, Acta Metall., **33**, 923-953, 1985.
9. T.W. BARBEE, L. SEAMAN, R. CREWDSON, D. CURRAN, *Dynamic fracture criteria for ductile and brittle metals*, J. Mater., **7**, 393-401, 1972.
10. J.D. CAMPBELL, W.G. FERGUSON, *The temperature and strain-rate dependence of the shear strength of mild steel*, Phil. Mag., **81**, 63-82, 1970.
11. M.M. CARROLL, A.C. HOLT, *Static and dynamic pore-collapse relations for ductile solids*, J. Appl. Phys., **43**, 1626-1636, 1972.
12. A.K. CHAKRABARTI, J.W. SPRETNAK, *Instability of plastic flow in the direction of pure shear*, Metallurgical Transactions, **6A**, 733-747, 1975.
13. S. CHENGWEI, Z. SHIMING, W. YANPING, L. CANGLI, *Dynamic fracture in metals at high strain rate*, in: High-Pressure Shock Compression of Solids, II. Dynamic Fracture and Fragmentation, L. DAVISON, D.E. GRADY and M. SHAHINPOOR [Eds.], 71-89, Springer-Verlag, New York 1996.
14. K. CHO, Y.C. CHI, J. DUFFY, *Microscopic observations of adiabatic shear bands in three different steels*, Brown University Report, 1989.
15. B.D. COLEMAN, M.E. GURTIN, *Thermodynamics with internal state variables*, J. Chem. Phys., **47**, 597-613, 1967.
16. B.D. COLEMAN, W. NOLL, *The thermodynamics of elastic materials with heat conduction and viscosity*, Arch. Rational Mech. Anal., **13**, 167-178, 1963.
17. H. CONRAD, *Thermally activated deformation of metals*, J. Metals, **16**, 582-588, 1964.
18. D.R. CURRAN, L. SEAMAN, D.A. SHOCKEY, *Dynamic failure in solids*, Physics Today, January, 46-55, 1977.
19. D.R. CURRAN, L. SEAMAN, D.A. SHOCKEY, *Linking dynamic fracture to microstructural processes*, in: Shock Waves and High-Strain Rate Phenomena in Metals: Concepts and Applications, M.A. MEYERS and L.E. MURR [Eds.], 129-167, Plenum Press, New York 1981.
20. D.R. CURRAN, L. SEAMAN, D.A. SHOCKEY, *Dynamic failure of solids*, Physics Reports, **147**, 253-388, 1987.
21. Y.F. DAFALIAS, *Corotational rates for kinematic hardening at large plastic deformations*, J. Appl. Mech., **50**, 561-565, 1983.
22. Y.F. DAFALIAS, *The plastic spin concept and simple illustration of its rule in final plastic transformations*, Mech. Mater., **3**, 223, 1984.
23. Y.F. DAFALIAS, *The plastic spin*, J. Appl. Mech., **52**, 865-871, 1985.

24. Y.F. DAFALIAS, *Issues on the constitutive formulation at large elastoplastic deformations, Part 1: Kinematics*, Acta Mechanica, **69**, 119, 1987.
25. Y.F. DAFALIAS, *Issues on the constitutive formulation at large elastoplastic deformations, Part 2: Kinetics*, Acta Mechanica, **73**, 121, 1988.
26. R. DAUTRAY, J.-L. LIONS, *Mathematical analysis and numerical methods for science and technology*, Vol. 6. Evolution Problems II, Springer, Berlin 1993.
27. W. DORNOWSKI, P. PERZYNA, *Constitutive modelling of inelastic solids for plastic flow processes under cyclic dynamic loadings*, Transaction of the ASME, J. Eng. Materials and Technology, **121**, 210-220, 1999.
28. W. DORNOWSKI, P. PERZYNA, *Numerical solutions of thermo-viscoplastic flow processes under cyclic dynamic loadings*, in: Proc. Euromech Colloquium 383, Inelastic Analysis of Structures under Variable Loads: Theory and Engineering Applications, D. WEICHERT and G. MAIER [Eds.], 69-94, Kluwer Academic Publishers, 2000.
29. W. DORNOWSKI, P. PERZYNA, *Localization phenomena in thermo-viscoplastic flow processes under cyclic dynamic loadings*, Computer Assisted Mechanics and Engineering Sciences, **7**, 117-160, 2000.
30. W. DORNOWSKI, P. PERZYNA, *Analysis of the influence of various effects on cycle fatigue damage in dynamic processes*, Arch. Applied Mechanics, **72**, 418-438, 2002.
31. W. DORNOWSKI, P. PERZYNA, *Localized fracture phenomena in thermo-viscoplastic flow processes under cyclic dynamic loadings*, Acta Mechanica, **155**, 233-255, 2002.
32. W. DORNOWSKI, P. PERZYNA, *Numerical analysis of macrocrack propagation along a bimaterial interface under dynamic loading processes*, Int. J. Solids and Structures, **39**, 4949-4977, 2002.
33. A.R. DOWLING, J. HARDING, J.D. CAMPBELL, *The dynamic punching of metals*, J. Inst. of Metals, **98**, 215-224, 1970.
34. M.K. DUSZEK, P. PERZYNA, *Plasticity of damaged solids and shear band localization*, Ing. Arch., **58**, 330-392, 1988.
35. M.K. DUSZEK, P. PERZYNA, *Influence of the kinematic hardening on the plastic flow localization in damaged solids*, Arch. Mech., **40**, 595-609, 1988.
36. M.K. DUSZEK, P. PERZYNA, *On combined isotropic and kinematic hardening effects in plastic flow processes*, Int. J. Plasticity, **7**, 351-363, 1991.
37. M.K. DUSZEK, P. PERZYNA, *The localization of plastic deformation in thermoplastic solids*, Int. J. Solids Structures, **27**, 1419-1443, 1991.
38. M.K. DUSZEK-PERZYNA, K. KORBEL, P. PERZYNA, *Adiabatic shear band localization in single crystals under dynamic loading processes*, Arch. Mechanics, **49**, 1069-1090, 1997.
39. M.K. DUSZEK-PERZYNA, P. PERZYNA, *Adiabatic shear band localization in elastic-plastic single crystals*, Int. J. Solids Structures, **30**, 1, 61-89, 1993.
40. M.K. DUSZEK-PERZYNA, P. PERZYNA, *Analysis of the influence of different effects on criteria for adiabatic shear band localization in inelastic solids*, in: Material Instabilities: Theory and Applications, ASME Congress, Chicago, 9-11 November 1994, R.C. BATRA and H.M. ZBIB [Eds.], 59-85, AMD-Vol. 183/MD-Vol.50, ASME, New York, 1994.

41. M.K. DUSZEK-PERZYNA, P. PERZYNA, *Acceleration waves in analysis of adiabatic shear band localization*, in: *Nonlinear Waves in Solids*, Proc. IUTAM Symposium, August 15–20, 1993, Victoria, Canada; J.L.WEGNER and F.R.NORWOOD [Eds.], 128–135, ASME Book No AMR 137, 1995.
42. M.K. DUSZEK-PERZYNA, P. PERZYNA, *Adiabatic shear band localization of inelastic single crystals in symmetric double slip process*, *Archive of Applied Mechanics*, **66**, 369–384, 1996.
43. M.K. DUSZEK-PERZYNA, P. PERZYNA, *Analysis of anisotropy and plastic spin effects on localization phenomena*, *Arch. Appl. Mechanics*, **68**, 352–374, 1998.
44. J. EFTIS, *Constitutive modelling of spall fracture*, in: *High-Pressure Shock Compression of Solids, II. Dynamic Fracture and Fragmentation*, L. DAVISON, D.E. GRADY and M. SHAHINPOOR [Eds.], 399–451, Springer-Verlag, New York 1996.
45. J. EFTIS, J.A. NEMES, *Constitutive modelling of spall fracture*, *Arch. Mech.*, **43**, 399–435, 1991.
46. J. EFTIS, J.A. NEMES, *Evolution equation for the void volume growth rate in a viscoplastic-damage constitutive model*, *Int. J. Plasticity*, **7**, 275–293, 1991.
47. J. EFTIS, J.A. NEMES, *Modelling of impact-induced spall fracture and post spall behaviour of a circular plate*, *Int. J. Fracture*, **53**, 301–324, 1992.
48. A.G. EVANS, R.D. RAWLINGS, *The thermally activated deformation of crystalline materials*, *Phys. Stat. Sol.*, **34**, 9–31, 1969.
49. P.S. FOLLANSBEE, *Metallurgical Applications of shock - wave and high-strain-rate phenomena*, L.E. MURR, K.P. STAUDHAMMER and M.A. MEYERES [Eds.], 451–480, Marcel Dekker, New York 1986.
50. K.O. FRIEDRICHS, *Symmetric hyperbolic linear differential equations*, *Comm. Pure Appl. Math.*, **7**, 345–392, 1954.
51. K.O. FRIEDRICHS, *Symmetric positive linear differential equations*, *Comm. Pure Appl. Math.*, **11**, 333–418, 1958.
52. I. GILATH, *Laser-induced spallation and dynamic fracture at ultra high strain rate*, in: *High-Pressure Shock Compression of Solids, II. Dynamic Fracture and Fragmentation*, L. DAVISON, D.E. GRADY and M. SHAHINPOOR [Eds.], 90–120, Springer-Verlag, New York 1996.
53. J.H. GIOVANOLA, *Adiabatic shear banding under pure shear loading*, *Mechanics of Materials*, **7**, 59–87, 1988.
54. A. GLEMA, T. ŁODYGOWSKI, P. PERZYNA, *Interaction of deformation waves and localization phenomena in inelastic solids*, *Computer Methods in Applied Mechanics and Engineering*, **183**, 123–140, 2000.
55. A. GLEMA, T. ŁODYGOWSKI, P. PERZYNA, *The role of dispersion for the description of strain localization in materials under impact loading*, *European Conference on Computational Mechanics*, June 26–29, Cracow, Poland, 2001.
56. A. GLEMA, T. ŁODYGOWSKI, P. PERZYNA, *Localization of plastic deformations as a result of wave interaction*, *CAM&ES*, **3**, 81–91, 2003.
57. J.A. GORMAN, D.S. WOOD, T. VREELAND, *Mobility of dislocation in aluminium*, *J. Appl. Phys.*, **40**, 833–841, 1969.

58. H.A. GREBE, H.R. PAK, M.A. MEYER, *Adiabatic shear band localization in titanium and Ti-6PctAl-4PctV alloy*, Met. Trans., **16A**, 761-775, 1985.
59. A.L. GURSON, *Plastic flow and fracture behaviour of ductile materials incorporating void nucleation, growth, and interaction*, PhD Thesis, Brown University, 1975.
60. A.L. GURSON, *Continuum theory of ductile rupture by void nucleation and growth - Part I - Yield criteria and flow rules for porous ductile media*, J. Eng. Mater. Technology, **99**, 2-15, 1977.
61. B. GUSTAFSSON, H.O. KREISS, J. OLIGER, *Time dependent problems and difference methods*, John Wiley, New York 1995.
62. H. HAKEN, *Cooperative phenomena in systems far from thermal equilibrium and in non-physical systems*, Reviews of Modern Physics, **47**, 67-121, 1975.
63. H. HAKEN, *Advanced Synergetics*, Springer, Berlin 1987.
64. H. HAKEN, *Information and self-organization*, Springer, Berlin 1988.
65. K.J. HALE, *Dynamic systems and stability*, J. Math. Anal. Appl., **26**, 39-59, 1969.
66. B. HALPHEN, *Sur le champ des vitesses en thermoplasticité finie*, Int. J. Solids Structures, **11**, 947, 1975.
67. K.A. HARTLEY, J. DUFFY, R.H. HAWLEY, *Measurement of the temperature profile during shear band formulation in steels deforming at high strain rates*, J. Mech. Phys. Solids, **35**, 283-301, 1987.
68. F.E. HAUSER, J.A. SIMMONS, J.E. DORN, *Strain rate effects in plastic wave propagation*, in: Response of Metals to High Velocity Deformation, 93-114, Wiley (Interscience), New York 1961.
69. R. HILL, J.R. RICE, *Constitutive analysis of elastic-plastic crystals at arbitrary strain*, J. Mech. Phys. Solids, **20**, 401-413, 1972.
70. R. HILL, J.R. RICE, *Elastic potentials and the structure of inelastic constitutive laws*, SIAM J. Appl. Math., **25**, 448-461, 1973.
71. K. HOHENEMSER, W. PRAGER, *Über die Ansätze der Mechanik isotroper Kontinua*, ZAMM, **12**, 216-226, 1932.
72. T.J.R. HUGHES, T. KATO, J.E. MARSDEN, *Well-posed quasilinear second order hyperbolic system with application to nonlinear elastodynamics and general relativity*, Arch. Rat. Mech. Anal., **63**, 273-294, 1977.
73. T.J.R. HUGHES, J.E. MARSDEN, *Classical elastodynamics as a linear symmetric hyperbolic systems*, J. Elasticity, **8**, 97-110, 1978.
74. K. IKEGAMI, *Experimental plasticity on the anisotropy of metals*, in: Proc. Euromech Colloquium 115, Mechanical Behaviour of Anisotropic Solids, J.P. BIEHLER [Ed.], 201-242, 1982.
75. I.R. IONESCU, M. SOFONEA, *Functional and numerical methods in viscoplasticity*, Oxford 1993.
76. G. JAUMANN, *Geschlossenes System physikalischer und chemischer Differentialgesetze*, Sitzgsber. Akad. Wiss. Wien (IIa), **120**, 385-530, 1911.

77. J.N. JOHNSON, *Dynamic fracture and spallation in ductile solids*, J. Appl. Phys., **52**, 2812–2825, 1981.
78. U.F. KOCKS, A.S. ARGON, M.F. ASHBY, *Thermodynamics and kinetics of slip*, Pergamon Press 1975.
79. J. KRATOCHVIL, *Finite-strain theory of crystalline elastic-inelastic materials*, J. Appl. Phys., **42**, 1104, 1971.
80. A. KUMAR, R.G. KUMBLE, *Viscous drag on dislocations at high strain rates in copper*, J. Appl. Physics, **40**, 3475–3480, 1969.
81. U.S. LINDHOLM, *Some experiments with the split Hopkinson pressure bar*, J. Mech. Phys. Solids, **12**, 317–335, 1964.
82. U.S. LINDHOLM, in: *Mechanical behaviour of materials under dynamic loads*, U.S. LINDHOLM [Ed.], 77–95, Springer Verlag 1968.
83. U.S. LINDHOLM, L.M. YEAKLEY, *Dynamic deformation of single and polycrystalline aluminium*, J. Mech. Phys. Solids, **13**, 41–53, 1965.
84. B. LORET, *On the effects of plastic rotation in the finite deformation of anisotropic elastoplastic materials*, Mech. Mater., **2**, 287–304, 1983.
85. T. ŁODYGOWSKI, P. PERZYNA, *Numerical modelling of localized fracture of inelastic solids in dynamic loading processes*, Int. J. Num. Meth. Engng., **40**, 4137–4158, 1997.
86. T. ŁODYGOWSKI, P. PERZYNA, *Localized fracture of inelastic polycrystalline solids under dynamic loading processes*, Int. J. Damage Mechanics, **6**, 364–407, 1997.
87. L.E. MALVERN, *The propagation of longitudinal waves of plastic deformation in a bar of material exhibiting a strain-rate effects*, J. Appl. Mech., **18**, 203–208, 1951.
88. J. MANDEL, *Plasticité classique et viscoplasticité*, CISM Lecture Notes No. 97, Udine, Springer-Verlag, Vien 1971.
89. J. MANDEL, *Equations constitutives et directeurs dans les milieux plastiques et viscoplastiques*, Int. J. Solids Structures, **9**, 725–740, 1973.
90. J. MANDEL, *Définition d'un repère privilégié pour l'étude des transformations anélastiques du polycrystal*, J. Méc. Théo. Appl., **1**, 7, 1982.
91. A. MARCHAND, K. CHO, J. DUFFY, *The formation of adiabatic shear bands in an AISI 1018 cold-rolled steel*, Brown University Report 1988.
92. A. MARCHAND, J. DUFFY, *An experimental study of the formation process of adiabatic shear bands in a structural steel*, J. Mech. Phys. Solids, **36**, 251–283, 1988.
93. J.E. MARSDEN, T.J.R. HUGHES, *Mathematical foundations of elasticity*, Prentice-Hall, Englewood Cliffs, New York 1983.
94. W.P. MASON, *Phonon viscosity and its effect on acoustic wave attenuation and dislocation motion*, J. Acoustical Soc. Amer., **32**, 458–472, 1960.
95. J.J. MASON, J.A. ROSAKIS, R. RAVICHANDRAN, *On the strain and strain rate dependence of the fraction of plastic work converted to heat: an experimental study using high speed infrared detectors and the Kolsky bar*, Mechanics of Materials, **17**, 135–145, 1994.
96. M.E. MEAR, J.E. HUTCHINSON, *Influence of yield surface curvature on flow localization in dilatant plasticity*, Mech. Mater., **4**, 395–407, 1985.

97. H.C. MEYERS, *Dynamic behaviour of materials*, John Wiley, New York 1994.
98. M.A. MEYERS, C.T. AIMONE, *Dynamic fracture (spalling) of metals*, Prog. Mater. Sci., **28**, 1-96, 1983.
99. S.K. MITRA, J.E. DORN, *On the nature of strain hardening in face-centered cubic metals*, Trans. AIME, **224**, 1062-1071, 1962.
100. F.R.N. NABARRO, *Theory of crystal dislocations*, Oxford 1967.
101. S. NEMAT-NASSER, *Phenomenological theories of elastoplasticity and strain localization at high strain rates*, Appl. Mech. Rev., **45**, S19-S45, 1992.
102. J. OLDROYD, *On the formulation of rheological equations of state*, Proc. R. Soc. Lond., **A200**, 523-541, 1950.
103. P. PERZYNA, *The constitutive equations for rate sensitive plastic materials*, Quart. Appl. Math., **20**, 321-332, 1963.
104. P. PERZYNA, *Fundamental problems in viscoplasticity*, Advances in Applied Mechanics, **9**, 243-377, 1966.
105. P. PERZYNA, *Thermodynamic theory of viscoplasticity*, Advances in Applied Mechanics, **11**, 313-354, 1971.
106. P. PERZYNA, *Thermodynamics of a unique material structure*, Arch. Mechanics, **27**, 791-806, 1975.
107. P. PERZYNA, *Coupling of dissipative mechanisms of viscoplastic flow*, Arch. Mechanics, **29**, 607-624, 1977.
108. P. PERZYNA, *Modified theory of viscoplasticity. Application to advanced flow and instability phenomena*, Arch. Mechanics, **32**, 403-420, 1980.
109. P. PERZYNA, *Thermodynamics of dissipative materials*, in: Recent Developments in Thermodynamics of Solids, G. LEBON and P. PERZYNA [Eds.], 95-220, Springer, Wien 1980.
110. P. PERZYNA, *Stability phenomena of dissipative solids with internal defects and imperfections*, in: Proc. XV-th IUTAM Congress, Toronto, August 1980, Theoretical and Applied Mechanics, F.P.J. RIMROTT and B. TABARROK [Eds.], 369-376, North-Holland, Amsterdam 1981.
111. P. PERZYNA, *Stability problems for inelastic solids with defects and imperfections*, Arch. Mechanics, **33**, 587-602, 1981.
112. P. PERZYNA, *Application of dynamical system methods to flow processes of dissipative solids*, Arch. Mechanics, **34**, 523-539, 1982.
113. P. PERZYNA, *Stability of flow processes for dissipative solids with internal imperfections*, ZAMP, **35**, 848-867, 1984.
114. P. PERZYNA, *Constitutive modelling of dissipative solids for postcritical behaviour and fracture*, ASME J. Eng. Materials and Technology, **106**, 410-419, 1984.
115. P. PERZYNA, *Dependence of fracture phenomena upon the evolution of constitutive structure of solids*, Arch. Mechanics, **37**, 485-501, 1985.
116. P. PERZYNA, *Internal state variable description of dynamic fracture of ductile solids*, Int. J. Solids Structures, **22**, 797-818, 1986.

117. P. PERZYNA, *Constitutive modelling for brittle dynamic fracture in dissipative solids*, Arch. Mechanics, **38**, 725–738, 1986.
118. P. PERZYNA, *Temperature and rate dependent theory of plasticity of crystalline solids*, Revue Phys. Appl., **23**, 445–459, 1988.
119. P. PERZYNA, *Influence of anisotropic effects on micro-damage process in dissipative solids*, in: Proc. IUTAM/ICM Symposium on Yielding, Damage and Failure of Anisotropic Solids, Villerd-de-Lance, August 1987, 483–507, Mech. Eng. Publ. Limited, London 1990.
120. P. PERZYNA, *Constitutive equations for thermoplasticity and instability phenomena in thermodynamic flow processes*, in: Progress in Computational Analysis of Inelastic Structures, E. STEIN [Ed.], 1–78, Springer-Verlag, Wien 1993.
121. P. PERZYNA, *Instability phenomena and adiabatic shear band localization in thermoplastic flow processes*, Acta Mechanica, **106**, 173–205, 1994.
122. P. PERZYNA, *Interactions of elastic-viscoplastic waves and localization phenomena in solids*, IUTAM Symposium on Nonlinear Waves in Solids, August 15–20, 1993, Victoria, Canada; J.L. WEGNER and F.R. NORWOOD [Eds.], 114–121, ASME 1995.
123. P. PERZYNA, *Constitutive modelling of dissipative solids for localization and fracture*, in: Localization and Fracture Phenomena in Inelastic Solids, P. PERZYNA [Ed.], 99–242, Springer, Wien, New York 1998.
124. P. PERZYNA, *Thermo-elasto-viscoplasticity and damage*, in: Handbook of Materials Behaviour Models, J. LEMAITRE [Ed.], 821–834, Academic Press, New York 2001.
125. P. PERZYNA, *Thermodynamical theory of inelastic single crystals*, Engineering Transactions, **50**, 107–164, 2002.
126. P. PERZYNA, A. DRABIK, *Influence of thermal effects on micro-damaged solids*, Arch. Mechanics, **40**, 795–805, 1988.
127. P. PERZYNA, A. DRABIK, *Description of micro-damage process by porosity parameter for nonlinear viscoplasticity*, Arch. Mechanics, **41**, 895–908, 1989.
128. P. PERZYNA, A. DRABIK, *Micro-damage mechanism in adiabatic processes*, Engineering Transactions, (in print), 2005.
129. P. PERZYNA, M.K. DUSZEK-PERZYNA, *Constitutive modelling of inelastic single crystals for localization phenomena*, in: Constitutive Laws: Experiments and Numerical Implementation, A.M. RAJENDRAN and R.C. BATRA [Eds.], 70–83, CIMME, Barcelona 1995.
130. P. PERZYNA, K. KORBEL, *Analysis of the influence of substructure of crystal on the localization phenomena of plastic deformation*, Mechanics of Materials, **24**, 141–158, 1996.
131. P. PERZYNA, K. KORBEL, *Analysis of the influence of various effects on criteria for adiabatic shear band localization in single crystals*, Acta Mechanica, **129**, 31–62, 1998.
132. A. PHILIPS, W.Y. LU, *An experimental investigation of yield surface and loading surface of pure aluminium with stress-controlled and strain-controlled paths of loading*, ASME J. Eng. Mater. Technol., **106**, 349–354, 1984.
133. W. PRAGER, *The theory of plasticity: a survey of recent achievements*, (J. Clayton Lecture), Proc. Inst. Mech. Eng., **169**, 41–57, 1955.
134. W. PRAGER, *Introduction to mechanics of continua*, Gin and Co., New York 1961.

135. R.D. RICHTMYER, *Principles of advanced mathematical physics*, Vol. I, Springer, New York 1978.
136. R.D. RICHTMYER, K.W. MORTON, *Difference methods for initial-value problems*, John Wiley, New York 1967.
137. H.C. ROGERS, C.V. SHASTRY, *Material factors in adiabatic shearing in steels*, in: *Shock Waves and High-Strain-Rate Phenomena in Metals*, M.A. MEYERS and L.E. MURR [Eds.], 285-298, Plenum, New York 1981.
138. A.R. ROSENFELD, G.T. HAHN, *Numerical description of the ambient low-temperature, and high-strain rate flow and fracture behaviour of plain carbon steel*, *Trans. Am. Soc. Metals*, **59**, 962-980, 1966.
139. L. SEAMAN, T.W. BARBEE, D.R. CURRAN, Stanford Res. Inst. Tech. Rep., No. AFWL-TR-71-156, Dec. 1971.
140. L. SEAMAN, D.R. CURRAN, D.A. SHOCKEY, Stanford Res. Inst. Tech. Rep., No. AFWL-TR-71-156, Dec. 1971.
141. L. SEAMAN, D.R. CURRAN, D.A. SHOCKEY, *J. Appl. Phys.*, **47**, 4814-4820, 1976.
142. L. SEAMAN, D.R. CURRAN, W.J. MURRI, *A continuum model for dynamic tensile microfracture and fragmentation*, *J. Appl. Mech.*, **52**, 593-600, 1985.
143. A. SEEGER, *The generation of lattice defects by moving dislocations and its application to the temperature dependence of the flow-stress of f.c.c. crystals*, *Phil. Mag.*, **46**, 1194-1217, 1955.
144. A. SEEGER, *Kristallplastizität*, in: *Handbuch der Physik VII/2*, S. FLÜGGE [Ed.], 1-208, Springer-Verlag 1958.
145. R.T. SHIELD, H. ZIEGLER, *On Prager's hardening rule*, *ZAMP*, **9a**, 260-276, 1958.
146. D.A. SHOCKEY, L. SEAMAN, D.R. CURRAN, in: *Metallurgical effects at high strain rates*, R.W. ROHDE, B.M. BUTCHER, J.R. HOLLAND and C.H. KARBES [Eds.], 473, Plenum Press, New York 1973.
147. D.A. SHOCKEY, L. SEAMAN, D.R. CURRAN, *The microstatistical fracture mechanics approach to dynamic fracture problem*, *Int. J. Fracture*, **27**, 145-157, 1985.
148. D.A. SHOCKEY, L. SEAMAN, K.C. DAO, D.R. CURRAN, *Kinetics of void development in fracturing A533B tensile bars*, *Trans. ASME J. Pressure Vessel. Tech.*, **102**, 14-21, 1980.
149. D. SIDEY, L.F. COFFIN, *Low-cycle fatigue damage mechanisms at high temperature*, in: *Fatigue Mechanisms*, Proc. ASTM STP 675 Symposium, Kansas City, Mo., May 1978, J.T. FONG [Ed.], 528-568, Baltimore 1979.
150. J.C. SIMO, T.J.R. HUGHES, *Computational inelasticity*, Springer, New York 1998.
151. L.J. SLUYS, *Wave propagation, localization and dispersion in softening solids*, Doctoral Thesis, Delft University Press, Delft 1992.
152. G. STRANG, G.J. FIX, *An analysis of the finite element method*, Prentice-Hall, Englewood Cliffs 1973.
153. G.I. TAYLOR, H. QUINNEY, *The latent energy remaining in a metal after cold working*, *Proc. R. Soc. Lond.*, **A143**, 307-326, 1934.

154. M.E. TAYLOR, *Partial differential equations*, vol. III Nonlinear Equations, Springer, New York 1996.
155. C. TEODOSIU, F. SIDOROFF, *A theory of finite elastoplasticity of single crystals*, Int. J. Engng. Sci., **14**, 165–176, 1976.
156. T.Y. THOMAS, *Plastic flow and fracture of solids*, Academic Press, New York 1961.
157. S.P. TIMOTHY, *The structure of adiabatic shear bands in metals: a critical review*, Acta Metall., **35**, 301–306, 1987.
158. C. TRUESDELL, *Rational thermodynamics*, Mc Graw–Hill, New York 1969.
159. C. TRUESDELL, W. NOLL, *The nonlinear field theories of mechanics*, [in:] Handbuch der Physik III/3, S. FLÜGGE [Ed.], Springer–Verlag, Berlin 1965.
160. V. TVERGAARD, *Effects of yield surface curvature and void nucleation on plastic flow localization*, J. Mech. Phys. Solids, **35**, 43–60, 1987.
161. E. VAN DER GIESSEN, *Continuum models of large deformation plasticity, Part I: Large deformation plasticity and the concept of a natural reference state*, Eur. J. Mech., A/Solids, **8**, 15, 1989.
162. E. VAN DER GIESSEN, *Continuum models of large deformation plasticity, Part II: A kinematic hardening model and the concept of a plastically induced orientational structure*, Eur. J. Mech., A/Solids, **8**, 89, 1989.
163. E. VAN DER GIESSEN, *Micromechanical and thermodynamic aspects of the plastic spin*, Int. J. Plasticity, **7**, 365–386, 1991.
164. J.C. WILLEMS, *Dissipative dynamical systems*, Arch. Rat. Mech. Anal., **45**, 321–393, 1972.
165. C.L. WITTMAN, M.A. MEYERS, H.–R. PAK, Met. Trans., **21A**, 707, 1990.
166. P.J. WRAY, *Strain–rate dependence of the tensile failure of polycrystalline material at elevated temperatures*, J. Appl. Phys., **46**, 4018–4029, 1969.
167. A.T. YOKOBORI, T.JR. YOKOBORI, K. SATO, K. SYO, *Fatigue crack growth under mixed modes I and II*, Fatigue Fract. Engng. Mater. Struct., **8**, 315–325, 1985.
168. S. ZAREMBA, *Sur une forme perfectionnée de la théorie de la relaxation*, Bull. Int. Acad. Sci. Cracovie, 594–614, 1903.
169. S. ZAREMBA, *Le principe des mouvements relatifs et les équations de la mécanique physique*, Bull. Int. Acad. Sci. Cracovie, 614–621, 1903.
170. H. ZIEGLER, *A modification of Prager's hardening rule*, Quart. Appl. Math., **17**, 55–65, 1959.

Received January 5, 2005; revised version April 14, 2005.